MODELING AND SIMULATION OF VIBRATIONS OF A TRACTOR GEARBOX

JAMES KURIA KIMOTHO

MASTER OF SCIENCE

(Mechanical Engineering)

JOMO KENYATTA UNIVERSITY OF

AGRICULTURE AND TECHNOLOGY

2008

Modeling and Simulation of Vibrations of a Tractor Gearbox

James Kuria Kimotho

A thesis submitted in partial fulfilment for the Degree of Master of Science in Mechanical Engineering in the Jomo Kenyatta University of Agriculture and Technology

2008

DECLARATION

This thesis is my original work and has not been presented for a degree in any other University.

Signature..... Date.....

James Kuria Kimotho

This thesis has been submitted for examination with my approval as the University Supervisor.

Signature..... Date.....

Eng. Prof. J. M. Kihiu

JKUAT, Kenya

DEDICATION

Dedicated to my loving wife *Janet*, for being the wind beneath my wings and to our daughter *Njeri*, for being the source of joy in my life.

ACKNOWLEDGEMENTS

I would like to thank my research supervisor, Dr. J. M. Kihiu for his support and instructions that were important in this study. His ingenious ideas and allowing me free reign in my investigation enabled me to discover and learn many new things.

I also express my appreciation to the Chairman of the Department of Mechanical Engineering, Dr. P. K. Kibicho for ensuring that the facilities needed for the research were available and for ensuring that our proposals were processed in good time. Special thanks go to the Chief Technician of the Department of Mechanical Engineering, Mr. E. Kibiro for his assistance in the computer laboratory and for providing essential softwares and materials.

The willingness of fellow graduate students, O. Mutuku, Z. Kithinji and C. Adenya to share research and programming experiences has been instrumental in the completion of my work. I also thank H. Ndiritu, A. Gitahi and M. Njuguna for their valuable support and encouragement in using Latex. I am also thankful to the entire staff members of the Department of Mechanical Engineering for their direct and indirect support and cooperation.

I am highly indebted to my wife, Janet Mutheu who has been consistently giving me support and encouragement. The countless sacrifices that she made for me to be able to accomplish this work are too numerous to list.

This work was entirely sponsored by Jomo Kenyatta University of Agriculture and Technology for which I am very grateful.

TABLE OF CONTENTS

LIST OF TABLES

LIST OF FIGURES

LIST OF APPENDICES

LIST OF ABBREVIATIONS

$AGMA$	American Gear Manufacturing Association
DTE	Dynamic Transmission Error
$NASA$	National Aeronautical and Space Administration

LIST OF SYMBOLS

Roman Symbols

$C_{gi}(t)$	Time varying gear mesh damping coefficient
C_{si}	Shaft damping coefficient
E	Young's Modulus of elasticity
E'	Effective Young's Modulus of elasticity
F	Gear face width
h	Time interval
J_i	Mass moment of inertia of rotor i
K	Stiffness matrix
$K_{gi}(t)$	Time varying gear mesh stiffness
N_p	Pinion rotational speed
p_c	Circular pitch
P_h	Hertzian pressure on gear teeth
q_i	generalized coordinate.
Q_i	generalized non-potential forces or moments
R	Mean radius of curvature
R_{bi}	Base circle radius of gear i
R_{ci}	Radius of curvature of gear i
S	Gear tooth surface roughness
SR	Gear teeth sliding ratio
t	Time
T	Total kinetic energy of the system.
T_1	Input torque
T_2, T_3	Output torque

T_p	Number of teeth on pinion
V	Change in potential energy of a system with respect to its potential energy in the static equilibrium position.
V_e	Entrainment velocity
V_R	Rolling velocity
V_s	Sliding velocity
W_{di}	Dynamic load
W_j	Load shared by the gear teeth
W'	Load per unit length of face width
y	Lewis tooth form factor

Greek Symbols

δ_i	Gear teeth relative displacement
$\dot{\delta}_i$	Gear teeth relative velocity
η_o	Lubricant absolute viscosity
μ	Coefficient of friction
ν_k	Lubricant kinematic viscosity
σ_i	Gear tooth bending stress
σ_L	Lewis gear tooth bending stress
τ_j	Time period for gear pair j
θ_i	Torsional displacement of rotor i
$\dot{\theta}_i$	Torsional velocity of rotor i
ζ_g	Gear teeth damping ratio
ζ_s	Shaft damping ratio

ABSTRACT

The vibration characteristics of a four-stage reduction tractor gearbox were studied. These characteristics are: displacement amplitudes, natural frequencies and mode shapes. The main aim of the study was to obtain accurate dynamic response of the system to time varying gear mesh stiffness and periodic frictional torque on the gear teeth and to analyze the effect of gear design parameters on the dynamic response in order to obtain the optimum configuration for the multistage gear train.

A mathematical model for torsional vibrations incorporating the periodic frictional torque on the gear teeth, the time varying mesh stiffness and time varying damping coefficients as the main sources of excitation was developed. Mesh coupling between the four reduction stages of the gear train and shaft flexibility were taken into consideration.

A computer program in FORTRAN that employs fourth order Runge-Kutta integration scheme was developed to simulate the model in the time domain. One of the challenges with models of multiple gear pairs encountered was predicting the initial conditions for the numerical integration. In this research, an iteration scheme was employed where the response after one period of each gear mesh was taken as the initial value for the next iteration until the difference between the initial values and the values after one mesh period was relatively small. This state corresponds to the steady state rotation of the gears. The model was verified by comparing the numerical results obtained with experimental data from NASA Lewis Research Center. The results were found to correlate very well both in the shape of the curves and in magnitude thus indicating that the model represents the physical behavior of gears in mesh. The numerical results obtained showed that gears exhibit large vibration amplitudes which influence the forces and stresses on the gear teeth under

dynamic load conditions. It was observed that the dynamic load on the gear teeth is much larger than the corresponding static load and as a result, the stresses, and hence, bending and contact fatigue lives of the gear set are influenced by its vibratory behavior.

The effect of varying gear design parameters (module, pressure angle and contact ratio) was also studied. The results obtained showed that increasing the contact ratio of a pair of gears in mesh reduces the vibration levels significantly. The results showed that by using gears with a contact ratio of 2.0, the vibration levels can be reduced by upto 75% while the peak dynamic stress on the gear teeth can be reduced by upto 45%. Gear pairs with a module of 2.5 and contact ratio close to 2.0 were found to yield the best combination of low vibrations and low bending stresses for the gearbox studied.

The eigenvalues and eigenvectors of the system were obtained using the Householder and QL algorithm. Prediction of the natural frequencies and mode shapes provided important information for keeping the natural frequencies above the operating speed range. For the gearbox system analyzed in this study, the natural frequencies predicted by the model were found to be way above the operating speed range and thus pose no danger of resonance occurring within the operating speed range. Results from this study showed that, by reducing the mass moment of inertia by about 20%, the natural frequency increases by about 11%.

The model developed in the study can thus be used as an efficient design tool to arrive at an optimal configuration for the gearing system that will result in minimum vibration levels and low dynamic gear root stresses in a cost effective manner.

CHAPTER 1

INTRODUCTION

1.1 Overview

Gears are some of the most critical components in a mechanical power transmission system and in most industrial rotating machinery. They are the most effective means of transmitting power in automobiles and other machines due to their high degree of reliability, compactness, constant transmission ratio, small overall dimensions and operating simplicity [1]. A gearbox usually used in a transmission system is also called a speed reducer, gear head, or a gear reducer, and consists of a set of gears, shafts, keys and bearings that are mounted in a lubricated housing [2]. The function of a gearbox is to convert the input power provided by a prime mover (usually an engine or an electric motor) into an output power at a lower speed and correspondingly higher torque and at times, a higher speed and correspondingly lower torque.

These power transmission systems are often operated under high rotational speeds or low speed and high torque and hence their dynamic analysis becomes a relevant issue. The dynamic behavior of gear systems is important for two main reasons:

i. durability of the gears

ii. vibration and noise

Forces at each gear mesh under dynamic conditions can be many times larger than the corresponding quasi-static forces. As a result of this, stresses and hence bending

and contact fatigue life of a gear set are influenced significantly by its vibratory behavior. Time varying dynamic gear mesh forces are transmitted to the surrounding structures through the housing and mountings to cause gear whine noise. Therefore, large vibration amplitudes typically result in higher noise levels as well.

The physical mechanism of gear meshing has a wide spectrum of dynamic characteristics including time varying mesh stiffness and damping changes during meshing cycle. Additionally, the instantaneous number of teeth in contact, governs the load distribution and sliding resistance acting on the individual teeth. These complexities of the gear meshing mechanism have led prior researchers [3–9] to adopt analytical or numerical approaches to analyze the dynamic response of a single pair of gears in mesh.

A large number of parameters are involved in the design of a gear system and for this reason, modeling becomes instrumental to understanding the complex behavior of the system. Provided all the key effects are included and the right assumptions made, a dynamic model will be able to simulate the experimental observations and hence the physical system considered. Thus a dynamic model can be used to reduce the need to perform expensive experiments involved in studying similar systems. The models can also be used as efficient design tools to arrive at an optimal configuration for the system in a cost effective manner.

Mechanical power transmission systems are often subjected to static or periodic torsional loading that necessitates the analysis of torsional characteristics of the system [10]. For instance, the drive train of a typical tractor is subjected to periodically varying torque. This torque variation occurs due to, among other reasons, the fluctuating nature of the combustion engine that supplies power to the gear-

box [10]. If the frequency of the engine torque variation matches one of the resonant frequencies of the drive train system, large torsional deflections and internal shear stresses occur. Continued operation of the gearbox under such a condition leads to early fatigue failure of the system components [10]. Dynamic analysis of gears is essential for the reduction of noise and vibrations in automobiles, helicopters, machines and other power transmission systems. Sensitivity of the natural frequencies and vibration modes to system parameters provide important information for tuning the natural frequencies away from operating speeds, minimizing response and optimizing structural design [11].

1.2 Problem Statement

The increasing demand for quiet and reliable power transmission systems in machines, automobiles, helicopters, marine vessels, et cetera, has created a growing demand for a more precise analysis of the characteristics of the gear systems. Gear design standards specified by American Gear Manufacturers Association (AGMA) and International Organization for Standardization (ISO), are widely accepted in industry. Mechanical Engineers use these standard values of gear parameters and gear geometries as the preliminary design parameters in designing gear systems. In reality, it is often found that these values give rise to lower than optimum performance, excessive noise, excessive vibrations and early failure when gear systems operate at high torques or at very high speeds. The development of a reliable numerical model to simulate the dynamic behavior of gear systems is therefore necessary.

Noise and vibration reduction in gearboxes is a constant development goal in production and automotive engineering emphasized by increasing requirements of reliability, efficiency and comfort. There are several factors that contribute to gear noise

and vibration. These include: shaft torsional stiffness; gear tooth loading and deformations; gear tooth spacing and profile errors; mounting misalignment; rotating speed; dynamic balance of rotating elements; gears and shaft masses and inertias; and the masses and inertias of driving (power) and driven (load) elements. However, the prime noise and vibration sources in a gear drive is the dynamic loading between gear teeth [12]. This effect is caused by the periodic variation of the stiffness of the meshing teeth which mainly depends upon gear tooth geometry and deflection.

In the past century, much research has been done to study the dynamic behavior of spur gears with more emphasis being focused on the optimal spur gear tooth profile that results in the minimal dynamic loading between the gear teeth [13–15]. Several strategies, namely, semi-empirical, analytical, numerical and experimental methods have been employed to study the problem. However, sufficient analysis for the optimal gear design parameters for a multi-mesh gear train has not been explored in detail.

In this research work, a numerical model that combines the time-varying gear mesh stiffness and periodic frictional torque to predict the vibration levels, dynamic load and dynamic stresses on the gear teeth of a multistage tractor gearbox is developed. The aim of the research is to obtain the optimum gear design parameters for minimum noise and vibrations of the gear train system. The proposed methods are easy to implement, computationally inexpensive and can be easily adapted to any multistage spur gearing system.

1.3 Research Objectives

The main objective of this report was to develop a computationally efficient and stable mathematical model to analyze the dynamics of a multistage tractor gearbox.

The specific research objectives were:

1. To compute the periodic gear mesh stiffness and periodic frictional torque on the gear teeth as a function of the contact position of the gear teeth.
2. To predict the vibratory behavior of the gear teeth of a four-stage tractor gear train both in the time and frequency domain.
3. To predict the dynamic load on the gear teeth of each gear pair in contact within the system.
4. To compute the dynamic stress on the gear teeth of each pair of gears in contact in the system and compare the results with those recommended by AGMA.
5. To predict the natural frequencies and mode shapes of the system and analyze the possibility of resonance occurring within the operating speed range.
6. To investigate the effect varying gear design parameters (module, contact ratio and pressure angle) on the dynamic behavior of the gear system and compare with those recommended by AGMA.
7. To validate the numerical model using existing experimental data available in literature.

1.4 Thesis Outline

The structure of this thesis is organized as follows:

1. Chapter 2 presents a critical literature review of studies that have been done on the dynamics of gears.

2. Chapter 3 describes a method of obtaining the gear tooth stiffness and consequently the mesh stiffness as a function of the contact position. A method of obtaining the periodic friction torque is also explained. Methods of obtaining the torsional natural frequencies and the gear tooth dynamic stress are also explained.

3. Chapter 4 presents the development of a multistage gear train model and the solution method employed to simulate the model.

4. Chapter 5 verifies the validity of the model using experimental data from a test rig developed at the NASA Lewis research center. It also discusses the results obtained from the model and the effects of varying gear design parameters on the vibration levels and bending stress on gears.

5. Chapter 6 sums up the presented research. At the end, the recommendations for future work have been addressed.

CHAPTER 2

LITERATURE REVIEW

2.1 Overview

A significant amount of work has been done in the area of gear modeling. The objectives in dynamic modeling of gears may be summarized as follows [2]:

- Noise and Vibration analysis of geared systems.
- Transmission efficiency prediction.
- Reliability and fatigue life predictions.
- Prediction of the natural frequencies of a geared system and their sensitivity to system parameters.
- Dynamic load analysis.
- Evaluating condition monitoring, fault diagnosis and prognosis.
- Stress analysis such as bending and contact stresses.

The models proposed by several investigators [3, 4, 16–19], show considerable variations in the effects and parameters included; in the basic assumptions made and in the solution technique applied. The current literature review attempts to classify gear literature into groupings with particular relevance to the research presented in this study. These are:

- Gear dynamics modeling.

- Gear stress analysis.
- Efficiency prediction of a geared system.
- Optimal design of gear sets.

2.2 Gear Dynamics Modeling

Numerous mathematical models for gear pair dynamics have been developed over the years. The available literature on gear dynamics modeling can be categorized into three groups:

i. Models for a spur gear pair

ii. Single stage gear train models

iii. Multistage gear train models

2.2.1 Modeling of a Spur Gear Pair

Most researchers have focused on the dynamic analysis of a single pair of gears in mesh [5, 6, 8, 9, 20–26]. Figure 2.1 shows the model used in this category. The gear mesh is modeled as a pair of rigid disks of base circle radii of the gears connected by a spring (mesh stiffness) and damper element set along the line of contact as shown. The differential equations of motion for this system can be expressed in the form [27]:

$$J_1\ddot{\theta_1} + C_g R_{b1}[R_{b1}\dot{\theta}_1 - R_{b2}\dot{\theta}_2] + R_{b1}K_m[R_{b1}\theta_1 - R_{b2}\theta_2] = T_1, \tag{2.1}$$

$$J_2\ddot{\theta_2} + C_g R_{b2}[R_{b2}\dot{\theta}_2 - R_{b1}\dot{\theta}_1] + R_{b2}K_m[R_{b2}\theta_2 - R_{b1}\theta_1] = -T_2. \tag{2.2}$$

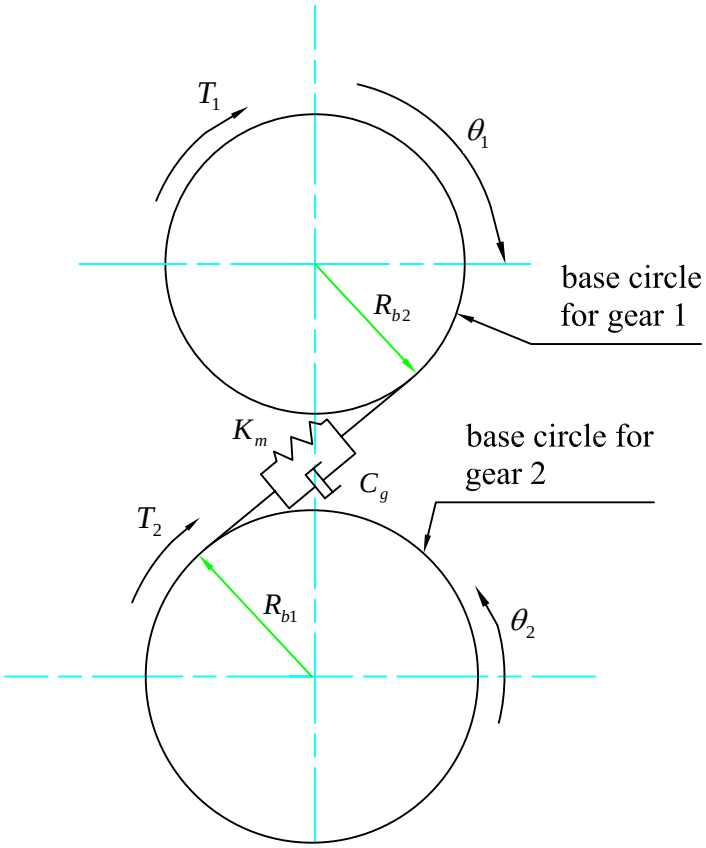

Figure 2.1: Mechanical model of a spur gear pair

where θ_i, $\dot{\theta}_i$, $\ddot{\theta}_i$ $(i = 1, 2)$ are the rotation angle, angular velocity and angular acceleration of the input pinion and output wheel, respectively. J_1 and J_2 are the mass moments of inertia of the gears. T_1 and T_2 denote the external torque loads applied on the system. R_{b1} and R_{b2} represent the base radii of the gears. K_m represents the mesh stiffness. The solution technique employed to solve the above equations differs depending on the investigators preference, reliability required, stability and ease of implementation.

Tamminana et al [26] used two different models, a finite element-based deformable model and a simplified discrete model to predict the dynamic behavior of spur gear

pairs. Finite element analysis was used to compute the relative deformations and stresses within the contact regions in the deformable model while non-linear time-varying model was used in the discrete model. Simple design formulas were proposed to relate the dynamic transmission error to the dynamic factor based on gear mesh forces and stresses.

$$(DF)_{tf} = \frac{(DTF)_{max}}{(STF)_{max}} \tag{2.3}$$

$$(DF)_{\sigma} = \frac{(\sigma_d)_{max}}{(\sigma_s)_{max}} \tag{2.4}$$

where,

$(DF)_{tf}$	Dynamic tooth force factor
$(DTF)_{max}$	Maximum value of dynamic tooth force in one complete mesh cycle
$(STF)_{max}$	Maximum value of static tooth force during the same mesh cycle
$(DF)_{\sigma}$	Dynamic stress factor
$(\sigma_d)_{max}$	Maximum value of the dynamic bending stress on the gear tooth during one mesh cycle
$(\sigma_s)_{max}$	Maximum value of the static bending stress on the gear tooth during one mesh cycle

Shaobin et al [28] developed a non-linear dynamic model of the coupled lateral-torsional vibrations of gear transmission system to estimate the dynamic response of a gear pair. Their results showed that the amplitude of every frequency response curve generated by the meshing vibration increases considerably around the resonance frequency. However, this analysis did not consider the torsional stiffness of the shafts.

Khang et al [27] investigated the parametrically excited vibrations of a gear pair in

mesh and compared the model results with actual experimental data from a test rig. It was concluded that the excitation function caused by the tooth errors is responsible for generating sidebands on the frequency spectrum. The computer simulation results were found to agree closely with results of measurements on the test rig. The study was however intended only to explain the appearance of sideband phenomenon generated by errors and distributed faults on gears.

Sejoong et al [29] developed equations of motion using Lagrange's equation, thus ensuring conservation of energy to study the effect of varying gear tooth stiffness on the dynamic response of a gear pair. The results of the power spectral density of the temporal response of a gear set at two different rotational speeds were presented based on (i) the exact energy conservation equations, (ii) the rigid kinematic Newtonian equations and (iii) the classic gear equation. The results showed that when the driving gear rotates at 4500 rpm,all three sets of equations define essentially the same response, hence justifying the use of the simpler classical equation for vibration analysis. However, with the driving gear rotating at 600 rpm, the exact results differ from the predictions of both the Newtonian equations and classical gear equations. The use of the Newtonian equation and classical gear equation would therefore not be recommended for the design of low speed gear sets.

Various techniques have been employed in gear analysis. Gelman et al [7] developed a statistical methodology and gear expressions for the ratio of the dynamic mean excitation to the transmitted mean load under the influence of important gear characteristics. Parker et al [30] investigated the dynamic response of a spur gear pair using finite element/ contact mechanics model. The dynamic mesh forces were calculated using a detailed contact analysis at each time step as the gears roll

through the mesh. The results showed that for the range of operating speeds and torques considered and in the absence of geometric imperfections, the response has spectral contents only at the mesh frequency. The results also showed that the resonant amplitudes of rotational modes changes more rapidly with torque than that for translational modes. The analysis did not consider the effect of shaft torsional stiffness.

Bonori et al [8] investigated the vibration problems in the gears of an industrial vehicle through the use of perturbation technique. A commercial software was used to generate the gear profiles in order to evaluate global mesh stiffness using finite element analysis. Results showed instability regions at speeds between 5600 and 22500 rpm. The effect of shafts and bearings on the mesh stiffness were neglected.

Some researchers have extended the use of a single gear pair to study the dynamics of gears by including friction between the gear teeth in their models [3–5, 23, 31–33]. In these models, empirical formulas for the instantaneous friction coefficient developed within the last three decades were employed in the computation of the frictional torque along the path of contact. Of particular interest was an empirical formula developed by Xu [33] based on non-newtonian thermo-elastohydrodynamic model (EHL). This formula was obtained by performing a multiple linear regression analysis to the massive EHL predictions under various contact conditions and takes into account most of the factors that influence the sliding friction on mating gears.

In all these studies, the interactions of the gear shafts, driving (power) and driven (load) elements have not been investigated in detail.

2.2.2 Single Stage Gear Models

Another category of gear models that has been used by many researchers to study the dynamic response of gears are the single stage models. These models incorporate the shaft stiffness and the driving and driven inertia elements. Figure 2.2 shows the gear system and its model used in this category. The mathematical model is a four degree of freedom torsional system that has been used by various researchers [18, 34–37]. The equations of motion for this system are given by equations 2.5 - 2.8.

$$J_1\ddot{\theta}_1 + C_{s1}(\dot{\theta}_1 - \dot{\theta}_2) + K_{s1}(\theta_1 - \theta_2) = T_1, \tag{2.5}$$

$$\begin{aligned} J_2\ddot{\theta}_2 + C_{s1}(\theta_2 - \theta_1) + C_g(t)R_{b1}(R_{b1}\dot{\theta}_2 - R_{b2}\dot{\theta}_3) + \\ K_{s1}(\theta_2 - \theta_1) + K_g(t)R_{b1}(R_{b1}\theta_2 - R_{b2}\theta_3) = 0, \end{aligned} \tag{2.6}$$

$$\begin{aligned} J_3\ddot{\theta}_3 + C_gR_{b2}(R_3\dot{\theta}_2 - R_3\dot{\theta}_3) + C_{s2}(\theta_3 - \theta_4) + \\ K_g(t)R_{b2}(R_{b2}\theta_3 - R_{b1}\theta_2) + K_{s2}(\theta_3 - \theta_4) = 0, \end{aligned} \tag{2.7}$$

$$J_4\ddot{\theta}_4 + C_{s2}(\dot{\theta}_4 - \dot{\theta}_3) + K_{s2}(\theta_4 - \theta_3) = -T_4. \tag{2.8}$$

where,

C_{si} (i=1,2) is the damping coefficients of the shafts

K_{si} (i=1,2) is the shaft torsional stiffness

$K_g(t)$ is the periodic gear mesh stiffness

$C_g(t)$ is the time varying gear mesh damping coefficient

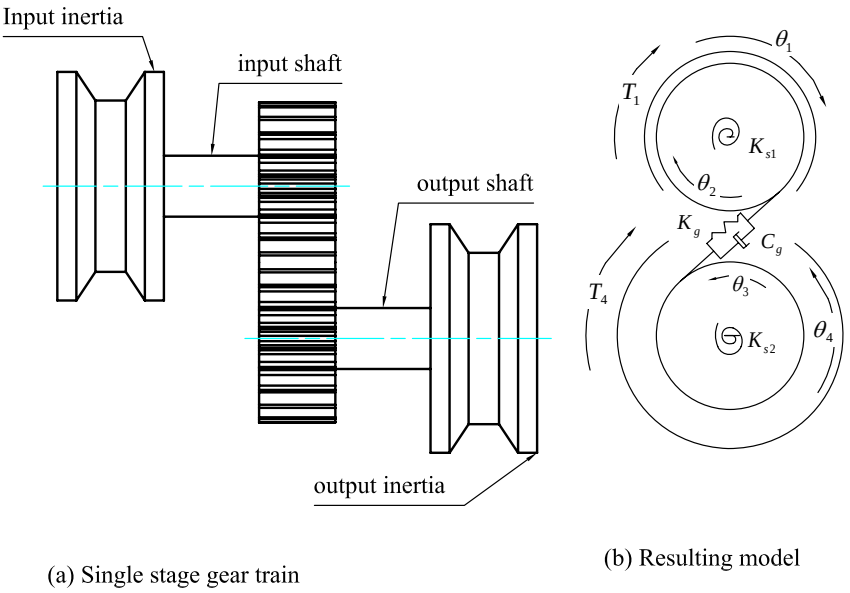

Figure 2.2: Single stage gear train and its model

Hsiang [18] developed an analytical approach specifically for the application of computer aided design and analysis of spur gear systems. The researcher proposed two design approaches to reduce the dynamic response within the operating speed range of a gearbox. One approach used geometric modification of the gear tooth profile while the other used modification of elements mass/ inertia. The results showed that tip relief reduces the peak dynamic loads over the entire speed range. The results also showed that by changing the inertias or stiffness values of a the system, a safe operating speed range with maximum magnitude can be obtained. The code developed in this study laid the base upon which the commercial software (DANST) used by National Aeronautical and Space Administration (NASA) in the analysis of helicopter transmission systems was developed. Leitner [38] developed a detailed dynamic model of a cylinder gear pair that includes the variable mesh stiffness along the line of contact, the non-linear characteristics of rolling element bearing and flexi-

bility of shafts by interfacing the transmission analysis software GESIM to ADAMS, a commercial software for dynamic analysis of rotored systems. The study demonstrated the use of these softwares for natural frequency analysis, vibration analysis or for investigation of deflection of shafts under dynamic loads. The results showed that the force application point changes along the path of contact.

Rao et al [39] determined lateral and torsional response due to torsional excitation of geared rotors. The study used a single stage gear train model to include coupling between bending and torsion of the gears as well as analyzing the effect of axial torque on bending vibrations. The results from this study showed that the lateral response due to short circuit excitation torques is very significant. Even if the rotor speed critical speed is far away from the operating speed, the lateral response at a multiple of the spin speed as well as torsional response in the fundamental mode are very large.

Kikaganesh [16] demonstrated the need to include rotor effects in gear dynamics. The study showed that the lateral whirling motion of the rotors (that model the gear and pinion) and torsional motion of the gears interact with each other and the degree of interaction depends on the proximity of the natural frequencies of the lateral and torsional motions. However, the study did not verify whether such coupling occurs in real systems. Hsiang and Ronald [40] investigated the effect of torsional stiffness of shafts and gear tooth loading and deflection on the dynamics of single stage gear train. The study showed that higher shaft stiffness yielded lower dynamic factors and higher rotating speed of peak response. Vasilios and Christos [41] simulated dynamically a single stage spur gear reducer using various scenarios of error distribution and profile modifications and the vibration amplitude and load

factor calculated in each case. The simulation results complied very well with practical results, confirming the well established standard guidelines of applying profile modifications equal to the maximum indexing error. In the test cases considered, dynamically induced overload was reduced by 35% by applying such modifications. The study also showed that excessive modification becomes a source of excitation.

In all the studies in this group, the effect of multi-mesh coupling of gears has not been investigated.

2.2.3 Multi-stage Gear Train Models

Less focus has been directed to this category of models. A dynamic model of three shafts and two pairs of gears in mesh was developed by Howard et al [19]. The effect of variable tooth stiffness, pitch and profile errors, friction and localized tooth crack on one of the gears were included in the model which was simulated using MATLAB and SIMULINK. The simulation results in this study showed indicated that the pitch and profile errors of 10 microns have a significant impact on the gearbox vibration. The main challenge with models of multiple gear pairs is recovering information about the vibrations from each shaft of interest. This was overcome by employing coherent-time, synchronous-signal averaging technique. This study did not consider the torsional stiffness of the shafts.

Krantz and Majidi [42] developed a mathematical model of a split path gearbox to study the effects of shaft angle, mesh phasing and the stiffness of shafts connecting spur gears to helical pinions on the natural frequencies and vibration energy of the gearbox. The study showed that mesh phasing strongly influenced the level of vibration. Mesh phasing at 0^o and 180^o produced low levels of vibration whereas mesh phasing at 90^o and 270^o produces relatively high vibration levels. The results also

showed that most of the natural frequencies of the vibration were not significantly influenced by varying the shaft angle.

The effect of mesh stiffness parameters, stiffness variation amplitudes, contact ratio, mesh frequencies and mesh phasing on the stability of a two-stage gear system was investigated by Lin and Parker [43]. The results from this study showed that the contact ratios and mesh phasing significantly impact the parametric instabilities and the excitations from the two meshes interact when one mesh frequency is an integer multiple of the other. The interactions between the stiffness variations at the two meshes were also studied.

Takuechi and Togai [44] described the use of Computer-Aided Engineering (CAE) model for the analysis of dynamic gear meshing behavior and for the prediction of dynamic transmission error from the input torque system. Results showed that the dynamic tooth-surface contact stress for a given transmission error value varies in the drive power train model in accordance with changes in the loading torque. The predicted and experimentally measured peak frequencies of the bearing under a dynamic load condition agreed well.

Peeters et al [45] investigated the internal dynamics of a drive train in a wind turbine using three types of multi-body models, with focus on the calculation of the eigen-frequencies and the corresponding mode shapes. The results showed that for the drive train considered, the normal modes lie in a frequency range below the operating frequency range of the drive train and therefore they do not affect the internal dynamics. Choy et al [46] presented an analysis for multi-mesh gear transmission systems. The analysis was used to predict the overall system dynamics and the transmissibility to the gearbox and or the enclosed structure by employing modal

synthesis approach to treat the uncoupled lateral/torsional modal characteristics of each stage or component independently. The results showed that gear tooth mesh frequency and torsional modal frequencies have substantial effect on rotation but not on lateral vibrations of the system.

Planetary gear trains have also received a great deal of attention by many researchers. Lin and Parker [11] investigated the natural frequencies and vibration mode sensitivities to system parameters. The aim of the study was to use the sensitivity of the natural frequencies to system parameters in order to tune resonances away from operating speed thereby minimizing response and optimizing the structural design. The results from this study showed that the rotational modes are independent of the transverse support stiffness and masses of the carrier, ring and sun. Translational modes are independent of the rotational support stiffness and moments of inertia of the carrier, ring and sun. Planet modes are remarkably insensitive to all support stiffnesses, mass and moments of inertia of the carrier, ring and sun. Translational mode natural frequency sensitivity to operating speed increases with component inertia and decreases with system stiffness.

Another study on the dynamic response of a planetary gear system was done by Parker et al [30]. In this study, a finite element/contact mechanics model was developed to study the dynamic response of a helicopter planetary gearbox system over a wide range of operating speeds and torques. Results from this study showed that resonance conditions may be excited by the l^{th} mesh frequency when a natura frequency coincides with $l\omega_m$, where ω_m is the mesh frequency. The results also showed that the response in rotational and translational modes have different sensitivity to changes in operating torque.

2.3 Gear Stress Analysis

A lot of attention on gear study has been devoted to analyzing the bending and contact stresses on gears. Ping-Hsua et al [47] developed procedures for designing compact gear sets by incorporating allowable tooth stress and dynamic response to obtain a feasible design region. The study showed that the required size of an optimal gear set is significantly influenced by the dynamic factor and the peak dynamic factor at system natural frequencies dominates the design of optimal gear sets that operate over a wide range of speeds. Zeping [2] investigated the characteristics of an involute gear system including contact stresses, bending stresses and transmission errors of gears in mesh. A commercial finite element method (FEM) software was employed in the analysis. The study showed that mesh stiffness variation as the number of teeth in contact changes is a primary cause of vibration and noise. Spitas et al [48] investigated numerically the use of spur gear teeth with circular instead of the standard trochoidal root fillet using Boundary Element Method (BEM). The strength of these new teeth was studied in comparison with the standard design by discretizing the tooth boundary using isoparametric Boundary Elements. The analysis demonstrated that the novel teeth exhibit higher bending strength (up to 70%) in certain cases without affecting the pitting resistance since the geometry of the load carrying involute was not changed.

Hsiang et al [49] presented an analytical study on using hob offset to balance the dynamic tooth strength of spur gears operated at a center distance greater than the standard value. The study was limited to offset values that ensure the pinion and gear teeth will neither be undercut nor become pointed. The analysis was done using DANST-PC, a NASA gear dynamics code. The results showed that the optimum

pinion hob offset varies with the rotational speed with the best value lying between 4.04 mm and 5.41 mm at most speeds. Sorin [50] investigated 2-D versus 3-D analysis for stress in the root region of gear teeth. The influence of non-uniform load along the contact line on the root stress was studied. The results showed that the stress distribution in the front plane of 3-D model proves the same shape as the 2-D model stress distribution but the values are smaller by 10% to 15%. Mohanty [51] presented an analytical method for calculating the load sharing amongst the meshing teeth in high contact ratio spur gearing. Contact stresses were computed from the applied load and tooth geometry. The results showed that the principal stress along the path of contact reaches its maximum value in the two pair contact zone at the same point where the normal load is maximum.

Mahbub et al [24] presented a study for stress analysis of spur gear teeth with the variation of tooth parameters; module, pressure angle and number of teeth. Gear tooth under tip load was considered as the worst condition. A computer code based on finite difference method was developed to solve the spur gear tooth as a plane strain problem with mixed boundary conditions. The study showed that gears with a larger module or a larger pitch radius undergo lower stresses. Likewise gears with a higher pressure angle have lesser effect of tooth stress. Glodez et al [52] presented a computational model for determination of service life of gears in regard to bending fatigue in a gear tooth root. The computational results for total service life were found to be in good agreement with available experimental results.

Herbert and Daniel [53] presented an analysis to determine the cyclic loads of the gear teeth of two classes of wind turbine gearboxes using a time-at-torque techniques. The analysis showed that the two gearboxes yielded different distribution of

the stress cycles imposed upon the gear tooth which led to the conclusion that gearboxes must be evaluated on an individual basis. Formulas for stress sensitivity and compliance of low and high contact ratio, involute spur gear teeth were developed by Cornell [21]. The stress sensitivity formula is a modified version of Heywood formula and was evaluated by comparing it with test, finite element and analytical transformation results for gears with various pressure angles, tooth proportions, number of teeth and load contact positions [21]. The formula also predicts fairly well the location of peak stress in the fillet. Results from the study showed that the peak dynamic stress occurs in the zone of single contact.

Mileta [54] presented an analysis on the effect of the teeth geometry and load distribution at simultaneously meshed teeth pairs on stress in the tooth root. Mathematical models were formed for determining the operating and critical stress at the tooth root relevant for checking the gear tooth volume strength based on analytical researches. Paisan et al [55] also added their contribution to gear stress analysis by developing a new innovative procedure called **Point load superposition** for determining the contact stresses in mating gear teeth. The accuracy of the method was demonstrated by comparison with results from classical methods for simple cases where the classical method is applicable. Bibel et al [56] demonstrated that bending stresses in thin rimmed spur gear tooth fillets and root areas differ from the stresses in solid gears due to rim deformations. In this investigation, finite element analysis on a segment of a thin rim gear was employed. The rim thickness was varied and the location and magnitude of the maximum bending stress reported.

2.4 Efficiency Prediction of Geared Systems

In gear transmissions, almost all efficiency or mechanical losses is transformed to heat thereby reducing gear performance, reliability and life. Several failure modes including scoring and contact fatigue failures can be directly impacted by the efficiency of a gear pair. A significant number of studies have been published on efficiency of gear trains [20, 23, 57–59].

Neil and stuart [57] developed a method of predicting power loss in spur gears and extended the method to include involute spur gears of non-standard proportions. The analysis showed that despite their higher sliding velocities, high contact ratio gears can be designed to levels of efficiency comparable to those of conventional gears while retaining their advantages through proper selection of gear geometry.

Xu et al [20] proposed a computational model for the prediction of friction-related mechanical efficiency losses of parallel-axis gear pairs. The friction model uses a validated non-Newtonian thermal elastohydrodynamic lubrication (EHL) model in conjunction with linear regression analysis. Mechanical efficiency predictions were shown to be within 0.1% of the measured values. The study showed that a gear pair having a tip relief of 15 μm is nearly 0.2% more efficient than its unmodified counterpart.

2.5 Optimal Design of Gear Sets

Several approaches to models of optimum design of gear sets have been presented in the recent literature. The methods range from varying the gear design parameters (addendum, module, pressure angle, center distance) to profile modifications of the gear teeth profile. The major goals in the optimization of gear sets vary from author

to author but can be summarized as follows:

- Reduction of static and dynamic transmission errors.
- Reduction of the dynamic loads on the gear teeth.
- Reduction of the root bending stress and contact stresses.

The methods of optimizing gear sets that have received a lot of attention are the use of high contact ratio gears and profile modification.

2.5.1 High Contact Ratio Gears

In high precision, heavily loaded gears, the effect of gear errors is negligible, so the periodic variation of tooth stiffness is the principal cause of noise and vibrations [60]. High contact ratio spur gears are normally used to reduce the variation of tooth stiffness. High contact ratio gears are defined as gear pairs with a contact ratio greater than two. This means that there will be at least two pairs of teeth in contact at any given time. Podzharov at al [60] presented an analysis of static and dynamic transmission error of spur gears cut with standard tools of 20^o pressure angle. A simple method of designing spur gears with contact ratios near 2.0 consisting of increasing the number of teeth of mating gears and simultaneously introducing profile shift in order to maintain same center distance was used in the analysis. It was demonstrated that gears with high contact ratios have much less static and dynamic transmission error than standard gears. High contact ratio gears can be designed in several ways:

1. By selecting a smaller value of the module (smaller teeth).

2. Increasing the length of the tooth addendum.

3. By choosing a smaller pressure angle.

These parameters can be changed individually or in combination to achieve the desired contact ratio [12]. Reducing the module increases the number of teeth and diminishes the tooth thickness, which will reduce the tooth strength. Augmenting the length of the addendum causes the tooth to become longer which increases the bending stress at the fillet region. A lower pressure angle increases the tangential force component acting on the tooth which increases the bending moment. Moreover, it raises the chances of interference, and reduces the tooth thickness at the fillet [12]. For a given pressure angle, the minimum number of teeth (N_{min}) to avoid interference can be calculated using equation 2.9 [61].

$$N_{min} = \frac{2K}{sin^2\phi}. \tag{2.9}$$

where, K is the tooth depth factor and ϕ is the pressure angle. Table 2.1 shows the minimum numbers of teeth to avoid undercutting and the contact ratio (CR) for standard gears [61].

Table 2.1: Minimum numbers of teeth to avoid undercutting for standard gears

System	ϕ	**K**	N_{min}	**CR**
Full depth	14.5^o	1	32	1.7-2.50
Full depth	20^o	1	18	1.45-1.85
Stub	20^o	0.8	14	1.35-1.65
Full depth	25^o	1	12	1.20-1.50

Increasing the tooth addendum is usually the preferred method to obtain high contact ratio gears because this can be done by adjusting the cutting depth of the generating rack during the manufacturing process. Figure 2.3 shows low contact and high contact ratio gears.

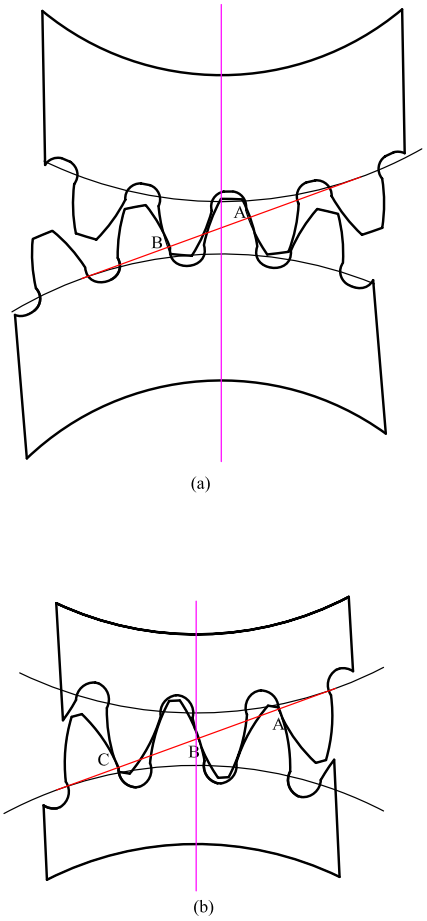

Figure 2.3: (a) Standard gear pair with 2 pairs of teeth in contact (b) High contact ratio gears with 3 pairs of teeth in contact

2.5.2 Tooth Profile Modification

Tooth profile modification is the method by which the tooth profile is subjected to change from the theoretical involute curve by means of reducing tiny amounts of tooth tip or root fillet of the tooth [14]. The modification could be tip relief or full profile modification, while the modified profile could be either linear or parabolic. Figure 2.4 shows an example of a gear tooth with profile modification.

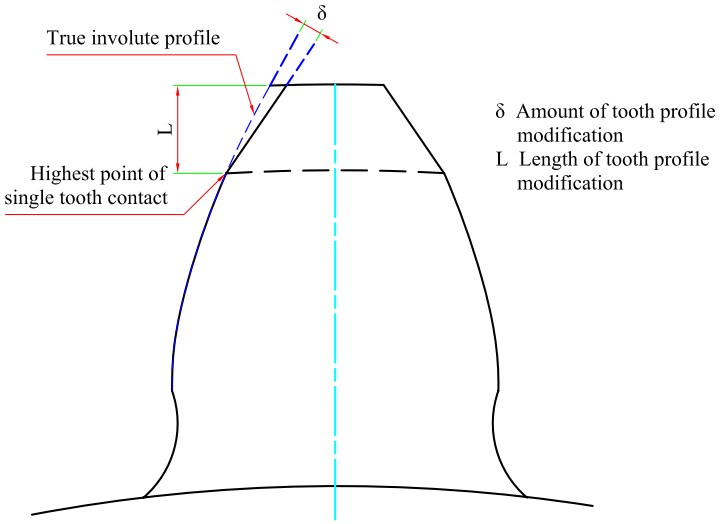

Figure 2.4: Example of a gear tooth with profile modification

Lin et al [13] presented a computer-aided procedure for minimizing the dynamic load and stress of HCRG system by using profile modifications. The total amount and length of tooth profile modification were varied to determine their effects on HCRG dynamics. Both linear and parabolic modifications were studied and their individual influence on the gear dynamic response were compared and discussed. Design charts describing the gear dynamic response for different profile modifications were also presented. The optimum length and amount of tooth profile modifications

for minimum dynamic load and stress can be determined from these charts.

Hyong et al [14] presented a study on how to calculate simultaneously the optimum amounts of tooth profile modifications, end relief and crowning by minimizing the vibration exciting force of helical gears. Automated Design Synthesis (ADS) was used as an optimization tool. Results from this study showed that for aspect ratio 0.25 and 0.5, linear end relief minimizes vibrational exciting force while for an aspect ratio of 1.0, quadratic end relief minimizes vibrations. Chinwai et al [15] investigated the use of linear profile modification and loading conditions on the dynamic tooth load and stresses of high contact ratio gears. The analysis showed that high contact ratio gears require less profile modification than standard low contact ration gears. The results also showed that the optimum profile modification for high contact ratio gears involves trade offs between minimum load (which affects stress) and minimum root bending stress.

2.6 Conclusion

All of the above literature analyzed the dynamics of gear transmission system in different aspects. Few models for the dynamic analysis of a multistage gear train have been developed and those that exist treat either the shafts of the gear system or the gear teeth as rigid bodies depending on the purpose of the analysis. Effect of varying gear design parameters on the dynamics of a multistage gearbox has also not been well explored in order to obtain the optimum parameters for a given gear train. Herbert and Daniel [53] showed that gearboxes must be evaluated for dynamic response on an individual basis. There is therefore the need to develop a general model for a multistage gear train vibrations and one that can be used to obtain the optimum gear design parameters (module, addendum and pressure angle) based on

vibration levels, dynamic load and dynamic root stress.

This work therefore involves the development of a general model to analyze the vibrations of a multistage gear train taking into account time varying mesh stiffness, time varying frictional torque and shaft torsional stiffness. The model is then used to analyze the effect of gear design parameters on the vibration levels and gear tooth root stress with the aim of obtaining the optimum gear design parameters mentioned above.

CHAPTER 3

THEORETICAL BACKGROUND

3.1 Introduction

Research on gears has shown that the varying mesh stiffness of a pair of gears, gear errors and periodic frictional torque are the principal causes of vibrations and noise of gears. However, in high precision, heavily loaded gears, the effect of gear errors is insignificant which leaves the time varying mesh stiffness and period frictional torque as the main sources of noise and vibration [60]. Therefore, in order to analyze the dynamics of gear trains, an accurate prediction of these two sources of vibration is necessary. This chapter focuses on methods of accurately estimating the mesh stiffness and frictional torque as a function of the contact position for a pair of gears in mesh. Methods of determining the natural frequencies and mode shapes, and the gear tooth dynamic stress are also presented.

3.2 Mesh Stiffness Estimation

A pair of meshing gears exhibit a stiffness associated with elastic tooth bending that varies as the gears rotate. This stiffness varies as a function of the contact position for two reasons. The number of teeth varies through each mesh cycle, with two pairs of teeth being in contact at one point in time and one pair of teeth being in contact at another, for example. In addition, the point of contact on any given pair of teeth continually moves along the teeth and thus changing the stiffness. The stiffness of a pair of teeth in mesh can be obtained by considering the elastic deflection of the teeth.

3.2.1 Elastic Deflection of a Tooth

The total static deflection of a pair of mating teeth is assumed to be composed of the following components [62]:

1. Deflection of the tooth as a cantilever beam including shear and compression deformation.

2. Local contact (Hertz) deformation at the contact point.

The total deflection of a gear tooth can be expressed along the line normal to the tooth profile, that is in the direction of the applied load [18]. The tooth is first assumed to be a non-prismatic cantilever beam with an effective length extending from the tip of the tooth to the root circle as shown in Figure 3.1.

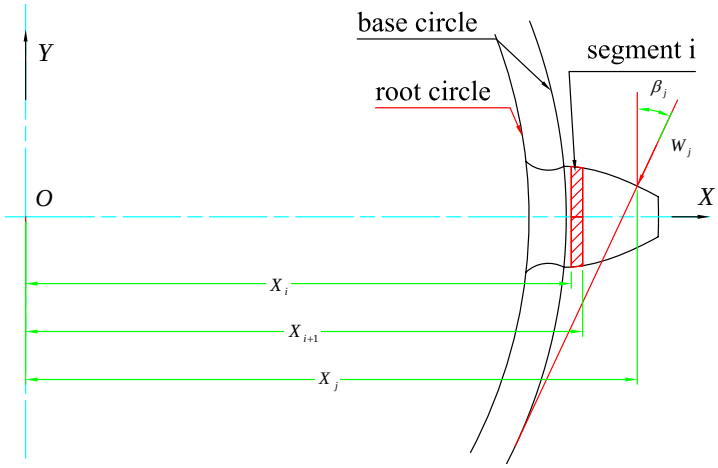

Figure 3.1: Gear tooth geometry for deflection computation

This section of the tooth is then divided into a sequence of segments of length T_i with each segment being considered as a cantilever beam with one end fixed and the remainder of the tooth adjacent to the other end of the segment as a rigid overhang.

The total deflection at the loading point and in the direction of the applied load is then obtained by applying the principle of superposition [63].

For each segment i, the height $\overline{Y_i}$, the cross-sectional area $\overline{A_i}$ and the area moment of inertia, $\overline{I_i}$ are taken as the average of these values at both faces. The applied load which is equal to the applied torque divided by the base circle radius can be resolved into an equivalent system of forces and moments at the right hand face of the segment as shown in Figure 3.2.

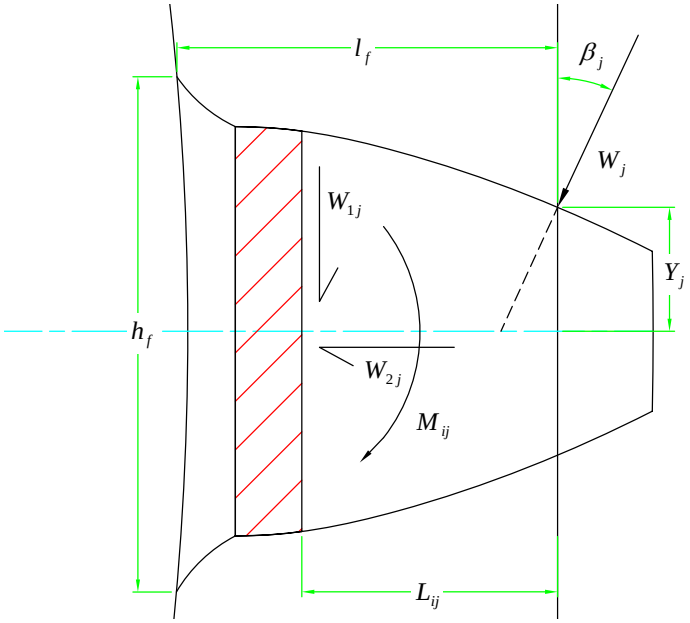

Figure 3.2: Components of the applied load

The components of this system of forces are given by:

$$W_{1j} = W_j \cos \beta_j, \tag{3.1}$$

$$W_{2j} = W_j \sin \beta_j, \tag{3.2}$$

$$M_{ij} = W_j(L_{ij} \cos \beta_j - Y_j \sin \beta_j). \tag{3.3}$$

Where i refers to the segment, j refers to the loading position, L_{ij} is the distance from j to i and,

W_j	is the transmitted load
W_{1j}, W_{2j}	are component loads at i
M_{ij}	is the resultant moment at i due to the load at j.

The contributions of bending, shear and axial deformations to the tooth deflection can can be computed separately as shown in the following sections.

3.2.2 Bending Deflection

The total deflection at the load position associated with bending is given by:

i. Displacements due to W_{1j}

$$(q_w)_{ij} = \frac{W_j \cos\beta_j}{3E_e\overline{I_i}}T_i^3 + \frac{W_j \cos\beta_j}{2E_e\overline{I_i}}T_i^2 L_{ij}, \tag{3.4}$$

ii. Displacement due to net moments M_{ij}

$$(q_m)_{ij} = \frac{W_j(L_{ij}\cos\beta_j - Y_j \sin\beta_j)}{2E_e\overline{I_i}} + \frac{W_j(L_{ij}\cos\beta_j - Y_j \sin\beta_j)}{E_e\overline{I_i}}. \tag{3.5}$$

The second terms of equations 3.4 and 3.5 are the displacements due to the rotations of the rigid overhang [63].

E_e is the effective 'Young's modulus of elasticity' whose value depends upon whether the tooth is 'wide' or 'narrow'. According to Cornell [21], a wide tooth is one for which,

$$\frac{F}{Y} > 5, \tag{3.6}$$

where Y is the tooth thickness at pitch point and F is the face width of the gear. For such a tooth, plane strain applies and,

$$E_e = \frac{E}{1-\nu^2}, \tag{3.7}$$

For a narrow tooth,

$$\frac{F}{Y} < 5, \tag{3.8}$$

and Plane stress applies:

$$E_e = E. \tag{3.9}$$

3.2.3 Shear Deformation

A deflection other than that due to bending moments occur in beams owing to the shearing forces on transverse sections of the beam. This deflection may be found approximately from strain energy principles and by making use of the equations for shear stress at a point in the transverse section of a beam [64].

For a gear tooth, the shear deformation is caused solely by the transverse component of the applied load. It displaces the centerline without causing any rotation [18]. For a rectangular cross-section, the shear deformation is calculated from equation 3.10.

$$(q_s)_{ij} = \frac{6}{5}\frac{W_j T_i \cos\beta_j}{G\overline{A}_i}. \tag{3.10}$$

where,

G is the shear modulus of rigidity.

The moduli of elasticity in tension and shear (E and G) of a material are related by equation 3.11 [65].

$$G = \frac{E}{2(1+\nu)}. \tag{3.11}$$

where,

ν is the poisson's ratio for the material.

Substituting for G in equation 3.10, we obtain:

$$(q_s)_{ij} = \frac{12}{5}\frac{W_j T_i(1+\nu)}{\overline{A}_i E_e}. \tag{3.12}$$

3.2.4 Deformation Due to Axial Compression

The axial compression is caused by the axial load component, W_{1j} and is given by the relation:

$$(q_c)_{ij} = \frac{W_j \sin\beta_j}{E_e \overline{A}_i} T_i. \tag{3.13}$$

The total displacement at the load position j, in the direction of the load, due to deformation of the segment i can be expressed as:

$$(q_1)_{ij} = (q_w + q_m + q_s)_{ij}\cos\beta_j + (q_c)_{ij}\sin\beta_j. \tag{3.14}$$

3.2.5 Deflection Due to Rim Flexibility

The deflection due to flexibility of the gear rim according to Cornell [21] are:

For plane stress case, narrow tooth,

$$(q_{fe})_j = \frac{W_j \cos^2\beta_j}{E_e F}[\frac{50}{3\pi}(\frac{l_f}{h_f})^2 + 2(1+\nu)(\frac{l_f}{h_f})], \tag{3.15}$$

For plane strain case, wide tooth,

$$(q_{fe})_j = \frac{W_j \cos^2\beta_j}{E_e F}(1-\nu^2)[\frac{50}{3\pi}(\frac{l_f}{h_f})^2 + 2\frac{(1-\nu-2\nu^2)}{1-\nu^2}(\frac{l_f}{h_f})]. \tag{3.16}$$

where h_f and l_f are defined in Figure 3.2. The first term in the brackets is the deflection at j due to the rotation caused by the moment at h_f. The second term is the sum of the deflection at j due to the displacement at h_f caused by the moment and rotation at h_f due to the shear force at h_f.

3.2.6 Hertzian Contact Deflection

When the surfaces of two solid bodies are brought into contact under load, they deform elastically. The "Theory of contact mechanics" is concerned with the stresses and deformations which arise for such surfaces [66]. Hertz considered the stresses and deformations in two perfectly smooth, ellipsoidal, contacting solids. The application of the classical elasticity theory to this problem forms the basis of stress and deformation calculations for machine elements such as ball and roller bearings, gears, cams and followers [67].

Hertzian theory of contact utilizes the following assumptions

- The materials are homogenous and yield stress is not exceeded.
- The dimensions of each body are large compared to the radius of the circle of contact.
- The radii of curvature of the contacting bodies are large compared with the radius of the circle of contact.
- The contacting bodies are in frictionless contact.
- The surfaces in contact are continuous and nonconforming.

The contact problem of a pair of gears can be assumed to be a parallel axis cylinder contact problem and therefore line contact deformation applies. The contact between parallel cylinders away from end effects is well represented by two-dimensional Hertz theory [66]. The contact area is assumed to have constant width $2b$ over the length of contact as shown in Figure 3.3.

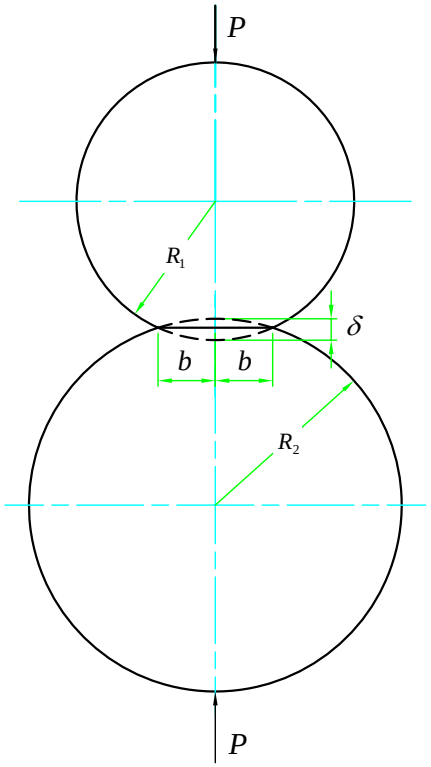

Figure 3.3: Two cylinders in contact with axis parallel

Contact modulus, E_c is given by:

$$\frac{1}{E_c} = \frac{1-\nu_1^2}{E_1} + \frac{1-\nu_2^2}{E_2}, \tag{3.17}$$

Relative radius, R_c is given by

$$\frac{1}{R_c} = \frac{1}{R_1} + \frac{1}{R_2}. \tag{3.18}$$

Half width of contact, b is given by equation 3.19

$$b = \left(\frac{4PR_c}{\pi E_c}\right)^{\frac{1}{2}}. \tag{3.19}$$

The normal displacement depends on the distance that the reference points R_1 and R_2 are from the contact point. This occurs because two dimensional theory only allows the load to spread out in one direction.

Normal displacement is given by:

$$\delta = \frac{P}{\pi E_c}\left\{ln\left(\frac{8R_1}{b}\right) + ln\left(\frac{8R_2}{b}\right) - 1\right\}. \tag{3.20}$$

Contact between a pair of meshing gear teeth can be assumed to be cylinders of radius equivalent to the radius of curvature of the gears at any instantaneous point of contact and then by applying equation 3.20, the contact deformation is obtained.

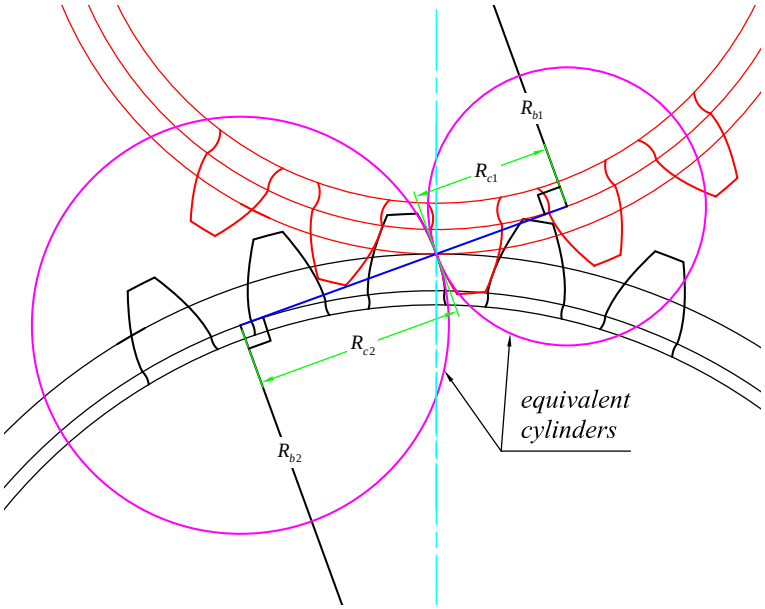

Figure 3.4: Contact model for a pair of gears

Figure 3.4 shows the equivalent contact model of a pair of gears in mesh.

The total deflection at load position j and in the direction of the load is the sum of all the deflections calculated above. If the number of segments is n, then

$$(q_t)_j = \sum_{i=1}^{n}[(q_1)_{ij}] + (q_{fe})_j + (\delta)_j. \tag{3.21}$$

The stiffness value $K_m(t)$ is defined, according to Peeters [45], as the normal distributed tooth force in the normal plane causing deflection of one or more engaging tooth pairs in the direction normal to the tooth profile divided by this deflection. This deflection results from the bending of the teeth in contact between the two gear wheels of which one is assumed to be fixed and the other loaded.

From a physical understanding, it is clear that the presented spring will only work under compression. To ensure that this limitation will not be exceeded during simulation, it is assumed that no contact loss between the mating teeth will occur, something that could happen for a system with backlash when the dynamic mesh force becomes larger than the static force transmitted.

3.2.7 The Individual Tooth Stiffness

The individual tooth stiffness of a pair of teeth in contact is obtained by assuming that one of the mating gears is rigid and applying load to the other. The individual stiffness K_j at any meshing position j can be obtained by dividing the applied load by the deflection of the tooth at that point as shown in equation 3.22 and 3.23. Subscripts p and g refer to the pinion and gear respectively.

$$K_{pj} = \frac{W_j}{q_{pj}}, \tag{3.22}$$

and

$$K_{gj} = \frac{W_j}{q_{gj}}. \tag{3.23}$$

3.2.8 Combined Mesh Stiffness

At any position in the mesh cycle, a pair of teeth in contact can be modeled as two linear springs connected in series [10]. The system stiffness against the applied load, called the combined mesh stiffness at contact point j can be calculated by the following equation;

$$K_{mj} = \frac{K_{pj} \cdot K_{gj}}{K_{pj} + K_{gj}}. \tag{3.24}$$

This equation is illustrated in Figure 3.5.

For a double pair of teeth in contact, the mesh stiffness is obtained by parallel superposition of the corresponding mesh stiffness of the tooth pairs in contact. This mesh stiffness is expressed as:

$$K_{Tj} = (K_{mj})_A + (K_{mj})_B. \tag{3.25}$$

Where $(K_{mj})_A$ and $(K_{mj})_B$ refer to the mesh stiffness of the single tooth pair at mesh positions A and B respectively. This equation is illustrated in Figure 3.6.

The procedures outlined in section 3.2 were coded into a FORTRAN program to generate the mesh stiffness as a function of the contact position. The process starts with the input of gear parameters and operating conditions. The actual profile of the gear tooth is computed and used in the estimation of the mesh stiffness.

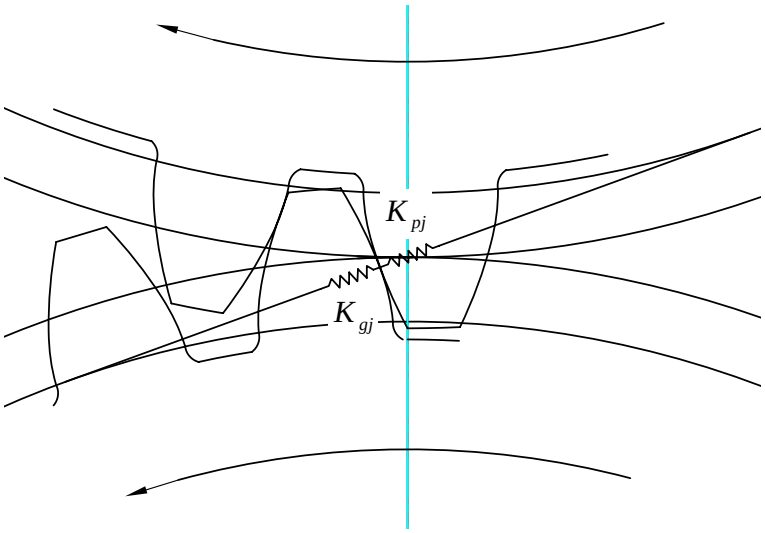

Figure 3.5: Single pair model of stiffness

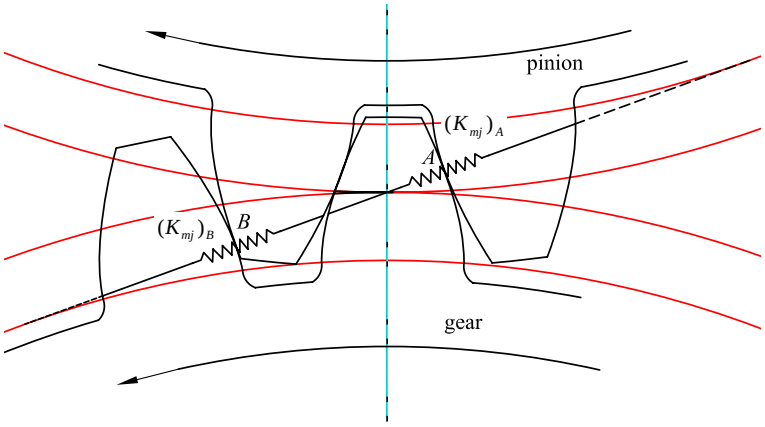

Figure 3.6: Double pair teeth stiffness model

3.3 Modeling Friction in Spur Gears

Sliding friction between gear teeth is recognized as one of the main sources of power loss in geared transmissions as well as a potential source of vibration and noise. Its accurate modeling is therefore of primary importance in vibration and efficiency analysis of geared transmissions. The free body diagram of an engaging spur gear pair is shown in Figure 3.7 where T_1 and T_2 denote the input and output torque

respectively. The contact loads at the contact points A and B are P_A and P_B respectively.

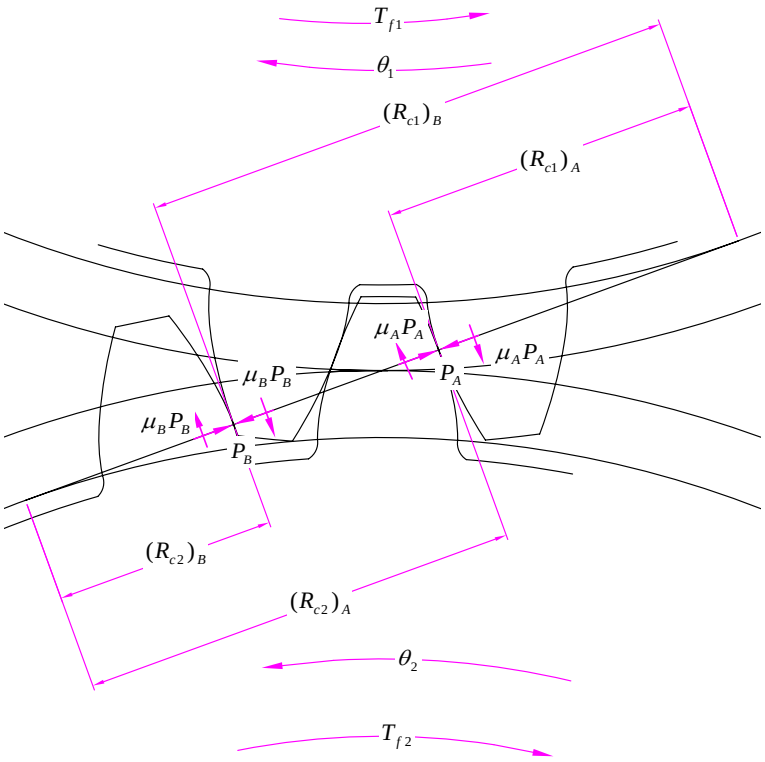

Figure 3.7: Free body diagram of a meshing gear pair

3.3.1 Frictional Torque

Sliding friction on the gear tooth surface causes frictional force F_t along the off-line of action direction and a frictional torque T_f about the gear axis. During gear meshing action, the tooth contact point moves along the line of action, and T_f changes continuously due to linearly varying values of the radius of curvature. The frictional torque can be obtained from the free body diagram of a meshing gear pair (Figure 3.7) as:

Double tooth pair contact zone

$$(T_{f1})_j = \mu_A P_A R_{c1}^A + \mu_B P_B R_{c1}^B \tag{3.26}$$

$$(T_{f2})_j = \mu_A P_A R_{c2}^A + \mu_B P_B R_{c2}^B \tag{3.27}$$

Single tooth pair contact zone

$$(T_{f1})_j = \mu P R_{c1} \tag{3.28}$$

$$(T_{f1})_j = \mu P R_{c2} \tag{3.29}$$

The magnitude of the frictional torque is directly related to the friction coefficient and the normal tooth load. Therefore, accurate determination of the friction coefficient is required.

3.3.2 Instantaneous Friction Coefficient

When gears operate near their maximum load capacity, very high contact pressure occurs at the mesh interface. This may lead to a partial breakdown of the lubricant film at the surface, thus resulting in two commonly encountered regimes, elastohydrodynamic (EHL) and boundary lubrication [3]. Furthermore, tribological parameters, such as radius of curvature and sliding velocity change over the whole gear tooth surface. Under EHL conditions, the friction coefficient is a function of the surface velocity, curvature, and the normal contact load W on the mating surfaces, such that $\mu = f(V_s, W, V_R, T_l, R_c, \eta_o, ...)$. Here , V_R is the rolling velocity, η_o is the lubricant dynamic viscosity and T_l is the fluid inlet temperature. Conversely, mixed lubrication condition is characterized by partial asperity contact and surface finish and surface finish becomes S, an additional parameter influencing friction properties and thus $\mu = f(V_s, W, V_R, T_l, R_c, \eta_o, S..)$.

As the gear teeth move through the mesh cycle, the normal contact force between the teeth changes its value as the number of teeth alternate between 1 and 2 as well as the coefficient of friction. A large number of empirical formulae for determining the coefficient of friction can be found in reference [3, 18, 20, 33]. Most of these formulae are obtained by curve fitting measured data from experimental tests. They have the following general formula $\mu = f(V_s, W, V_R, P_{max}, R_c, \eta_o, S..)$, where P_{max} is the contact pressure.

Commonly cited empirical formulas for coefficient of friction are shown in Table 3.1. Other details of these formulas can be found in references [4, 20].

These formulae were shown to be inaccurate under certain conditions representing the contact of a gear pair [20]. Specifically, as V_s approaches zero when the contact nears the pitch point, most of these formulae predict a very large value of the friction coefficient while in real sense, the coefficient of friction should be zero under no sliding. Consequently as indicated in Table 3.1, some of these formulas are only valid in certain parameter ranges, specific roughness and lubricant types and therefore cannot be used as a general means of predicting the friction coefficient along the path of contact for different gears. Figure 3.8 shows the curves for the friction coefficient along the path of contact resulting from these formulas. Table 3.2 shows some typical parameters used in the analysis.

Table 3.1: Commonly cited formulas for μ

Formula and author	Parameter ranges	specific units
Drozdov and Gavrikov [20] $\mu = [0.8\sqrt{\nu_k}V_s + V_r\phi + 13.4]^{-1}$ $\phi = 0.47 - 0.13(10)^{-4}P_{max} - 0.4(10)^{-3}\nu_k$	$\nu_k \epsilon [4, 500]$ $V_s \leq 15,$ $V_r \epsilon [3, 20]$	$V_s, V_r (m/s)$ $P_{max} (kg/cm^2$
Benedict and Kelley [20] $\mu = 0.127[\frac{50}{50-S}]log_{10}[\frac{3.17(10)^8 W^{'}}{\nu_k V_s V_r^2}]$	$\frac{50}{50-S} \leq 3$	$S(\mu in)$ $W^{'}(lbf/in)$
ISO TC60 [20] $\mu = 0.12[W^{'}S/(RV_r\nu)]^{0.25}$		$V_r (m/s)$ $S(\mu m),$ $W^{'}(N/mm)$
Kuang [4] $\mu = \frac{V_s}{P_A t_A} \int_{-a}^{+a} \eta_A dx$		V_s (m/s)

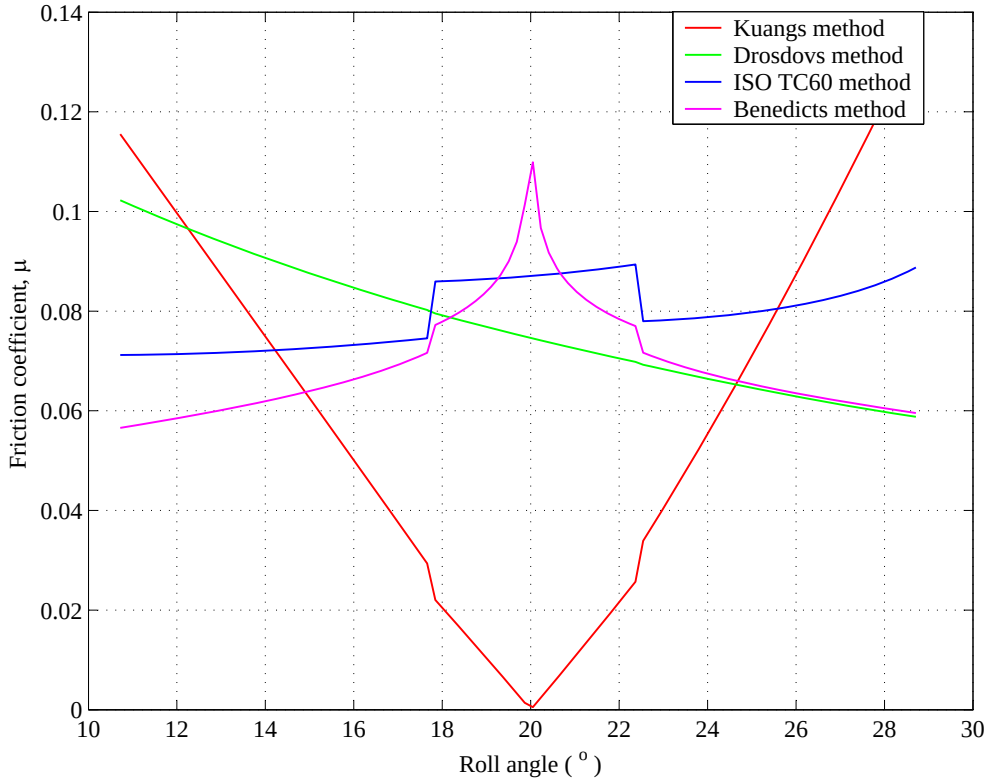

Figure 3.8: Friction Coefficients from different empirical formulas

Table 3.2: Parameters and operating conditions used in the analysis of coefficient of friction

module (m)	$3.0mm$
pressure angle ϕ	20^o
pinion	$28T$
gear	$20T$
speed (N)	$1500rpm$
power	$4847KW$

In this study, an empirical formula developed by Xu and Kahraman [20] was adopted as it was found to accurately model the instantaneous coefficient of friction along the path of contact of a pair of gears in mesh. This model is based on Electro-hydrodynamic lubrication (EHL) and was obtained by multiple linear regression analysis. This model includes the key parameters influencing friction at the contacting gear surfaces, namely sliding velocity, contacting pressure, surface roughness, lubricant dynamic viscosity, radius of curvature and entrainment velocity. The formula was found to correlate very well with experimental data [20]. The formula can therefore be used with confidence for the prediction of friction coefficient for a pair of contacting gears. This formula is written as:

$$\mu = e^{f(SR,P_h,\eta,S)} P_h^{b_2} |SR|^{b3} V_e^{b_6} \eta^{b_7} R^{b_8}. \tag{3.30}$$

where,

$$f(SR, P_h\eta, S) = b_1 + b_4|SR|P_h log_{10}(\eta) + b_5 e^{-|SR|P_h log_{10}(\eta)} + b_9 e^s \tag{3.31}$$

$$\begin{aligned}
V_e &= \tfrac{u_1+u_2}{2} \\
V_r &= u_1 + u_2 \\
V_s &= u_1 - u_2 \\
SR &= \tfrac{V_s}{V_e} \\
P_h &= \sqrt{\tfrac{W' E'}{2\pi R}} \\
R &= \tfrac{R_{c1} R_{c2}}{R_{c1}+R_{c2}} \\
E' &= 2[\tfrac{1-\nu_1}{E_1} + \tfrac{1-\nu_1}{E_2}]^{-1}
\end{aligned}$$

The above set of equations were coded in a FORTRAN program and simulated. The results are presented in chapter 5.

3.4 Natural Frequencies of the System

An $n-$degree-of-freedom system has n natural frequencies, and for each natural frequency there is a corresponding normal mode shape that defines a distinct relationship between the amplitudes of the generalized coordinates for that mode. The squares of the natural frequencies and the corresponding sets of coordinate values describing the normal mode shapes are referred to as *eigenvalues* and *eigenvectors* respectively, and they are of fundamental importance in the analysis of free or forced vibration of multi-degree-of-freedom systems [68]. Prediction of the natural frequencies and vibration modes of a system provides important information for tuning resonances away from the operating speeds and minimizing response [11]. Equations of motion for undamped systems, under the assumption of constant stiffness, mass inertia and free oscillations, can be represented in matrix form (equation 3.32) and are used to find the natural frequencies of the system.

$$[J]\{\ddot{\theta}\} + [K]\{\theta\} = \{0\}, \tag{3.32}$$

Where the inertia matrix $[J]$ is given by:

$$\begin{pmatrix} J_1 & 0 & 0 & 0 & 0 & 0 & 0 & 0 & 0 & 0 & 0 & 0 & 0 \\ 0 & J_2 & 0 & 0 & 0 & 0 & 0 & 0 & 0 & 0 & 0 & 0 & 0 \\ 0 & 0 & J_3 & 0 & 0 & 0 & 0 & 0 & 0 & 0 & 0 & 0 & 0 \\ 0 & 0 & 0 & J_4 & 0 & 0 & 0 & 0 & 0 & 0 & 0 & 0 & 0 \\ 0 & 0 & 0 & 0 & J_5 & 0 & 0 & 0 & 0 & 0 & 0 & 0 & 0 \\ 0 & 0 & 0 & 0 & 0 & J_6 & 0 & 0 & 0 & 0 & 0 & 0 & 0 \\ 0 & 0 & 0 & 0 & 0 & 0 & J_7 & 0 & 0 & 0 & 0 & 0 & 0 \\ 0 & 0 & 0 & 0 & 0 & 0 & 0 & J_8 & 0 & 0 & 0 & 0 & 0 \\ 0 & 0 & 0 & 0 & 0 & 0 & 0 & 0 & J_9 & 0 & 0 & 0 & 0 \\ 0 & 0 & 0 & 0 & 0 & 0 & 0 & 0 & 0 & J_{10} & 0 & 0 & 0 \\ 0 & 0 & 0 & 0 & 0 & 0 & 0 & 0 & 0 & 0 & J_{11} & 0 & 0 \\ 0 & 0 & 0 & 0 & 0 & 0 & 0 & 0 & 0 & 0 & 0 & J_{12} & 0 \\ 0 & 0 & 0 & 0 & 0 & 0 & 0 & 0 & 0 & 0 & 0 & 0 & J_{13} \end{pmatrix} \tag{3.33}$$

and the stiffness matrix $[K]$ is given by:

$$\begin{pmatrix} K_{1,1} & -K_{1,2} & 0 & 0 & 0 & 0 & 0 & 0 & 0 & 0 & 0 & 0 & 0 \\ -K_{2,1} & K_{2,2} & -K_{2,3} & 0 & 0 & 0 & 0 & 0 & 0 & 0 & 0 & 0 & 0 \\ 0 & -K_{3,2} & K_{3,3} & -K_{3,4} & 0 & 0 & 0 & 0 & 0 & 0 & 0 & 0 & 0 \\ 0 & 0 & -K_{4,3} & K_{4,4} & -K_{4,5} & 0 & 0 & 0 & 0 & 0 & 0 & 0 & 0 \\ 0 & 0 & 0 & -K_{5,4} & K_{5,5} & -K_{5,6} & 0 & 0 & 0 & 0 & 0 & 0 & 0 \\ 0 & 0 & 0 & 0 & -K_{6,5} & K_{6,6} & -K_{6,7} & 0 & 0 & 0 & 0 & 0 & 0 \\ 0 & 0 & 0 & 0 & 0 & -K_{7,6} & K_{7,7} & -K_{7,8} & 0 & -K_{7,10} & 0 & 0 & 0 \\ 0 & 0 & 0 & 0 & 0 & 0 & -K_{8,7} & K_{8,8} & -K_{8,9} & 0 & 0 & 0 & 0 \\ 0 & 0 & 0 & 0 & 0 & 0 & 0 & -K_{9,8} & K_{9,9} & 0 & 0 & 0 & -K_{9,13} \\ 0 & 0 & 0 & 0 & 0 & 0 & -K_{10,7} & 0 & 0 & K_{10,10} & -K_{10,11} & 0 & 0 \\ 0 & 0 & 0 & 0 & 0 & 0 & 0 & 0 & 0 & -K_{11,10} & K_{11,11} & -K_{11,12} & 0 \\ 0 & 0 & 0 & 0 & 0 & 0 & 0 & 0 & 0 & 0 & -K_{12,11} & K_{12,12} & 0 \\ 0 & 0 & 0 & 0 & 0 & 0 & 0 & 0 & -K_{13,9} & 0 & 0 & 0 & K_{13,13} \end{pmatrix}$$

Where,

$$K_{1,1} = K_{s1} \qquad K_{1,2} = -K_{s1}$$

$$K_{2,1} = -K_{21} \qquad K_{2,2} = K_{s1} + K_{g1}r_2^2 \qquad K_{2,3} = -K_{g1}r_2r_3$$

$$K_{3,2} = -K_{g1}r_2r_3 \qquad K_{3,3} = K_{g1}r_3^2 + K_{s2} \qquad K_{3,4} = -K_{s2}$$

$$K_{4,3} = -K_{s2} \qquad K_{4,4} = K_{s2} + K_{g2}r_4^2 \qquad K_{4,5} = -K_{g2}r_4r_5$$

$$K_{5,4} = -K_{g2}r_4r_5 \qquad K_{5,5} = K_{g2}r_5^2 + K_{s3} \qquad K_{5,6} = -K_{s3}$$

$$K_{6,5} = -K_{s3} \qquad K_{6,6} = K_{s3} + K_{g3}r_6^2 \qquad K_{6,7} = -K_{g3}r_6r_7$$

$$K_{7,6} = -K_{g3}r_6r_7 \qquad K_{7,7} = K_{g3}r_7^2 + 2K_{s4} \qquad K_{7,8} = -K_{s4} \quad K_{7,10} = -K_{s4}$$

$$K_{8,7} = -K_{s4} \qquad K_{8,8} = K_{s4} + K_{g4}r_8^2 \qquad K_{8,9} = -K_{g4}r_8r_9$$

$$K_{9,8} = -K_{g4}r_8r_9 \qquad K_{9,9} = K_{g4}r_9^2 + K_{s5} \qquad K_{9,13} = -K_{s5}$$

$$K_{10,7} = -K_{s4} \qquad K_{10,10} = K_{s4} + K_{g5}r_{10}^2 \qquad K_{10,11} = -K_{g5}r_{10}r_{11}$$

$$K_{11,10} = -K_{g5}r_{10}r_{11} \qquad K_{11,11} = K_{g5}r_{11}^2 + K_{s5} \qquad K_{11,12} = -K_{s5}$$

$$K_{12,11} = -K_{s5} \qquad K_{12,12} = K_{s5}$$

$$K_{13,9} = -K_{s5} \qquad K_{13,13} = K_{s5}$$

Since the mesh stiffness for the gears varies with the contact position, it is expected that the natural frequencies should vary with the contact position. Therefore, equation 3.32 should be solved for each contact position of the gears in mesh.

Equation 3.32 was solved for the eigenvalues and eigenvectors by the **householder** method and **QL Algorithm with Implicit Shifts** [69]. The Householder algorithm reduces an $n \times n$ symmetric matrix **A** to tridiagonal form by $n-2$ orthogonal transformations. Each transformation annihilates the required part of a whole column and whole corresponding row. Once the original, real, symmetric matrix has been reduced to tridiagonal form, the **QL Algorithm** obtains all the eigenvalues

and associated eigenvectors simultaneously and has been found to work well in practice [69].

Equation 3.32 can be reformulated into equation 3.34 through a series of steps.

$$J^{-1}K\theta = \lambda\theta. \tag{3.34}$$

Although the matrices J and K are both symmetric, the matrix $J^{-1}K$ is not symmetric which means that the right hand side of equation 3.34 cannot be solved directly by the Householder and QL algorithms. The matrix J is generally decomposed by employing **Cholesky Decomposition procedure** so that J is written as:

$$J = LL^T \tag{3.35}$$

in which L is the lower triangular matrix and L^T is the upper triangular transpose of J. A symmetric matrix can thus be obtained and expressed as:

$$[L^{-1}K(L^{-1})^T]\{L^T\theta\} = \lambda\{L^T\theta\}, \tag{3.36}$$

$$AY = \lambda Y. \tag{3.37}$$

where

$$\begin{aligned} A &= L^{-1}K(L^{-1})^T, \\ Y &= L^T\theta. \end{aligned} \tag{3.38}$$

With K being a symmetric matrix, A will also be symmetric, and thus equation 3.37 can be solved by the Householder and QL algorithms. The eigenvalues of equation 3.37 are identical to those of the equation in its original form (Equation 3.34). However, it should be apparent from the second expression of equation 3.38

that the eigenvectors θ of the original equation must be obtained from:

$$\theta = (L^T)^{-1}Y = (L^{-1})^T Y. \tag{3.39}$$

3.5 Dynamic Stress Analysis

Tooth bending failure at the root is a major concern in gear design. If the bending stress exceeds the fatigue strength, the gear tooth has a high probability of failure. In this study, a modified Heywood formula [47] for tooth root stress was used for the dynamic stress calculation at the root of a gear tooth. This formula has been found to correlate well with experimental data and finite element analysis results [47]. This formula is expressed as:

$$\sigma_j = \frac{W_j \cos\beta_j}{F}\Big[1 + 0.26\Big(\frac{h_f}{2R_f}\Big)^{0.7}\Big]\Big[\frac{6l_f}{h_f^2} + \sqrt{\frac{0.72}{h_f l_f}}\Big(1 - \frac{h_l}{h_f}\tan\beta_j\Big) - \frac{\tan\beta_j}{h_f}\Big]. \tag{3.40}$$

where, σ_j is the root bending stress, h_f is the tooth thickness at the critical section, R_f is the fillet radius, l_f is the length of the tooth from the projected point of contact on the neutral axis to the critical section and γ is the angle between the form circle and the critical section. The formula of equation 3.40 consists of five factors:

i. Stress concentration at the fillet, $\frac{W_j cos\beta_j}{F}\Big[0.26\Big(\frac{h_f}{2R_f}\Big)^{0.7}\Big]\Big[\frac{6l_f}{h_f^2} + \sqrt{\frac{0.72}{h_f l_f}}\Big(1 - \frac{h_l}{h_f}tan\beta_j\Big) - \frac{tan\beta_j}{h_f}\Big]$.

ii. Beam cantilever bending stress, $\frac{W_j \cos\beta_j}{F}\frac{6l_f}{h_f^2}$.

iii. Bending load proximity stress, $\frac{W_j \cos\beta_j}{F}\sqrt{\frac{0.72}{h_f l_f}}\frac{6l_f}{h_f^2}$.

iv. Axial load proximity stress, $\frac{W_j \cos\beta_j}{F}\sqrt{\frac{0.72}{h_f l_f}}\frac{h_l}{h_f}\tan\beta_j$

v. Axial stress, $\frac{W_j \cos\beta_j}{F}\frac{\tan\beta_j}{h_f}$

The formula has the proximity effects decreasing as the bending and axial load get further from the fillet and closer to the neutral axis. Figure 3.9 shows the tooth geometry for root stress calculation.

Lewis obtained the critical section of a gear tooth by inscribing a parabola within the tooth profile [70], where the point of contact of the parabola with the tooth root rounding determines the critical cross section. Other researchers, [18, 47] assumed an average value of $\gamma = 30^o$ to obtain the cross section for maximum root stress. However in this study, the tooth root stress was calculated at each point in the tooth root area and subsequently the location for the maximum root stress was obtained. Force application at the highest point of single tooth contact was found to yield the maximum root stress in most cases.

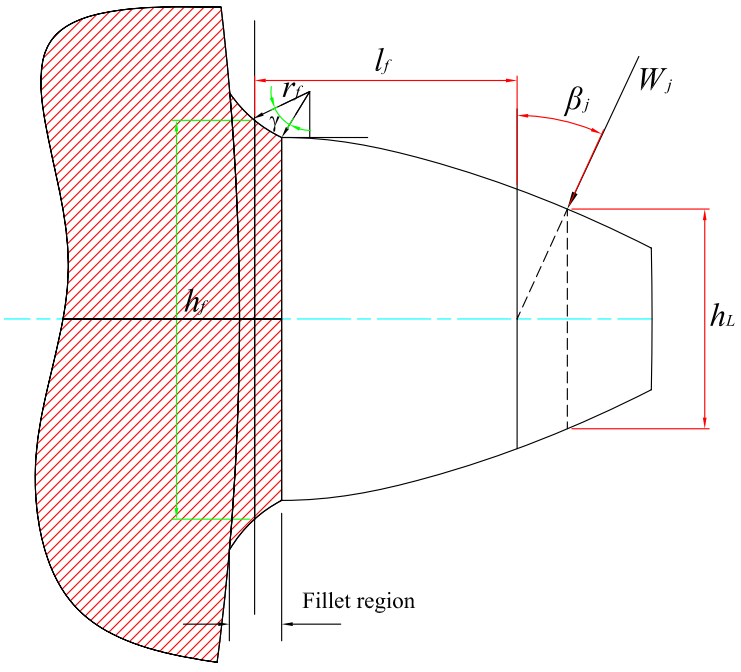

Figure 3.9: Tooth geometry nomenclature for root stress calculation

CHAPTER 4

MODEL DEVELOPMENT

4.1 Model Description

The model for the gear train system was developed based on a four stage tractor gearbox explained in appendix A. The essential elements of the gear train model (Figure 4.1) are shown in Figure 4.2. The model contains five pairs of gear meshes each with a periodic mesh stiffness and its damping constant, the moments of inertia of the gears, moments of inertia of the input and output masses and the torsional stiffness of the shafts. This yielded a thirteen (13) degree of freedom system which was modeled as a purely torsional vibratory system.

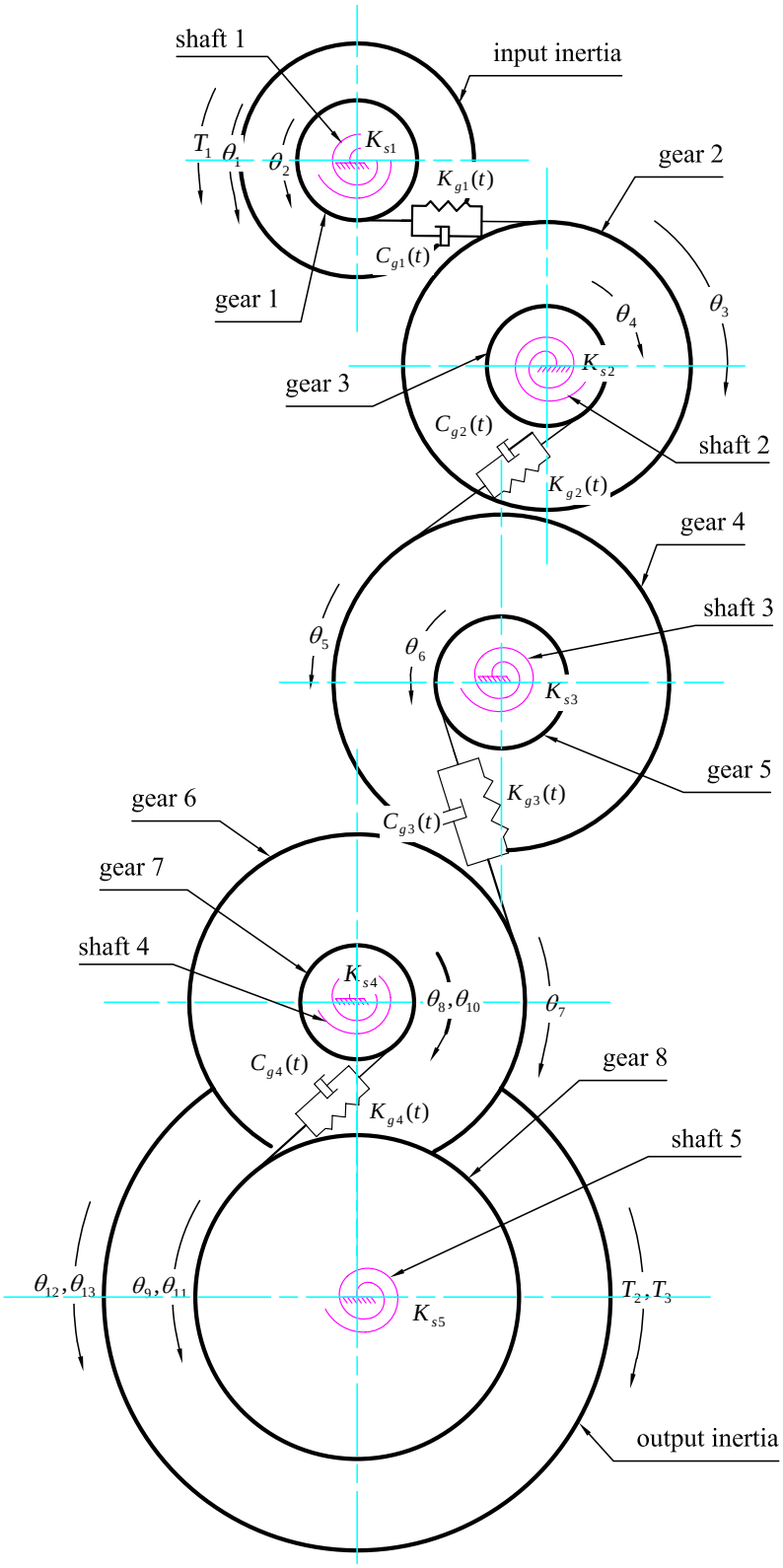

Figure 4.1: Gear train model

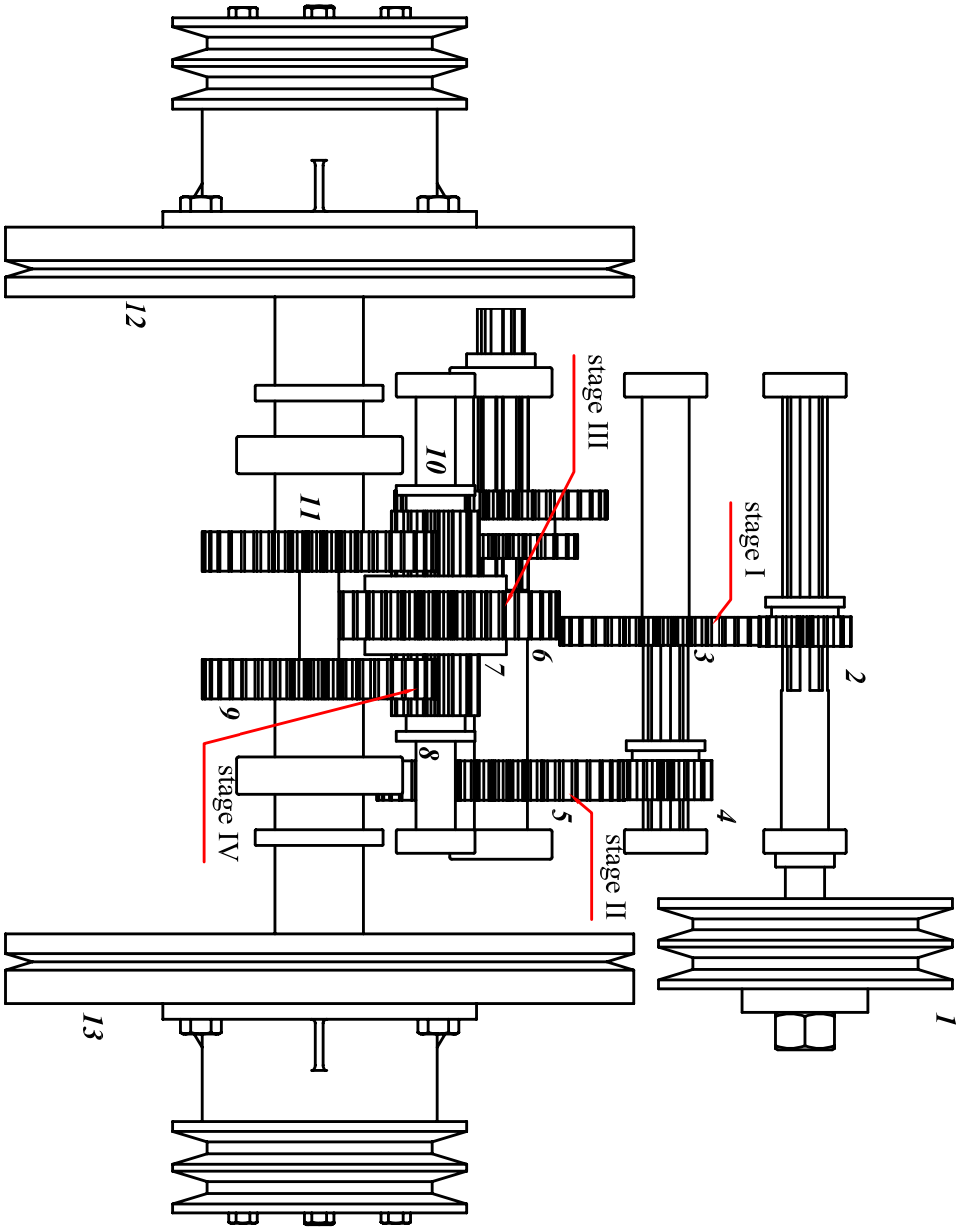

Figure 4.2: Gear train for bottom gear ratio

The major assumptions on which the dynamic model is based are as follows:

i. Gears are modeled as rigid disk with radius equal to the base circle radius and flexibility at the gear teeth.

ii. Bearings and the casing are assumed to be rigid (deflections of the bearings are much smaller than the deflections of the gear teeth and shafts and can be neglected.)

iii. Static transmission error effects are much smaller than the dynamic transmission error so they can be neglected [19].

iv. Gear teeth are assumed to be perfectly involute and manufacturing and assembly errors are ignored.

v. Backlash is not considered in this model. This is because while running at steady state, the gears are loaded in a single direction only and thus tooth separation is not considered.

A set of governing equations of motion for the model was derived using the standard Lagrangian equation, which is given here without proof [68]:

$$\frac{d}{dt}\left(\frac{\partial T}{\partial \dot{q}_i}\right) - \frac{\partial T}{\partial q_i} + \frac{\partial V}{\partial q_i} = Q_i, \tag{4.1}$$

Where,

q_i generalized coordinate.

T Total kinetic energy of the system.

V Change in potential energy of a system with respect to its potential energy

in the static equilibrium position.

Q_i generalized non-potential forces or moments resulting from excitation forces or moments that add energy into the system, and damping forces and moments that remove energy from it.

The kinetic energy of the system is given by:

$$T = \frac{1}{2}\Sigma J_i \dot{\theta}_i^2. \tag{4.2}$$

The generalized non-potential forces or moments (Q_i) result from excitation forces or moments that add energy into the system, and damping forces and moments that remove energy from it. The potential energy is classified into two groups of stored energy caused by:

1. Distortion of the gear meshes, for example the potential energy stored in gear mesh 1 is expressed as:

$$V_{m1} = \frac{1}{2}K_{g1}(t)[R_2\theta_2 - R_3\theta_3]^2, \tag{4.3}$$

2. Twisting of gear shafts, for example the potential energy stored in shaft 1 is expressed as:

$$V_{s1} = \frac{1}{2}K_{s1}[\theta_1 - \theta_2]^2. \tag{4.4}$$

The application of equation 4.1 to the gear train system yielded 13 equations of motion (4.5 - 4.17) given below:

$$J_1\ddot{\theta}_1 + C_{s1}(\dot{\theta}_1 - \dot{\theta}_2) + K_{s1}(\theta_1 - \theta_2) = T_1, \tag{4.5}$$

$$J_2\ddot{\theta_2} + C_{s1}(\theta_2 - \theta_1) + C_{g1}(t)R_2(R_2\dot{\theta_2} - R_3\dot{\theta_3}) +$$
$$K_{s1}(\theta_2 - \theta_1) + K_{g1}(t)R_2(R_2\theta_2 - R_3\theta_3) = -T_{f1}(t), \tag{4.6}$$

$$J_3\ddot{\theta_3} + C_{g1}(t)R_3(R_3\dot{\theta_2} - R_3\dot{\theta_3}) + C_{s2}(\theta_3 - \theta_4) +$$
$$K_{g1}(t)R_3(R_3\theta_3 - R_2\theta_2) + K_{s2}(\theta_3 - \theta_4) = -T_{f2}(t), \tag{4.7}$$

$$J_4\ddot{\theta_4} + C_{s2}(\theta_4 - \theta_3) + C_{g2}(t)R_4(R_4\dot{\theta_4} - R_5\dot{\theta_5}) +$$
$$K_{s2}(\theta_4 - \theta_3) + K_{g2}(t)R_4(R_4\theta_4 - R_5\theta_5) = -T_{f3}(t), \tag{4.8}$$

$$J_5\ddot{\theta_5} + C_{g2}(t)R_5(R_5\dot{\theta_5} - R_4\dot{\theta_4}) + C_{s3}(\theta_5 - \theta_6) +$$
$$K_{g2}(t)R_5(R_5\theta_5 - R_4\theta_4) + K_{s3}(\theta_5 - \theta_6) = -T_{f4}(t), \tag{4.9}$$

$$J_6\ddot{\theta_6} + C_{s3}(\theta_6 - \theta_5) + C_{g3}(t)R_6(R_6\dot{\theta_6} - R_7\dot{\theta_7}) +$$
$$K_{s3}(\theta_6 - \theta_5) + K_{g3}(t)R_6(R_6\theta_6 - R_7\theta_7) = -T_{f5}(t), \tag{4.10}$$

$$J_7\ddot{\theta_7} + C_{g3}(t)R_7(R_7\dot{\theta_7} - R_6\dot{\theta_6}) + C_{s4}(\dot{\theta_7} - \dot{\theta_8})$$
$$C_{s4}(\dot{\theta_7} - \dot{\theta_9}) + K_{g3}(t)R_7(R_7\theta_7 - R_6\theta_6) + K_{s4}$$
$$(\theta_7 - \theta_8) + K_{s4}(\theta_7 - \theta_9) = -T_{f6}(t), \tag{4.11}$$

$$J_8\ddot{\theta_8} + C_{s4}(\theta_8 - \theta_7) + C_{g4}(t)R_8(R_8\dot{\theta_8} - R_9\dot{\theta_9})$$
$$+K_{s4}(\theta_8 - \theta_7) + K_{g4}(t)R_8(R_8\theta_8 - R_9\theta_9) = -T_{f7}(t), \tag{4.12}$$

$$J_9\ddot{\theta_9} + C_{g4}(t)R_9(R_9\dot{\theta_9} - R_8\dot{\theta_8}) + C_{s5}(\theta_9 - \theta_{13}) +$$
$$K_{g4}(t)R_9(R_9\theta_9 - R_8\theta_8) + K_{s5}(\theta_9 - \theta_{13}) = -T_{f8}(t), \tag{4.13}$$

$$J_{10}\ddot{\theta_{10}} + C_{s4}(\theta_{10} - \theta_7) + C_{g5}(t)R_{10}(R_{10}\dot{\theta_{10}} - R_{11}\dot{\theta_{11}})$$
$$+K_{s4}(\theta_{10} - \theta_7) + K_{g5}(t)R_{10}(R_{10}\theta_{10} - R_{11}\theta_{11}) = -T_{f9}(t), \tag{4.14}$$

$$J_{11}\ddot{\theta_{11}} + C_{g5}(t)R_{11}(R_{11}\dot{\theta_{11}} - R_{10}\dot{\theta_{10}}) + C_{s5}(\theta_{11} - \theta_{12}) +$$
$$K_{g4}(t)R_{11}(R_{11}\theta_{11} - R_{10}\theta_{10}) + K_{s5}(\theta_{11} - \theta_{12}) = -T_{f10}(t), \tag{4.15}$$

$$J_{12}\ddot{\theta_{12}} + C_{s5}(\dot{\theta_{12}} - \dot{\theta_{11}}) + K_{s5}(\theta_{12} - \theta_{11}) = -T_2, \tag{4.16}$$

$$J_{13}\ddot{\theta_{13}} + C_{s4}(\dot{\theta_{13}} - \dot{\theta_9}) + K_{s4}(\theta_{13} - \theta_9) = -T_3. \tag{4.17}$$

As can be observed from equations 4.6 to 4.15, the non-linear interactions of the gear mesh couple the moment equations of each stage to each other. The gear mesh moments are evaluated as functions of relative motion and rotation between two

meshing meshing gears and the corresponding gear mesh stiffnesses and damping constants. The relative dynamic displacement and relative velocity of any pair of gears in mesh are the most important factors that influence the dynamics of the gear teeth and are given by equations 4.18 and 4.19.

$$\delta_i(t) = R_i\theta_i(t) - R_{i+1}\theta_{i+1}(t), \tag{4.18}$$

$$\dot{\delta}_i(t) = R_i\dot{\theta}_i(t) - R_{i+1}\dot{\theta}_{i+1}(t). \tag{4.19}$$

where, δ_i, $\dot{\delta}_i$, $(i = 1 - 5)$ represent the relative displacement and relative velocity of the gear teeth in mesh 1-5.

4.1.1 Damping Coefficients

The equations of motion contain damping terms for all components in the system. Damping results from viscous damping which occurs as a result of a system vibrating in a fluid. Most mechanical systems have damping which is quite complex but can be represented by viscous damping [71]. It is usually convenient to represent the damping coefficient in the differential equation as a factor of the critical damping as given by equation 4.20.

$$\zeta = \frac{C}{C_c}. \tag{4.20}$$

The damping factor can be determined experimentally for a system by obtaining a free vibration record of the system showing how its amplitude of vibration varies with time.

Since the mathematical description of the damping effect in gears is very complicated, a simplified damping model between two lumped masses was introduced in the study and the effective damping coefficients for the shafts and gears were given

by equations 4.21 and 4.22 respectively.

$$C_{gi}(t) = 2\zeta_g \sqrt{K_{gi}(t) \frac{J_i J_{i+1}}{J_{i+1} R_i^2 + J_i R_{i+1}^2}}, \tag{4.21}$$

$$C_{si} = 2\zeta_s \sqrt{K_{si} \frac{J_i J_{i+1}}{J_i + J_{i+1}}}. \tag{4.22}$$

The damping ratio for the shafts is mainly due to material damping which by experiment has been found to range between 0.05 and 0.07 [18]. In this study, a value of 0.05 was adopted. This value has been found to correlate very well with experimental results for shafts running in an oil bath [3, 4, 18]. On the other hand, the magnitude of the damping ratio for a gear mesh depends upon the lubrication film between the contacting teeth and values ranging between 0.1 and 0.2 were suggested by Kuang [4] by obtaining a correlation between analytical and experimental results. A value of 0.1 was adopted in this study as it was found to correlate very well with experimental results for gears running in an oil bath [3, 4, 18].

4.1.2 Gear Shaft Torsion

To calculate gear shaft torsion, equivalent torsional spring constants for the shafts were determined. The complex shaft shapes were approximated by using a series of sections having constant cross sections. The torsional spring constants for each section were calculated by:

$$K_s = \frac{JG}{L}. \tag{4.23}$$

where L is the section length, J is the polar moment of inertia, and G is the material's shear modulus. The equivalent torsional spring constants for the shafts were then determined by treating the shafts as a set of torsional springs in series.

4.2 Numerical Simulation

The time domain behavior of the system was studied by integrating the set of governing differential equations using **4$^{\text{th}}$ order Runge-Kutta** method. The differential equations were linearized by dividing the mesh period of the output pair into many small intervals. The mesh period for any pair of teeth in mesh was taken as the time interval from the initial point of contact to the highest point of single tooth pair contact.

To integrate initial value problems, one needs an appropriate set of initial conditions. In this study, all generalized coordinates were set to zero. Starting with these initial estimates of $\theta_i(0)$ and $\dot{\theta}_i(0)$ at the initial contact point, the values of $\theta_i(t)$ and $\dot{\theta}_i(t)$ were calculated for one mesh period of the output pair of gears.

The calculated value of the relative displacement $\delta_i(\tau_j)$ and relative velocity $\dot{\delta}_i(\tau_j)$ after the end of one period τ_j of each pair of gears j in mesh were compared with the initial values $\delta_i(0)$ and $\dot{\delta}_i(0)$. Unless the difference between them is sufficiently small as defined by the tolerance in equation 4.24, an iteration procedure was used to obtain the $(i+1)^{th}$ iteration values of $\theta_i(t)$ and $\dot{\theta}_i(t)$ by taking the i^{th} iteration values of $\theta_i(\tau_j)$ and $\dot{\theta}_i(\tau_j)$ as the new initial trial conditions. Once the solution has converged, this state corresponds to the steady state rotational speed of the shafts. Figure 4.3 shows a sample plot of the convergence of the relative displacement. For this particular case, the solution converges to an acceptable percentage difference (0.001%) after about 25 iterations.

$$tol_i = \frac{\delta_i(\tau_j) - \delta_i(0)}{\delta_i(\tau_j)}. \tag{4.24}$$

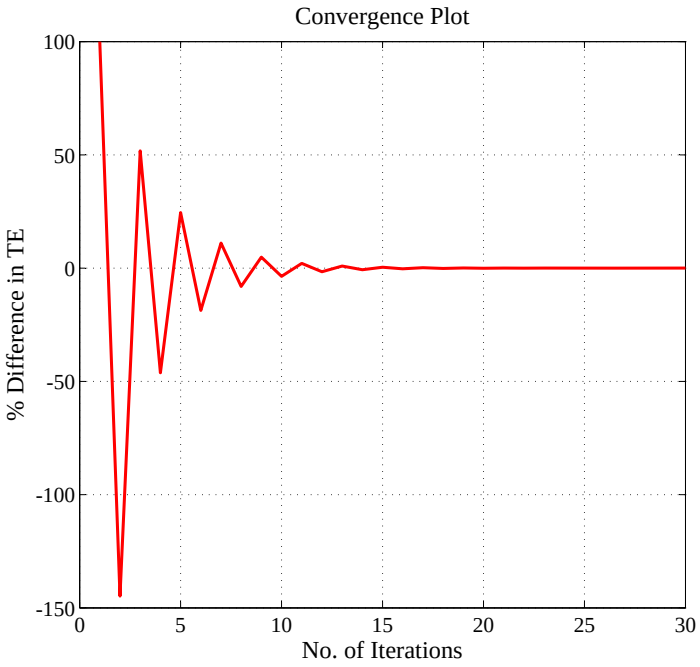

Figure 4.3: Sample plot of the convergence of relative displacement of a gear pair

The **optimum time step** was initially selected as the period for the path of contact of the gears in stage I divided by 100. The time step was then reduced and the model simulated for each time step until the point where further reduction in the time step did not yield any appreciable change in the response and the time step at this point was taken as the optimum time step.

The Runge-Kutta integration scheme requires values of $K_{gi}(t+\frac{h}{2})$, $K_{gi}(t+h)$, $C_{gi}(t+\frac{h}{2})$, $C_{gi}(t+h)$, $T_{fi}(t+\frac{h}{2})$, $T_{fi}(t+h)$. These values were obtained by employing cubic spline interpolation technique [69]. The procedure described above for the time domain studies yielded the response to both the time varying mesh stiffness and time varying frictional torque. Figure 4.4 is the flow chart showing the computational procedure.

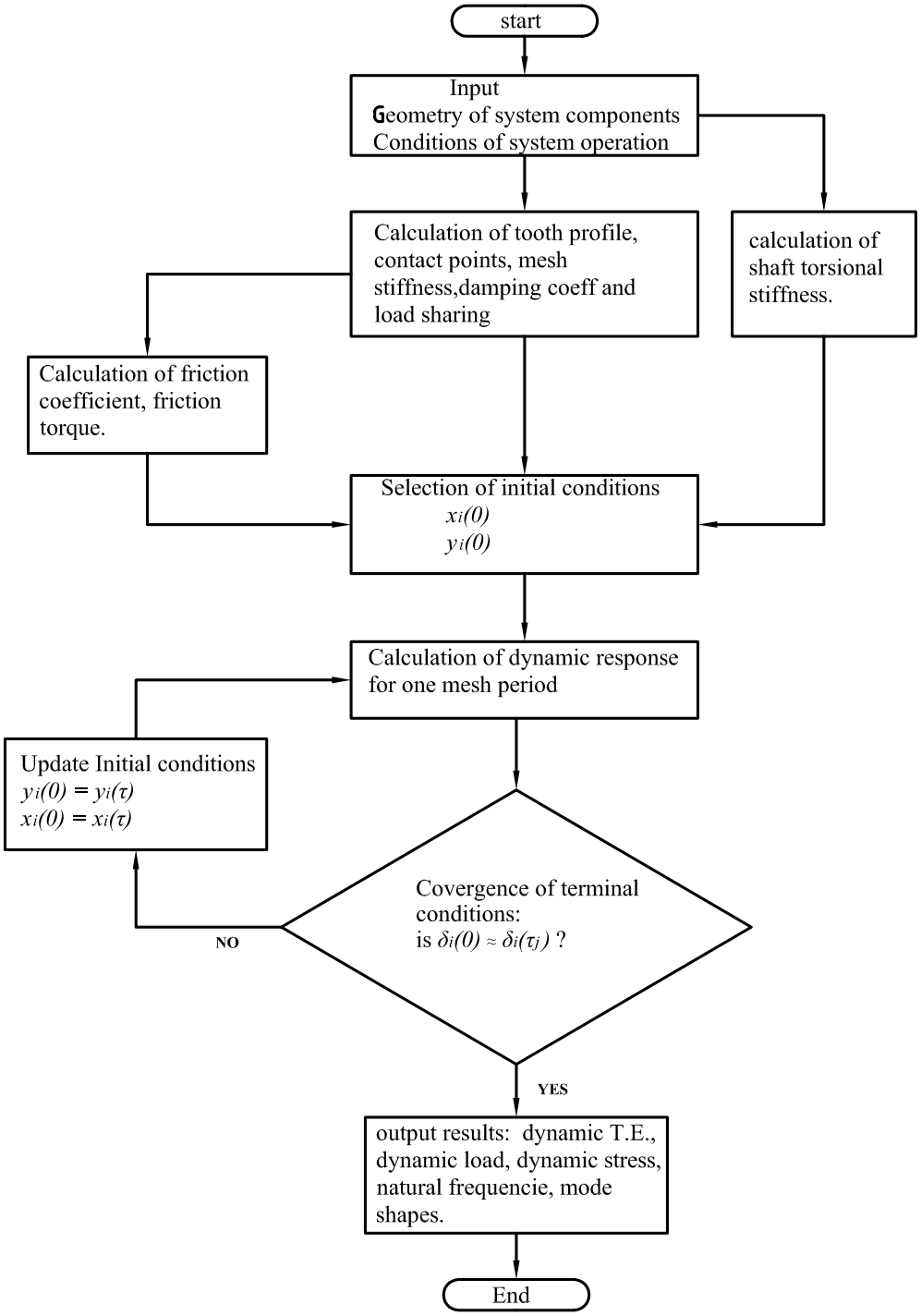

Figure 4.4: Flowchart for the computational procedure

CHAPTER 5

RESULTS AND DISCUSSIONS

5.1 Introduction

The main objective of the study was to develop a mathematical model to analyze the vibrations of a multistage tractor gearbox and to study the influence of gear design parameters on the relative levels of vibration of the gears. The results of the mesh stiffness, frictional torque, time domain vibration levels, frequency spectrum, dynamic load and dynamic stress are presented and discussed in the following sections.

5.2 Mesh Stiffness

Figure 5.1 shows a sample plot of the normalized mesh stiffness on the face width. A gear tooth enters contact at point A and between points A and B we have two pairs of teeth in contact. In this region, the stiffness of one tooth falls as the contact point moves towards the tip of the tooth while the stiffness of the mating tooth increases as the contact point moves towards the root circle. This accounts for the variation of the stiffness in this region. At point B, the stiffness falls drastically as the gear moves from double pair contact zone to single pair contact zone. Again, the stiffness varies along the single pair zone due to the movement of the contact point towards the root circle for one tooth and towards the tip for the other. At point C another pair of teeth enters contact and the cycle is repeated. Table 5.1 shows the gear parameters used in the computation of the stiffness. In order to apply the stiffness in the equations of motion, we need to be able to represent the stiffness as a function of time.

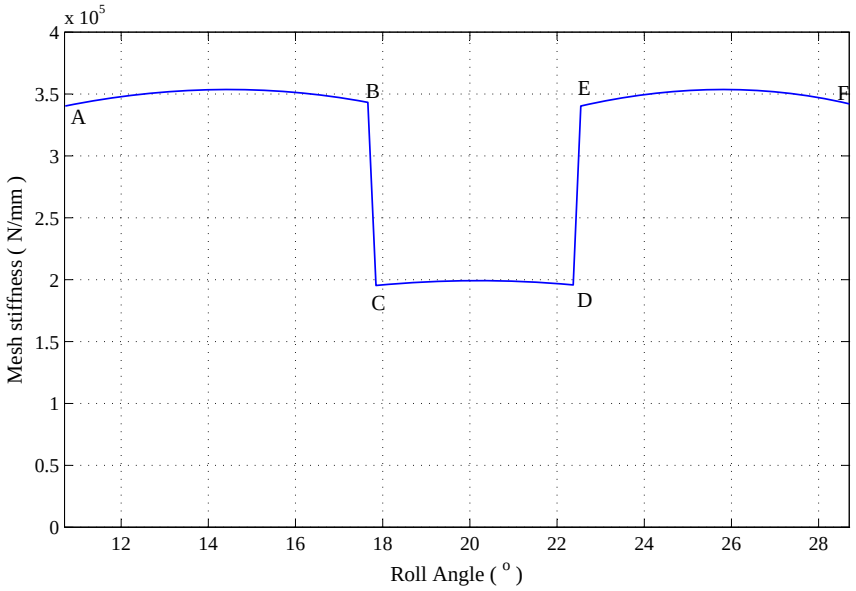

Figure 5.1: Gear mesh stiffness as a function of the contact position

Table 5.1: Gear set data and operating conditions for stiffness prediction

Parameter	Pinion	Gear
Module	*3.0* mm	*3.0* mm
No. of teeth	*28*	*20*
Clearance	*0.157* module	*0.157* module
Pressure angle	20^o	20^o
Input speed	*1500* rpm	
Power	*4847* W	

In practice, the stiffness will be a function of the angular rotation of the gear set and this will only be known as a function of time if the mean rotational speed can be assumed to be (or approximated as) constant [29].

Figure 5.2 is a plot of the periodic mesh stiffness for various face widths of the gear pair. τ_i is the mesh period which can be computed from equation 5.4.

$$\tau_i = \frac{60}{N_i \times Nt_i} \tag{5.1}$$

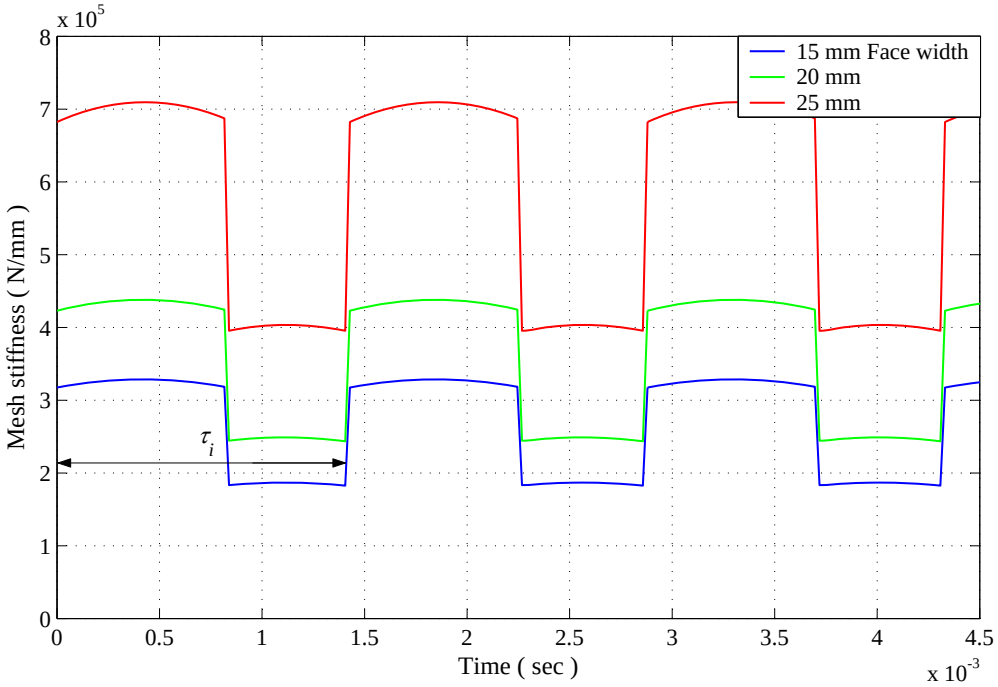

Figure 5.2: Periodic mesh stiffness for various face widths of the same gear set

The mesh stiffness increases significantly with the increase in the face width as seen in Figure 5.2. By increasing the face width by 67% (from 15 mm to 25 mm), the stiffness model developed in this study predicts that the mesh stiffness increases by 113%.

The discontinuities in the mesh stiffness as the number of pairs of teeth alternate between one and two can be eliminated by increasing the contact ratio of the gear set. Figure 5.3 shows the stiffness curves for various contact ratios. The contact ratio was increased by increasing the addendum of the gear teeth. Increasing the contact ratio reduces the bandwidth of the single contact zone and also the values of the stiffness. For a contact ratio of 2.0, the zone of single contact is eliminated and the only variation in the mesh stiffness is due to the change of the contact position.

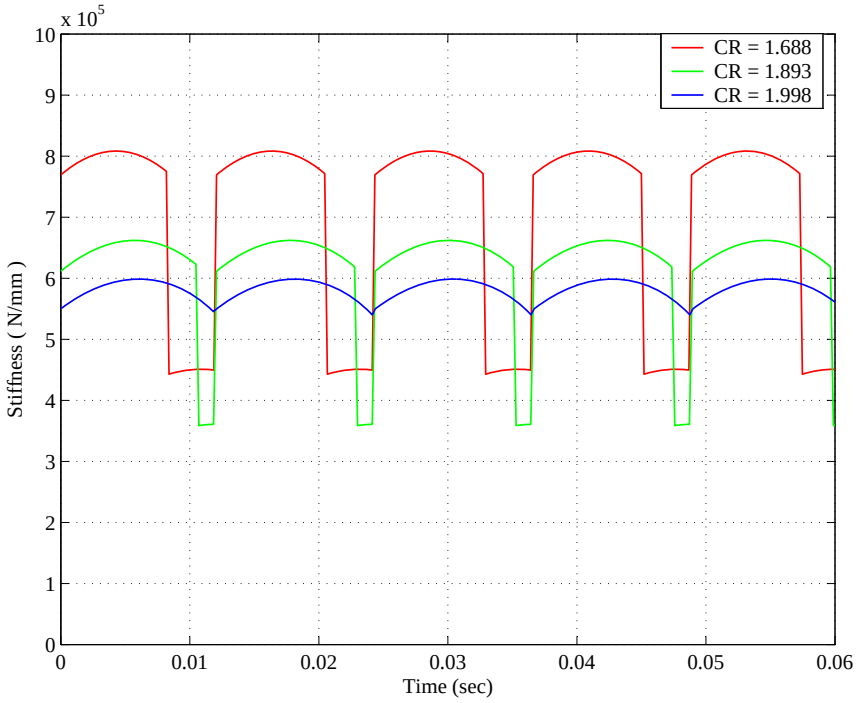

Figure 5.3: Periodic stiffness for different contact ratios

5.3 Frictional Torque

Figure 5.4 shows the variation of friction coefficient along the path of contact of a mating pair of gears. The analysis was carried out using the parameters and operating conditions given in Table 3.2. As seen from Figure 5.4, the friction coefficient approached zero as the contact point nears the pitch point. This is because the rate of sliding decreases towards the pitch point, becomes zero at the pitch point, changes the direction and increases as the contact point moves away from the pitch point. Points A and B are points of transition from double tooth pair contact to single tooth pair contact and from single tooth pair contact to double tooth pair contact respectively. For a pair of gears with equal number of teeth, the curve on the path of approach seems like a mirror of the curve of approach with the vertical

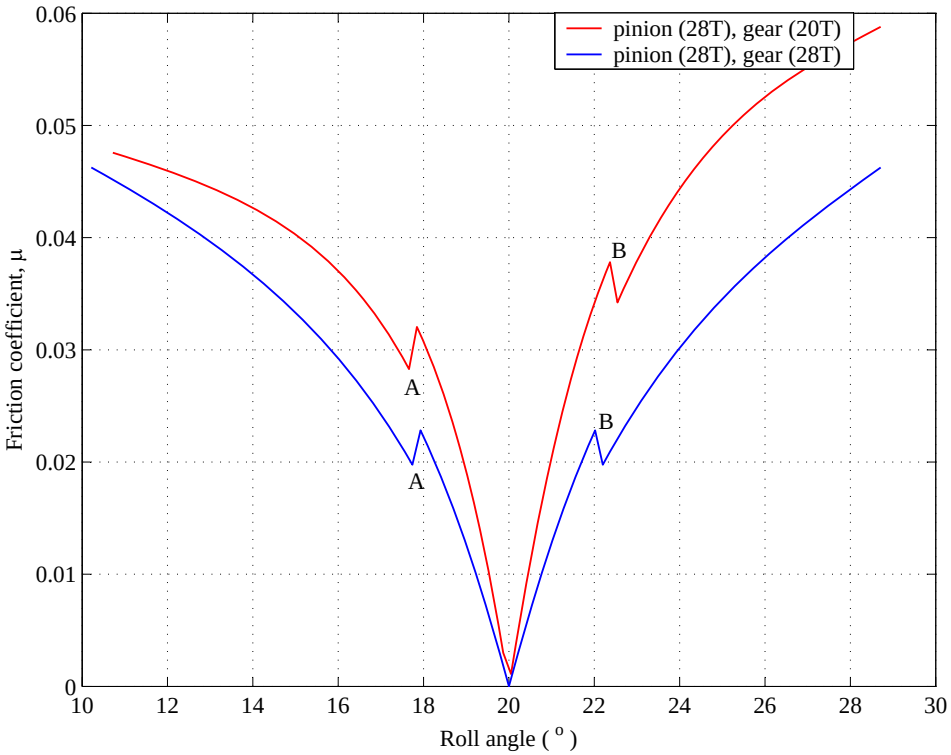

Figure 5.4: Instantaneous friction coefficient using EHL model

line through the pitch point as the mirror line as seen in Figure 5.4.

Figure 5.5 shows the frictional torque on a spur gear pair. The frictional torque depends upon the magnitude of the shared load, the instantaneous friction coefficient and the varying radius of curvature. At point A (Figure 5.5 (a)), the gear pair moves from double tooth pair contact into single tooth pair contact zone. The frictional torque decreases from point B, highest point of single tooth pair contact zone, up to zero at the pitch point, C, where it becomes zero. It then increases up to point D, lowest point of single tooth pair contact zone. This point is a transition point from single tooth pair contact to double tooth pair contact and the frictional torque

experiences an impulsive change. At point E, another pair of teeth enters into contact beginning another double tooth pair contact zone. In practice, the frictional torque will be a function of the angular rotation of the gear set and this will only be known as a function of time if the mean rotational speed of the gears can be assumed to be constant in which case the frictional torque will be periodic with a time period of τ which is taken as the time that elapses before a successive pair of teeth to enters into contact.

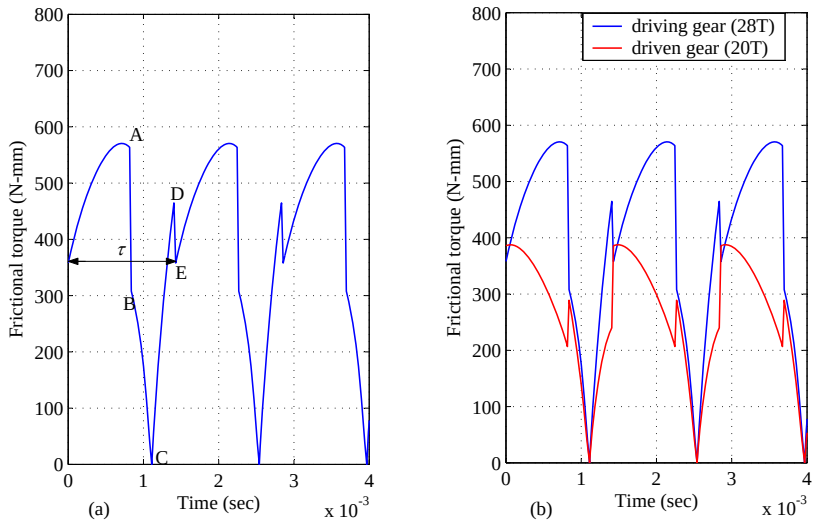

Figure 5.5: Periodic frictional torque (a) on the driving gear, (b) on both gears

The frictional torque changes abruptly at the transition points from single tooth pair to single tooth pair and vice versa. This sudden change in the frictional torque acts as a source of excitation for a gear pair and will be included in the dynamic model of the spur gear train. Figure 5.5 (b) shows the frictional torque on both the pinion and the gear. The shape of the curve for the gear torque is a scaled mirror of the pinion torque. The parameters and operating conditions used in the simulation are those in Table 3.2. Figure 5.6 shows the frictional torque curves for gears with

different contact ratios. It can be observed that the plot for a contact ratio close to 2.0 is quite different from that of a contact ration less than 2.0. The zone of single contact is not visible for a contact ratio close to 2.0 and the torque changes impulsively only when a pair of teeth approaches end of contact and a new pair of teeth enters into contact.

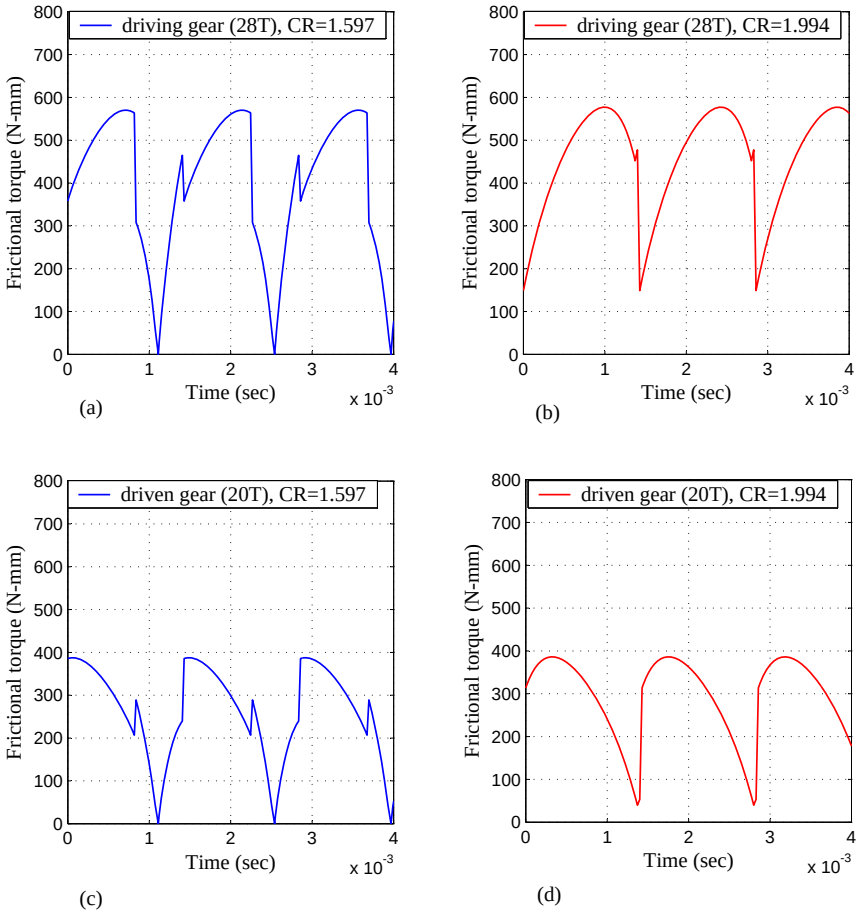

Figure 5.6: Frictional torque for different contact ratios

5.4 Code Validation

Computer codes in gear applications are usually developed to allow designers to investigate the effect of various design parameters and optimum gear configurations

on vibrations and gear dynamics which would either be difficult to analyze experimentally or that would require very expensive tests. Though the computer codes provide a cheaper alternatives to analyze the gear dynamics, their validity must be tested for the designer to be sure that the results obtained are within acceptable limits. Usually, a code is validated by comparing the results obtained from the code with those obtained from a simple experimental set up. In this study, the results obtained from the code developed were compared with results obtained from tests performed on the NASA gear noise rig [34].

The rig features a single mesh gearbox powered by a 150 KW variable speed electric motor. An eddy current dynamometer loads the output shaft. The gearbox can operate at speeds up to 6000 rpm. The rig was built to carry out fundamental studies of gear noise and the dynamic behavior of gear systems [34]. Table 5.2 shows the test rig parameters.

To compare the experimental and numerical results, the measured dynamic loads from Oswald et al [34] were placed next to dynamic load plots predicted by the model developed in this study. Figures 5.7 to 5.10 show the measured and predicted dynamic loads for four speeds with five different torque levels on each plot (20 operating conditions). The numerical and measured values match each other rather well both in the general pattern and magnitude especially at 2000 and 4000 rpm, where the percentage error between the measured and predicted peak load was found to be between 0.07% and 1.2%. There are some differences in the waveforms at 800 and 6000 rpm which could have arisen from external factors not considered in the model. Example of such factors are:

- Load fluctuations from the motor and / belt drive.

Table 5.2: Test rig parameters

Gear tooth type	Standard, full depth
No. of Teeth	28 and 28
module	3.175 mm
Face width	6.35 mm
Pressure angle	20^o
Tooth root radius	1.35 mm
Mesh damping coeff.	10% of critical
Gear inertia	301.55 $Kg\text{-}mm^2$
Motor inertia	1100 $Kg\text{-}mm^2$
Load inertia	1400 $Kg\text{-}mm^2$
Input stiffness	17×10^6 $N\text{-}m/rad$
Output stiffness	17×10^6 $N\text{-}m/rad$

- Coupling between lateral and torsional vibrations.
- Low frequency vibration modes of the long shafts connecting the motor and dynamometer to the gearbox [34]

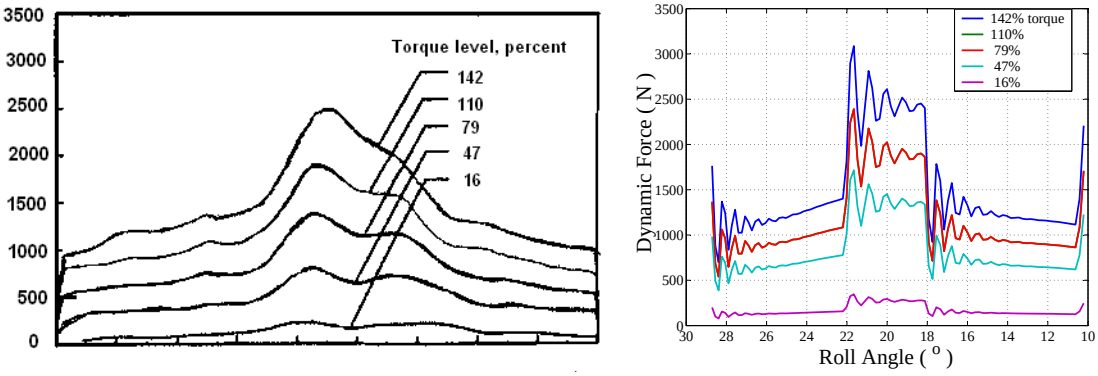

(a) Measured dynamic loads (b) Predicted dynamic loads

Figure 5.7: Dynamic loads at different torques levels for 800 rpm

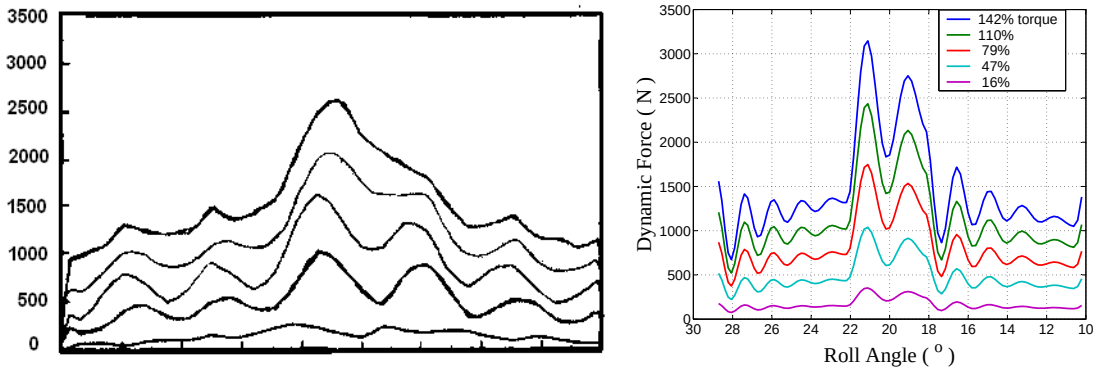

(a) Measured dynamic loads (b) Predicted dynamic loads

Figure 5.8: Dynamic loads at different torques levels for 2000 rpm

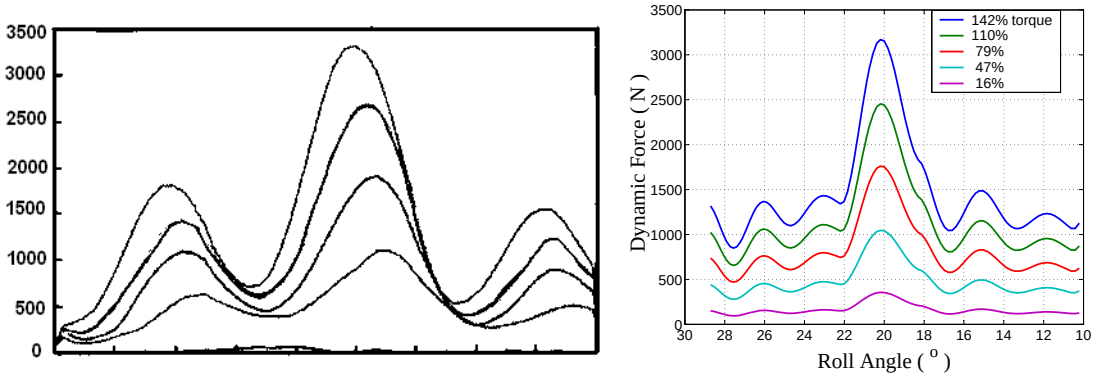

(a) Measured dynamic loads (b) Predicted dynamic loads

Figure 5.9: Dynamic loads at different torques levels for 4000 rpm

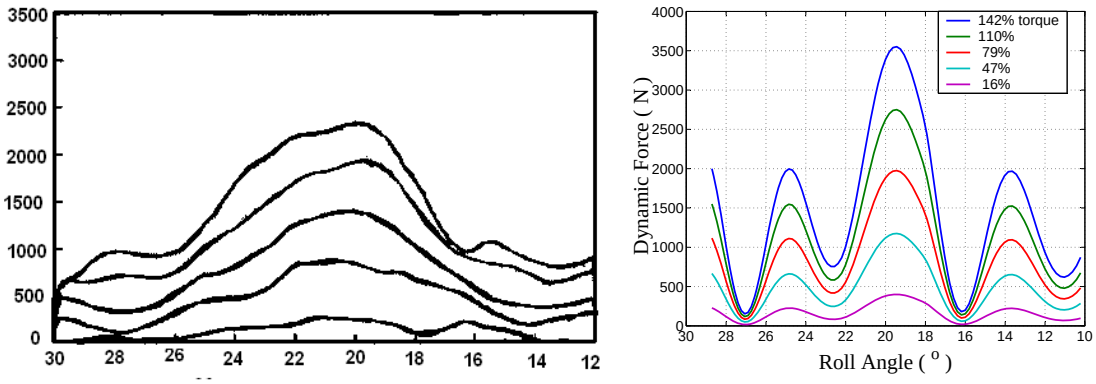

(a) Measured dynamic loads (b) Predicted dynamic loads

Figure 5.10: Dynamic loads at different torques levels for 6000 rpm

Correlation between the dynamic loads predicted by the model developed in this study and the experimental results from Oswald et al [34], the peak dynamic loads predicted by the model were plotted against the experimental results for all the 20 conditions as shown in Figure 5.11. The diagonal line shows the line of best fit where the numerical and experimental values agree. The results show that apart from the four conditions (142%, 110% and 79% nominal torque at 6000 rpm and 142% at 800 rpm), the numerical peak load agrees well with measured peak loads within an average error of 5.5%

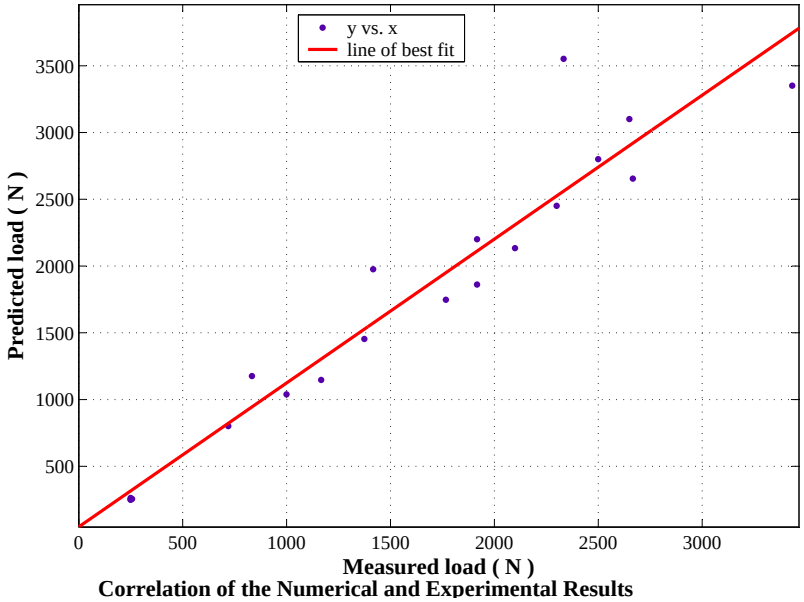

Figure 5.11: Comparison of the peak loads predicted by the model with experimental data

5.5 Multistage Gear Train Results

Two gear train configurations are presented in this study:

1. Bottom Gear Ratio; in this case, the gear train that produces the highest reduction ratio is analyzed. This ratio produces the the maximum torque with low speed at the wheel axles. This configuration is normally used when moving the tractor from rest, ploughing land and moving up a steep hill whilst loaded. The nominal output torque used in the design of the gears is 1300 Nm, i.e, 650 Nm at each axle.

2. Top Gear Ratio; in this case, the gear train that produces the highest speed at the axles is analyzed. The design torque used in this case is 130 Nm, i.e, 65 Nm at each axle.

5.5.1 Bottom Gear Ratio Configuration

The gear train for this configuration is shown in Figure 4.2. Table 5.3 shows the rotor properties for this system while Table 5.4 shows the operating conditions and gear parameters. In this thesis, this gear train will be referred to as **gear train 1**. The pinions in this gear train have a number of teeth less than the minimum required to avoid undercut and therefore the addendum has been modified to avoid undercut. Short and long addendum with standard center distance have been used.

Table 5.3: Rotor properties for gear train 1

Rotor No.	Description	No. of teeth for gears	Addendum modification factor	Face width (mm)	Moment of inertia (Kg mm^2)	Theoretical contact ratio
1	Input pulley assembly	-	-	-	10697.8	-
2	Stage I pinion	14	1.2987 m	15	51.2	1.516
3	Stage I gear	34	0.7013 m	15	1249.5	
4	Stage II pinion	14	1.3106 m	20	63.9	1.523
5	Stage II gear	40	0.6894 m	20	3191.1	
6	Stage III pinion	15	1.2385 m	25	96.3	1.552
7	Stage III gear	40	0.7615 m	25	4892.7	
8	Stage IV pinion	14	1.3106 m	50	140.2	1.523
9	Stage IV gear	40	0.6894 m	30	4786.7	
10	Stage IV pinion	14	1.3106 m	50	140.2	1.523
11	Stage IV gear	40	0.6894 m	30	4786.7	
12	Output inertia	-	-	-	291179.0	-
13	Output inertia	-	-	-	291179.0	-

Table 5.4: Operating conditions and gear parameters for gear train 1

Input speed	1500 rpm
Nominal Torque	1300 Nm
module (m)	3 mm
Pressure angle	20^o
ζ_g	0.1
ζ_s	0.05

The relative dynamic displacement of gear i and $i+1$ represents the deflection of the gear teeth from their mean position. If gear i is the driving gear, the following situations will occur [18]:

i. $\delta_i > 0$ This represents the normal operation case and the dynamic mesh force is given by:

$$W_{di} = K_{gi}(t)\delta_i + C_{gi}\dot{\delta}_i, \tag{5.2}$$

ii. $\delta_i \leq 0$ and $|\delta_i| \leq bh$,

where bh is the backlash between the gears.

In this case, gears will separate and contact between the gear teeth will be lost.

$$W_{di} = 0,$$

iii. $\delta_i < 0$ and $bh < |\delta_i|$

In this case, gear $i+1$ will collide with gear i on the back side, and the mesh force will be given by:

$$W_{di} = K_{gi}(t)(\delta_i - bh) + C_{gi}\dot{\delta}_i. \tag{5.3}$$

where, W_{di} is the dynamic load and bh is the backlash. In this study, one of the assumptions in the development of the model was that there was no backlash, therefore only the first case will be analyzed. Figures 5.12 to 5.15 show the dynamic transmission error in the time domain and frequency domain for the various gear meshes. The frequency analysis of the dynamic transmission error (DTE) was performed by taking the Fast Fourier Transform (FFT) of its time wave. The FFT process transforms time domain data to the frequency domain creating a spectrum. Signals that

are periodic in the domain appear as peaks in the frequency domain. The amplitude of each peak is proportional to the vibration created by the source. While the time domain analysis examines the level or shape of the vibration signal as a function of time, frequency domain examines the harmonic content (repeating) elements of a signal as a function of frequency.

In all the time plots, Figures 5.12(a), 5.13(a), 5.14(a) and 5.15(a), the tooth cycle is clearly visible with the two distinct regions corresponding to single and double tooth contact. The response is periodic with a period equal to the mesh period τ (shown explicitly in Figure 5.12(a)) as the fundamental meshing period, given by equation 5.4. Larger displacements are seen to occur at the single tooth contact zone due to the lower mesh stiffness in this region.

$$\tau = \frac{60}{N_p T_P}. \tag{5.4}$$

The effect of reversal of the frictional torque at the pitch point can be seen in Figure 5.12(a), point P. The effect of friction is visible on stages I and II where the rotational speeds are higher. However, at very low speeds, the effect of frictional torque are minimal.

Referring to Figures 5.12(b), 5.13(b), 5.14(b) and 5.15(b), it can be seen that the dynamic response corresponds proportionately to the tooth mesh frequency which is the product of the shaft speed and the the number of teeth on the gear. For a perfect tooth, the peak amplitude of the DTE is found at the mesh frequency. The amplitudes of higher harmonics are relatively small and their contribution can be neglected. Table 5.5 shows the tooth mesh frequencies for the various meshes in the gear train. Both time and frequency spectra indicate that parametric excitations have significant effect on the system response.

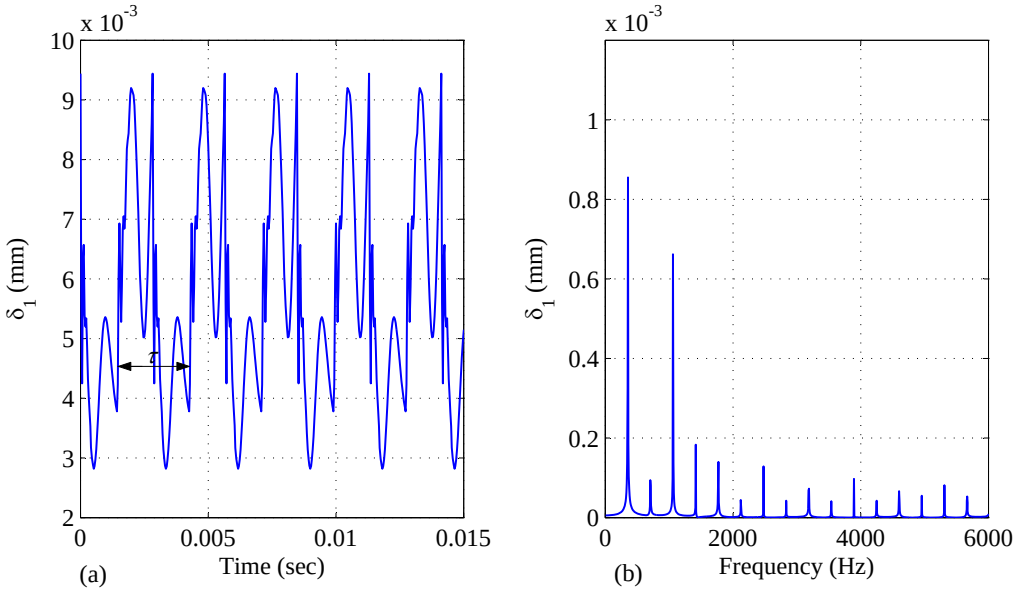

Figure 5.12: Vibration signatures for gears in stage I (gear train 1)

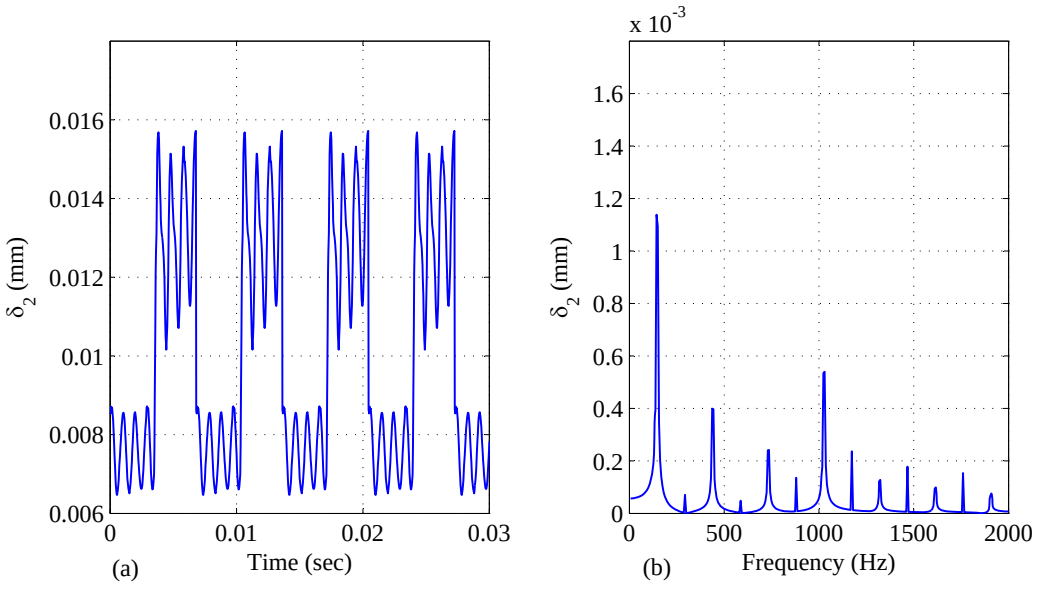

Figure 5.13: Vibration signatures for gears in stage II (gear train 1)

The dynamic relationship between all the gear stages are coupled through the nonlinear interactions in the gear mesh. The gear mesh forces and moments were eval-

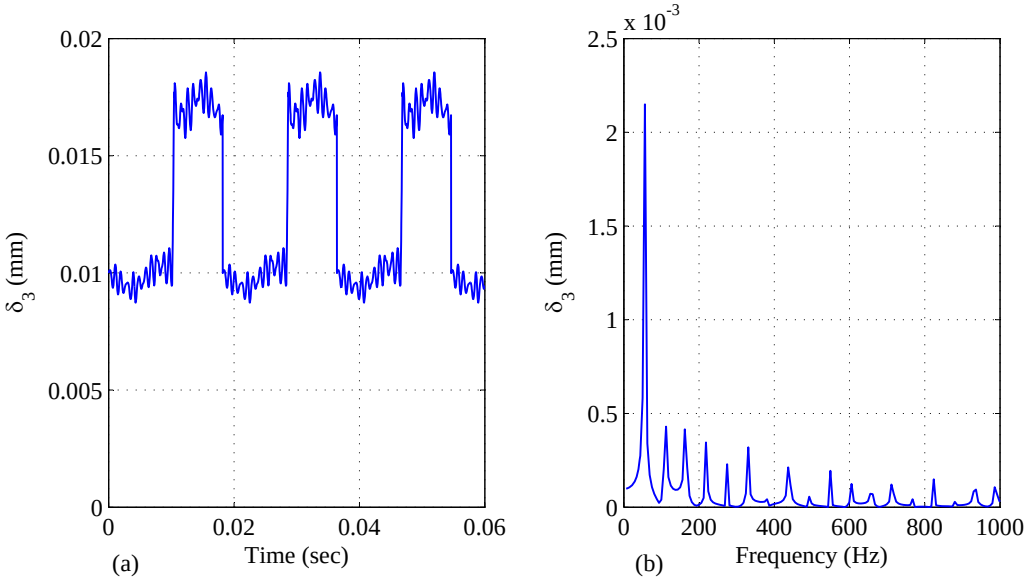

Figure 5.14: Vibration signatures for gears in stage III (gear train 1)

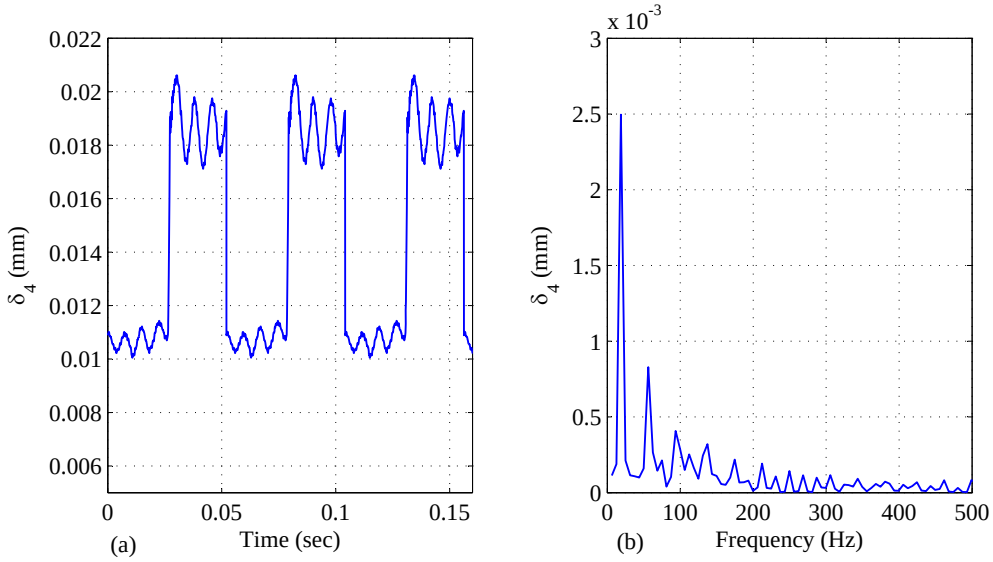

Figure 5.15: Vibration signatures for gears in stage IV (gear train 1)

uated as functions of relative motion and rotation between two meshing gears and the corresponding mesh stiffness as shown in equation 5.2.

Table 5.5: Mesh frequencies for gear train 1

mesh	mesh frequency (HZ)
I	350.0
II	144.1
III	54.0
Iv	18.9

Figure 5.16 shows the static load and the dynamic load response for a single tooth in mesh for all the reduction stages. The dynamic load is basically a static load sharing in phase with the stiffness change due to the change in the number of teeth in contact superimposed by an oscillating load.

The peak tooth force under dynamic conditions is much higher than the static load especially in the single pair contact region as can be seen in Figure 5.16. Thus if the gear teeth are designed using the static load, there are high possibilities of tooth failure due to the resulting high bending and contact stresses. The dynamic load is also influenced by the pitch-line velocity as shown on Table 5.6. The percentage difference between the peak dynamic load and static load decreases as the pitch line velocity reduces.

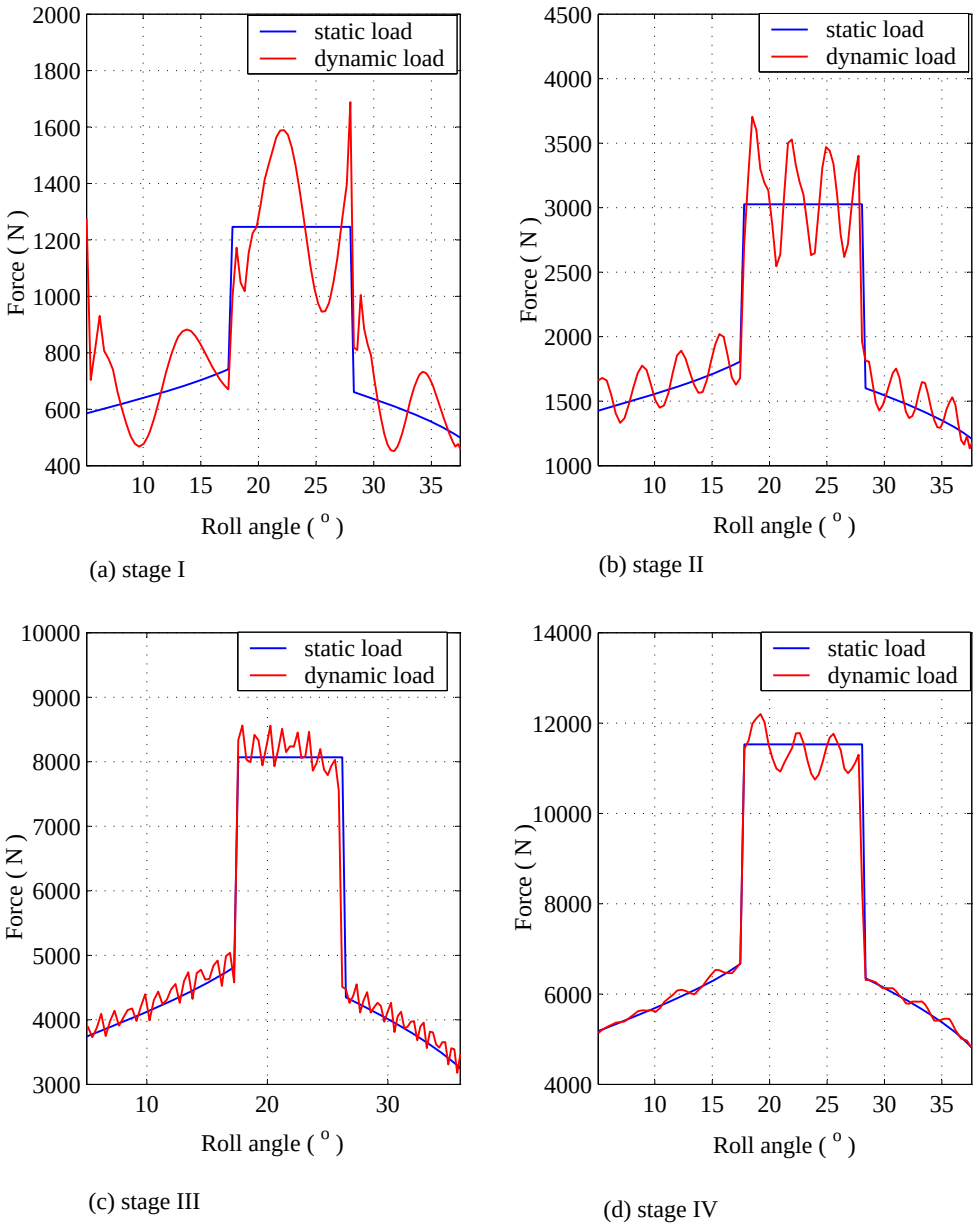

Figure 5.16: Comparison of the dynamic and static load on a single tooth over the path of contact (gear train 1)

Table 5.6: Percentage difference between peak dynamic load and maximum static load for gear train 1

Gear mesh	velocity (m/s) (m/s)	static load (N)	Peak dynamic load (N)	% difference
I	3.299	1246.11	1610.58	29.25
II	1.358	3026.26	3727.95	23.19
III	0.509	8070.02	8586.22	6.02
IV	0.178	11528.59	12120.45	5.13

Figures 5.17 to 5.20 compare the static and dynamic stress on a single tooth of all the gears in mesh. The pattern of the stress curves is similar to that of the dynamic load pattern in that the dynamic stress is basically the static stress in phase with the stiffness change superimposed by an oscillating stress. The figures show that both the dynamic and static stress reach maximum in the single pair contact zone. The only difference is that the root stress is determined not only by the magnitude of the load (and hence the speed) but also by the position of the load along the tooth profile as seen in Figures 5.17 to 5.20. For the driving gear, the point of contact moves from the lowest point of contact along the tooth profile to the highest point of contact and thus the cantilever beam length of the gear tooth increases along the path of contact. This explains why both the static and dynamic stresses increase with time for the driving gear. The converse is true for the driven gear.

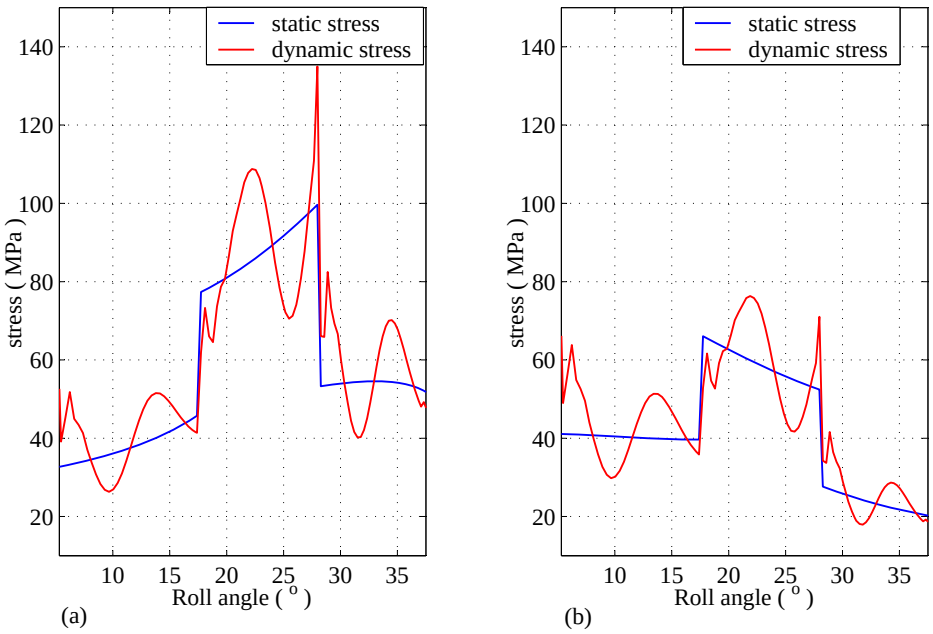

Figure 5.17: Tooth bending stress as a function of the contact position for gears in stage I (gear train 1), (a) pinion, (b) gear

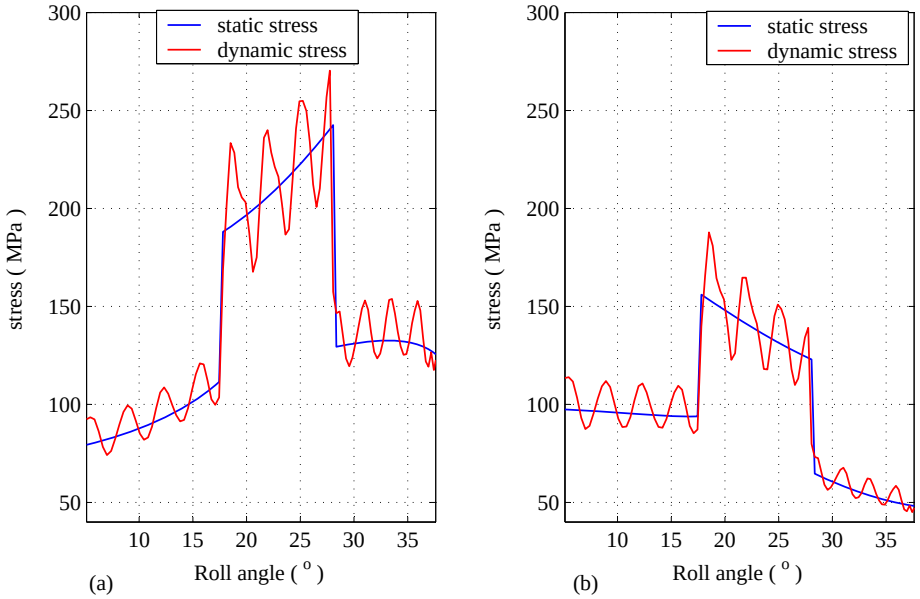

Figure 5.18: Tooth bending stress as a function of the contact position for gears in stage II (gear train 1), (a) pinion, (b) gear

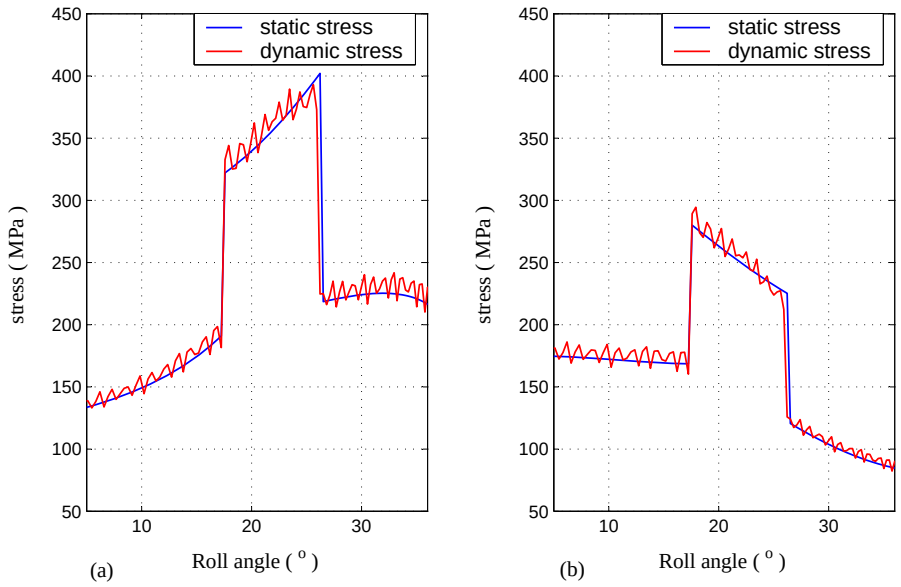

Figure 5.19: Tooth bending stress as a function of the contact position for gears in stage III (gear train 1), (a) pinion, (b) gear

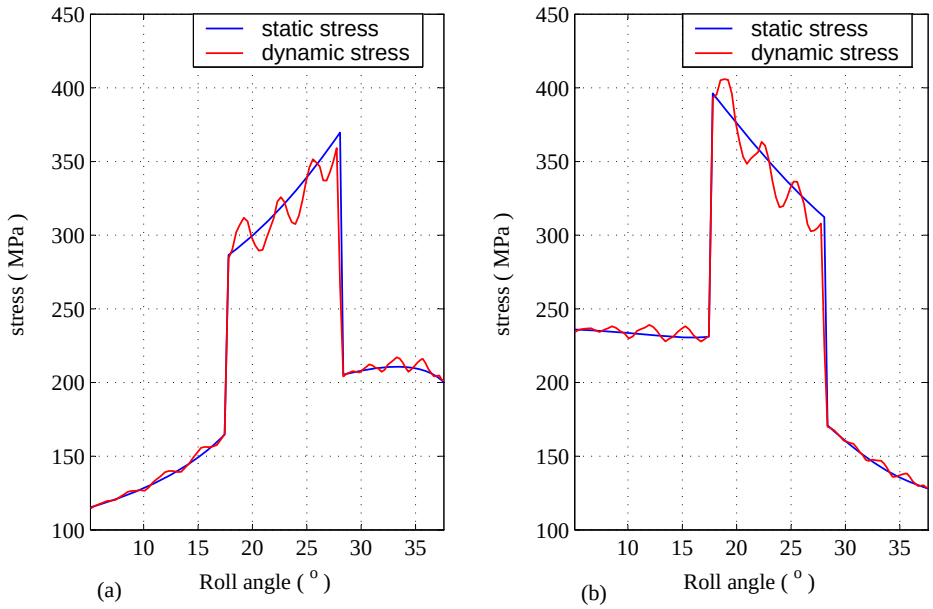

Figure 5.20: Tooth bending stress as a function of the contact position for gears in stage IV (gear train 1), (a) pinion, (b) gear

The peak dynamic stress during single pair contact is much higher than the static stress which makes the dynamic analysis an important design tool for the gears. To avoid tooth failure, the bending stress should be limited to the allowable bending strength of the material suggested by AGMA [72]. AGMA bending strength equation is given by:

$$\sigma_{all} = \frac{S_t K_L}{K_T K_R K_V}. \tag{5.5}$$

where,

σ_{all}	allowable bending stress
K_L	life factor
S_t	AGMA bending strength
K_T	temperature factor
K_R	reliability factor
K_V	dynamic factor

The dynamic factor is used to account for inaccuracies in the manufacture and meshing of gear teeth in action. AGMA has defined a set of quality control numbers to define the tolerances of gears of various sizes manufactured to a specified class. More details on these classes can be found in reference [72]. The following equations for the dynamic factor are based on these quality control numbers.

$$K_V = \Big[\frac{A}{A + \sqrt{200V}}\Big]. \tag{5.6}$$

where

A	$= 50 + 56(1 - B)$
B	$= \frac{(12-Q_v)^{\frac{2}{3}}}{4}$

Q_v = quality control number

V = pitch-line velocity (m/s)

The allowable stress depends on the nature of heat treatment and surface hardness of the material. Typical values used in this study are given in Table 5.7 [72]. In this study, a typical value of $450MPa$ was used for the allowable stress for a case hardened low carbon steel alloy [73]. Based on a life cycle of 10^7, the life factor can

Table 5.7: Values of allowable stress

Material	Heat Treatment	Hardness	$S_t\ MPa$
Steel	induction hardened	50-54 HRC	310-380
	carburised	55 HRC	380-450
	case hardened	60 HRC	380-480

be taken as $K_L = 1.0$ with a corresponding reliability of 0.99 whose reliability factor is 1.0. For oil or gear blank temperatures of up to 120^oC, the temperature factor is taken as 1.0. The allowable bending stress recommended by AGMA depends on the magnitude of the pitch line velocity and from Table 5.8, it can be seen that the allowable bending stress increases as the pitch line velocity increases.

The face width of the current gearbox design was obtained based on the modified Lewis equation given by:

$$\sigma_L = \frac{W_t}{K_v F p_c y}, \tag{5.7}$$

where

$$K_v = \frac{6.1}{6.1 + V}. \tag{5.8}$$

Thus to analyze the possibility of gear tooth failure at the root, the values obtained

Table 5.8: Allowable root bending stress based on AGMA equation

Reduction stage	Gear	V (m/s)	K_v	*AGMA* σ_{all} *(MPa)*
I	14 T	3.29867	0.78409	573.91
	34 T			
II	14 T	1.35828	0.84784	530.76
	40 T			
III	15 T	0.50935	0.89995	500.03
	40 T			
IV	14 T	0.17827	0.93783	479.83
	40 T			

from the Lewis equation and the peak values obtained from the dynamic analysis need to be compared with AGMA allowable stress. Table 5.9 shows the factors

Table 5.9: Factors used to compute the bending stress using Lewis equation

Reduction stage	Gear	*V (m/s)*	K_v	*y*	W_t *(N)*	σ_L *(MPa)*
I	14 T	3.29867	0.64903	0.149	1469.414	107.481
	34 T			0.227		70.549
II	14 T	1.35828	0.81788	0.149	3568.577	155.352
	40 T			0.233		99.345
III	15 T	0.50935	0.92293	0.156	9516.204	233.765
	40 T			0.233		156.511
IV	14 T	0.17827	0.97160	0.149	13594.578	199.274
	40 T			0.233		212.388

used to compute the bending stress based on the Lewis equation, while Table 5.10 shows a comparison of the dynamic stress obtained from this study with the bending stress obtained using the Lewis equation and the allowable stress recommended by AGMA. The Lewis equation predicts low values of the bending stress than that obtained from the dynamic analysis of the gear train as show on Table 5.10. This implies that dynamic analysis of a geared system is necessary in the design stage in order to analyze possibility of gear tooth failure and to predict the fatigue life of

Table 5.10: Comparison of the dynamic stress, Lewis stress and AGMA allowable stress

Reduction stage	Gear	σ_j *(MPa)*	σ_L *(Mpa)*	*AGMA* σ_{all} *(MPa)*
I	14 T	119.61	107.48	573.91
	34 T	93.95	70.55	
II	14 T	274.62	155.35	530.76
	40 T	188.98	99.35	
III	15 T	388.34	233.77	500.03
	40 T	294.28	156.51	
IV	14 T	359.39	199.27	479.83
	40 T	409.61	212.39	

a gear. The gear pairs in all the stages have a peak dynamic stress less than the recommended AGMA bending stress for 10^7 cycles.

Figure 5.21 shows the variation of the natural frequencies with the contact position of the first gear mesh for the first three modes. Table 5.11 shows the natural frequencies range corresponding the the system configuration shown in Figure 4.2 while the corresponding mode shapes are shown in Figures 5.22 to 5.24.

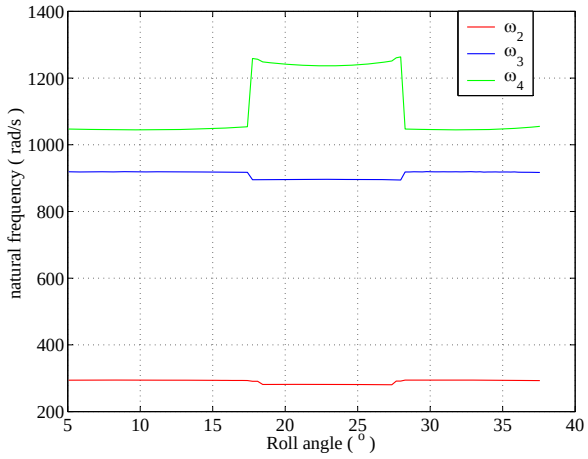

Figure 5.21: Variation of natural frequency with the contact position of the gears

Table 5.11: System Natural Frequencies corresponding to gear train 1

Natural frequency	Predicted value (rad/s)
ω_1	0
ω_2	252 – 264
ω_3	894 – 920
ω_4	1044 – 1264
ω_5	7174 – 7580
ω_6	11722 – 12540
ω_7	16000 – 17180
ω_8	21647 – 27620
ω_9	43812 – 57240
ω_{10}	47743 – 60323
ω_{11}	61935 – 79593
ω_{12}	73167 – 83534
ω_{13}	131292 - 169520

The mode shapes show the relative rotational displacements between the rotors when the system is responding purely to the corresponding natural frequency. Figure 4.2 is a free-free (unconstrained) system and is also referred to as a *semi definite system*. One of the natural frequencies of such a system will be zero, corresponding to the zero root of the eigenfrequency equation when the body moves as a rigid body. The rigid body motion corresponding to $\omega_1 = 0.0$ is not actually vibratory motion and is of no importance.

Figure 5.22(a) shows the mode shape of the system corresponding to ω_2. This mode is influenced by the input pulley assembly, (element 1) which rotates at a maximum angular speed of 157.08 rad/s. This speed is below the fundamental frequency which implies that this gear train configuration operates at speeds below the natural frequencies of the system and hence it is highly unlikely that resonance would occur during normal operation.

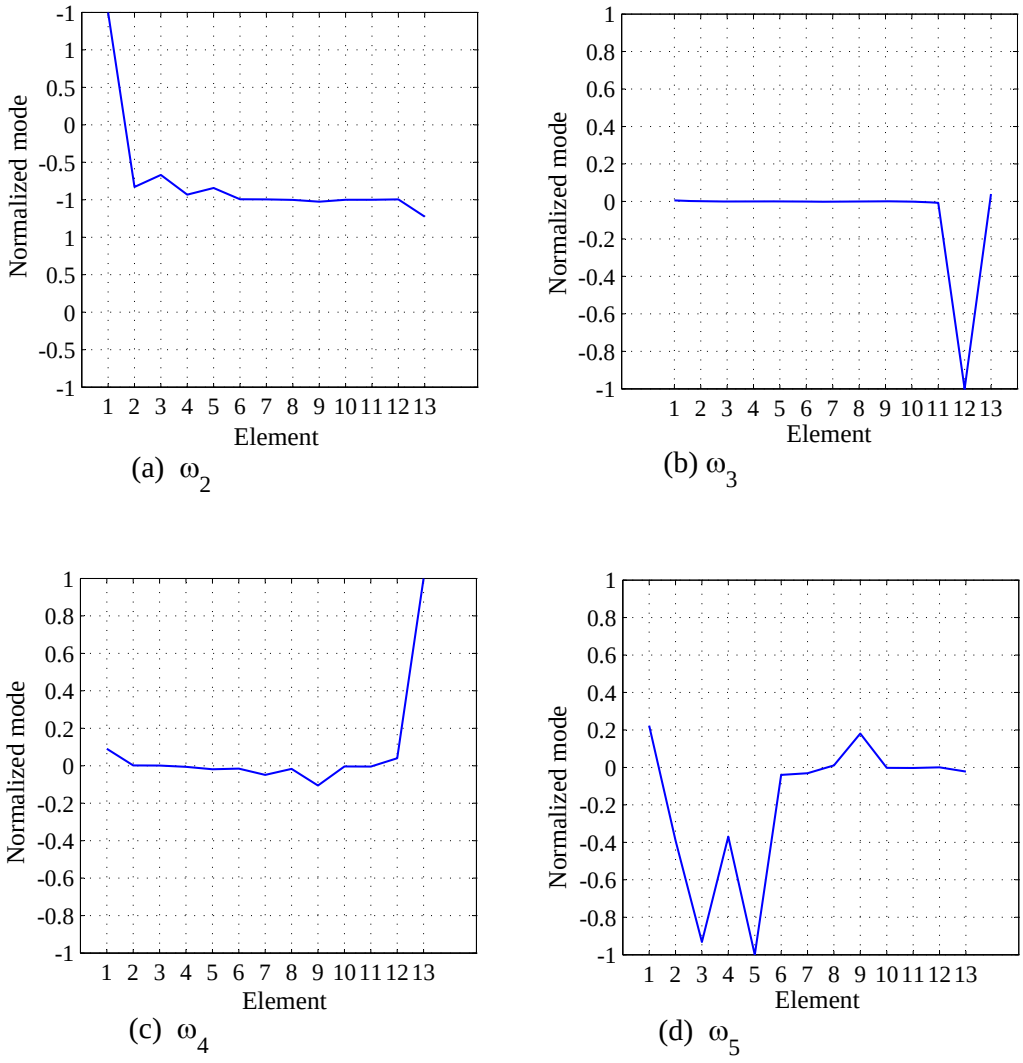

Figure 5.22: Mode shape corresponding to $\omega_2 - \omega_5$ for gear train 1

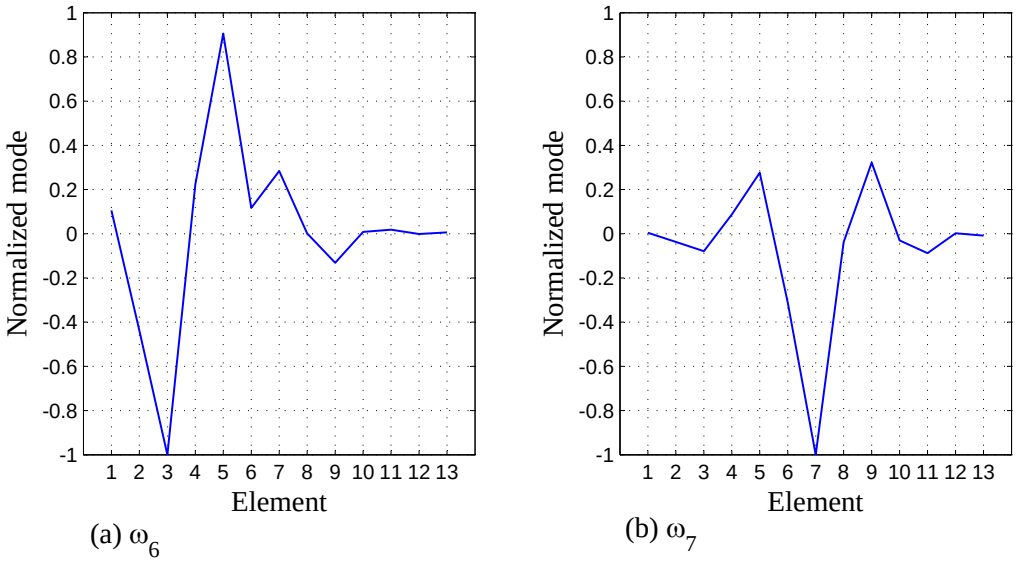

(a) ω_6 (b) ω_7

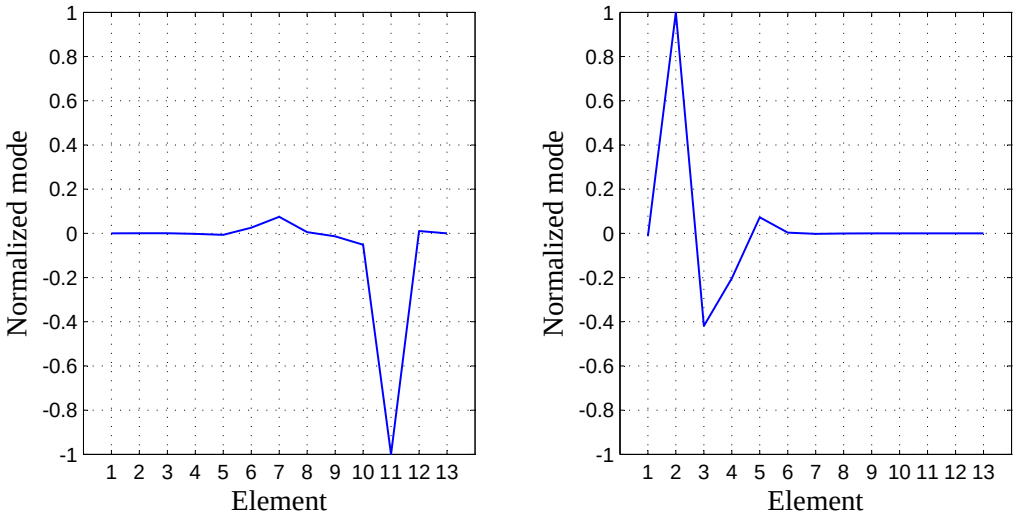

(c) ω_8 (d) ω_9

Figure 5.23: Mode shape corresponding to $\omega_6 - \omega_9$ for gear train 1

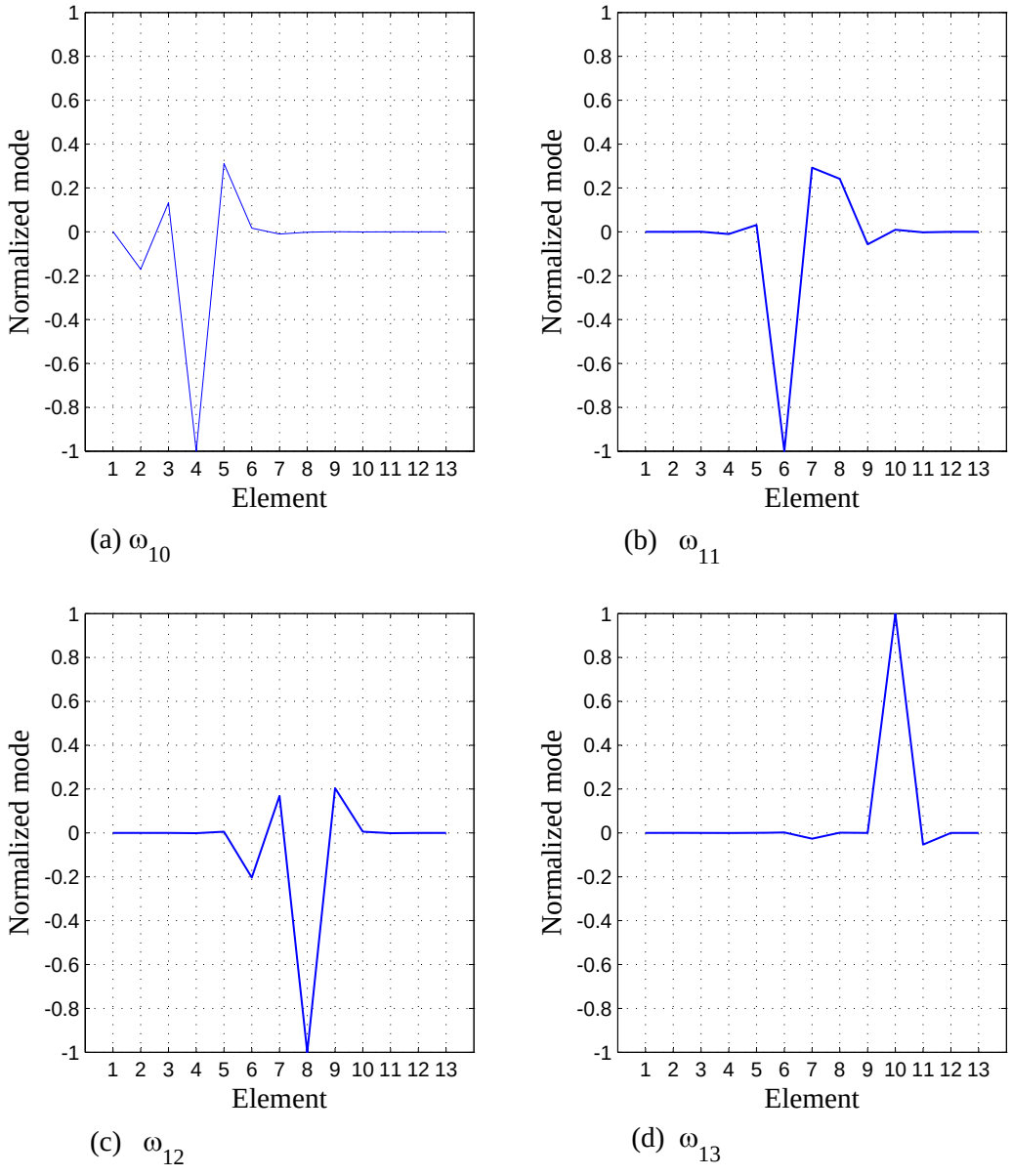

Figure 5.24: Mode shape corresponding to $\omega_{10} - \omega_{13}$ for gear train 1

To demonstrate the sensitivity of the eigenvalues to rotor properties, we reduced the inertia of the input pulley by 20% (from 10697 $Kgmm^2$ to 8558 $Kgmm^2$) and observed that the fundamental frequency increased by about 11% as shown in Table 5.12. Only the first four modes are given since the higher modes have no impact on the system. The effect of shaft stiffness is negligible as seen in Table 5.12 where an increase in the torsional stiffness of the shaft connecting the input pulley to gear 1 by about 90% (from $2.45 \times 10^7 Nm/rad$ to $4.60 \times 10^7 Nm/rad$) by increasing the shaft diameter from 24 mm to 28 mm results to an increase in the natural frequency by only 0.8%. Thus it is possible to tune the natural frequencies away from the operating speed range by either reducing or increasing the mass moment of inertia of the system components.

Table 5.12: Predicted natural frequencies with modified system properties

Natural frequency	Initial value (rad/s)	With modified Inertia (rad/s)	With modified shaft stiffness (rad/s)
ω_2	252 – 264	280 – 295	254 – 267
ω_3	894 – 920	895 – 920	895 – 920
ω_4	1044 – 1264	1044 – 1264	1044 – 1260
ω_5	7174 – 7580	7200 - 7600	8078 – 8728

5.5.2 Top Gear Ratio Configuration

Gear arrangement for this configuration is shown in Figure 5.25. In this report, this gear train will be referred to as **gear train 2**.

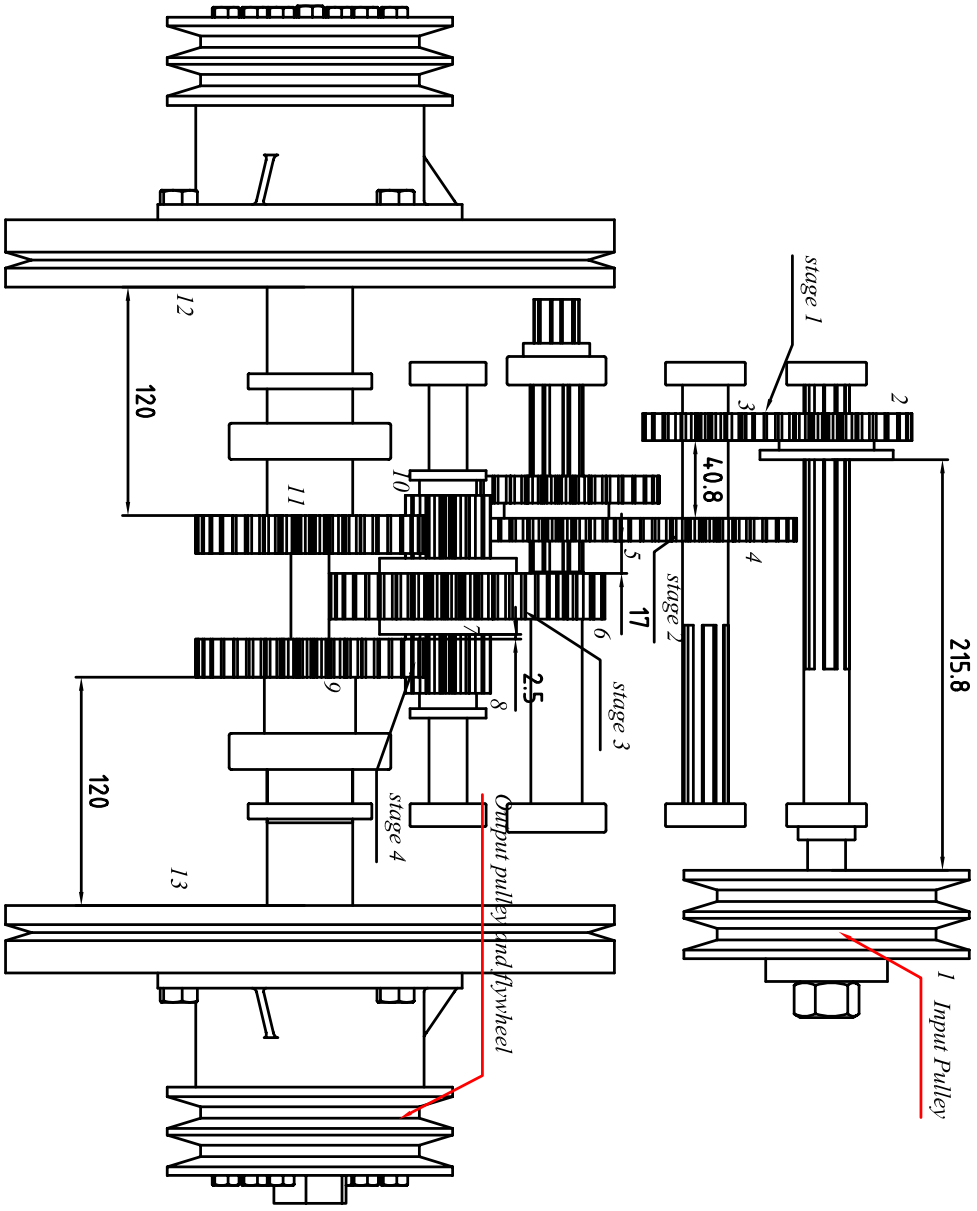

Figure 5.25: Gear train for top gear ratio

Table 5.13 show the system properties for the gear train 2 while Table 5.14 shows the operating conditions for this gear train.

Table 5.13: Rotor properties for gear train 2

Rotor No.	Description	No. of teeth for gears	Face width (mm)	Addendum modification factor	Moment of inertia (Kg mm^2)	Theoretical contact ratio
1	Input pulley assembly	-	-		10697.8	-
2	Stage I pinion	28	15	-	722.5	1.597
3	Stage I gear	20	15	-	151.1	
4	Stage II pinion	30	20	-	759.2	1.628
5	Stage II gear	24	20	-	1631.9	
6	Stage III pinion	15	25	1.2385 m	96.3	1.552
7	Stage III gear	40	25	0.7615 m	4892.7	
8	Stage IV pinion	14	50	1.3106 m	140.2	1.522
9	Stage IV gear	40	30	0.6894 m	4786.7	
10	Stage IV pinion	14	50	1.3106 m	140.2	1.522
11	Stage IV gear	40	30	0.6894 m	4786.7	
12	Output inertia	-	-		291179.0	-
13	Output inertia	-	-		291179.0	-

Table 5.14: Operating conditions and gear parameters for gear train 2

Input speed	1500 rpm
Nominal Torque	130 Nm
module (m)	3 mm
Pressure angle	20^o

Figures 5.26 to 5.29 show the dynamic response of the gears on each mesh. Similarly,

the response is periodic and the zones of single tooth contact and double tooth pair contact are clearly visible in all the time plots. The effect of damping is more significant on high speed and low torque applications as can be seen in Figures 5.26(a) and 5.27(a). The peak amplitude of relative displacement occurs at the fundamental mesh frequency. The fundamental mesh frequency for the various meshes are given in Table 5.15.

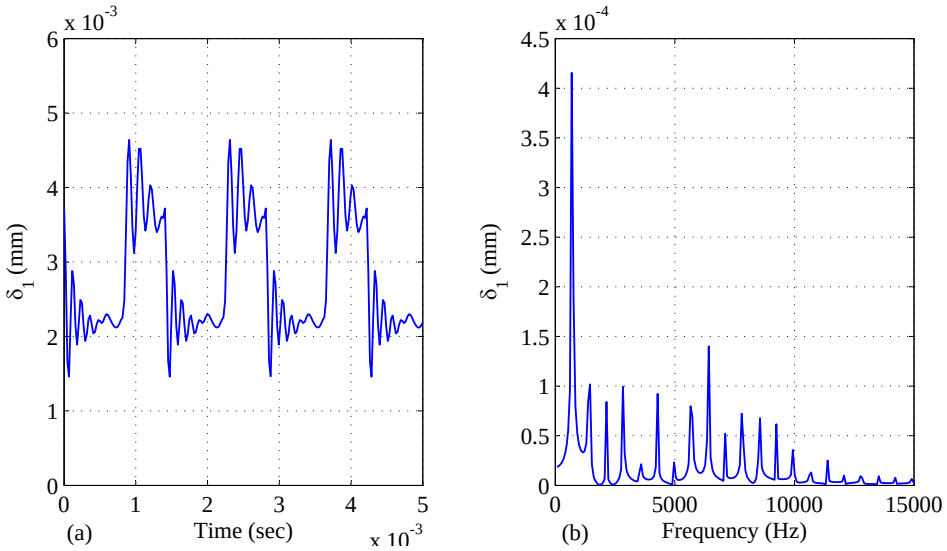

Figure 5.26: Vibration signatures for gears in stage I (gear train 2)

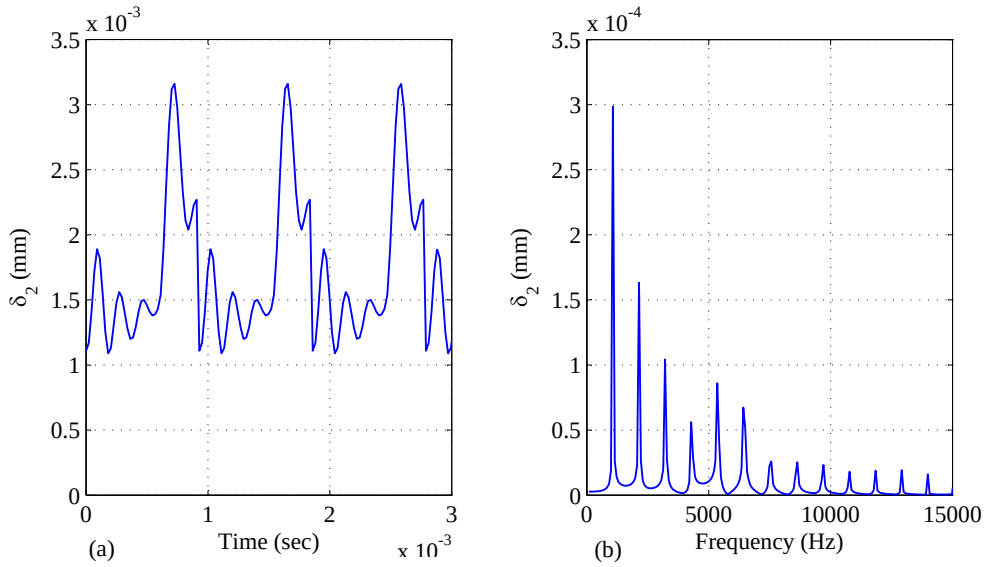

Figure 5.27: Vibration signatures for gears in stage II (gear train 2)

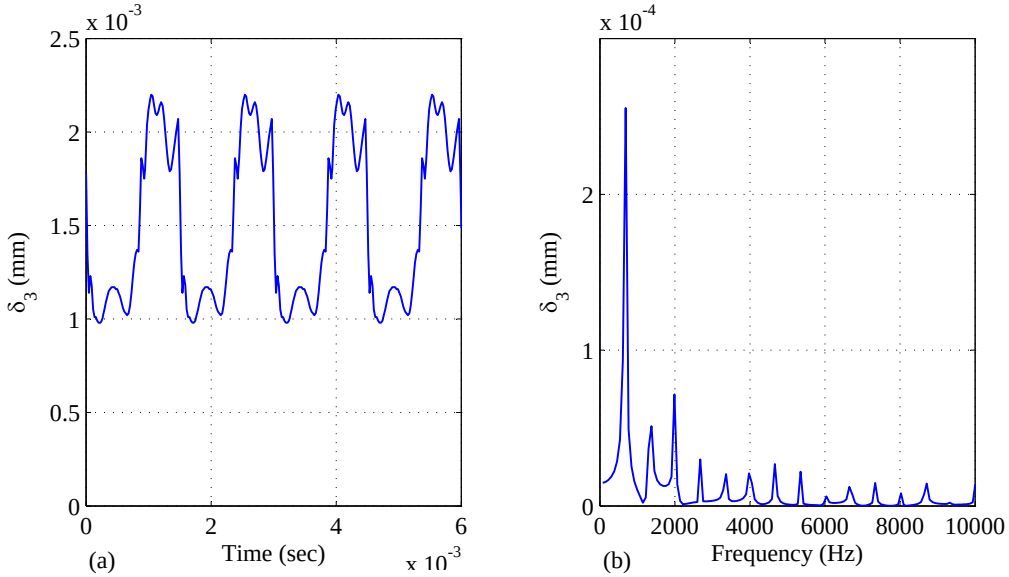

Figure 5.28: Vibration signatures for gears in stage III (gear train 2)

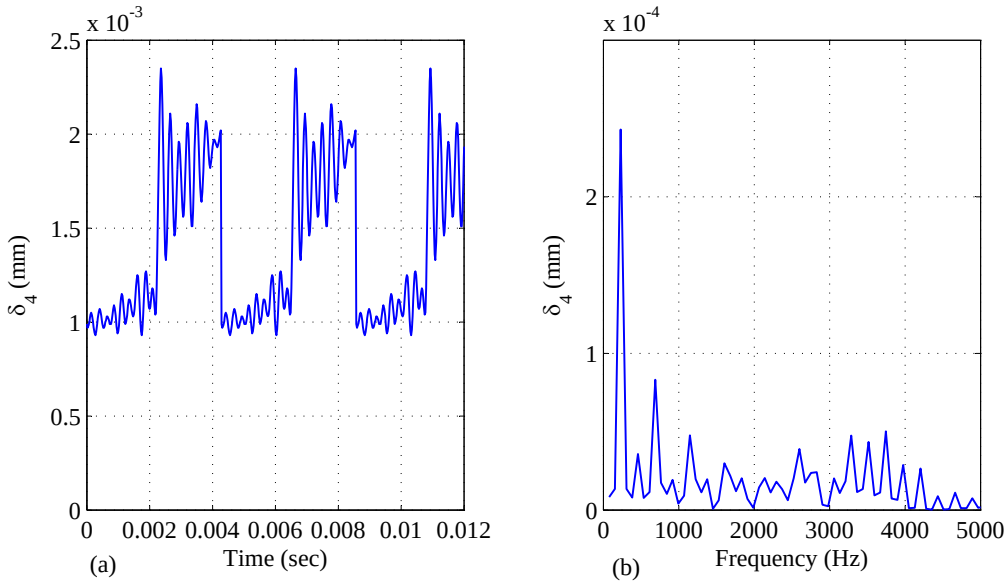

Figure 5.29: Vibration signatures for gears in stage IV (gear train 2)

Table 5.15: Fundamental mesh frequencies for gear train 2

mesh	mesh frequency (HZ)
I	700.0
II	1050.0
III	656.3
Iv	229.7

Figure 5.30 shows a comparison of the dynamic and static load on a gear tooth along the path of contact. As previously discussed, the dynamic load is higher than the static load and the percentage difference is shown in Table 5.16.

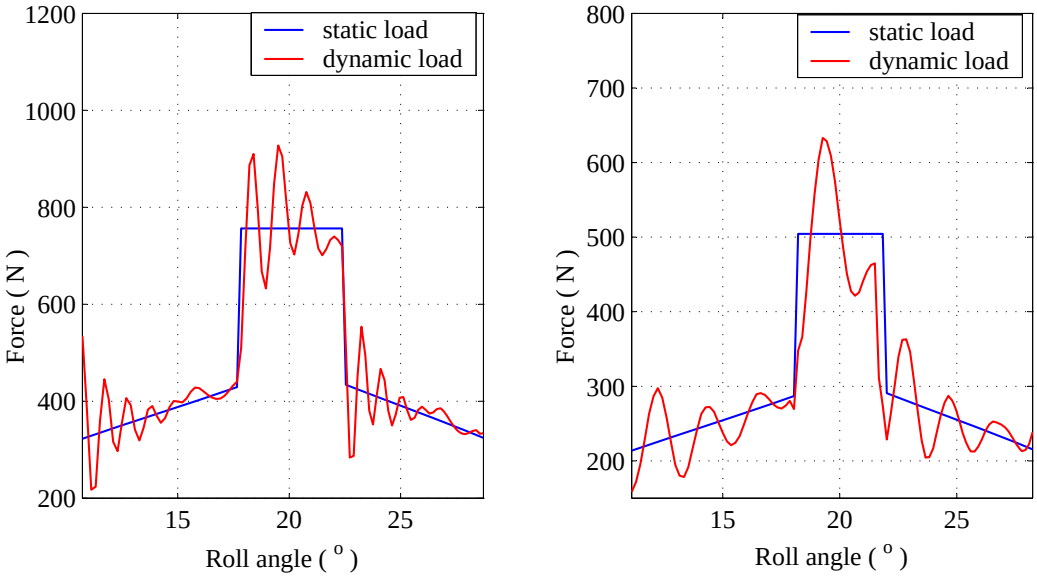

(a) stage I

(b) stage II

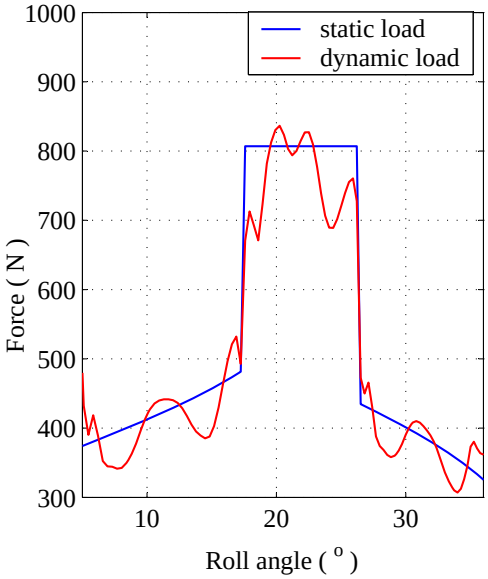

(c) stage III

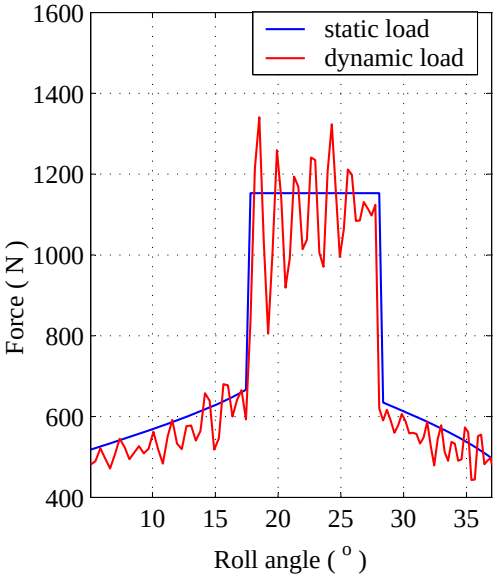

(d) stage IV

Figure 5.30: Comparison of the dynamic and static load on a single tooth over the path of contact (gear train 2)

Table 5.16: Percentage difference between peak dynamic load and maximum static load for gear train 2

Gear mesh	velocity (m/s) (m/s)	static load (N)	Peak dynamic load (N)	% difference
I	6.597	756.56	909.44	20.21
II	9.896	504.38	644.09	27.70
III	6.185	807.00	862.84	6.92
IV	2.010	1152.86	1378.34	19.56

Figures 5.31 to 5.34 show the comparison of the dynamic stress and static stress over the path of contact. In all the plots, the peak dynamic stress on a gear tooth is higher than the static stress.

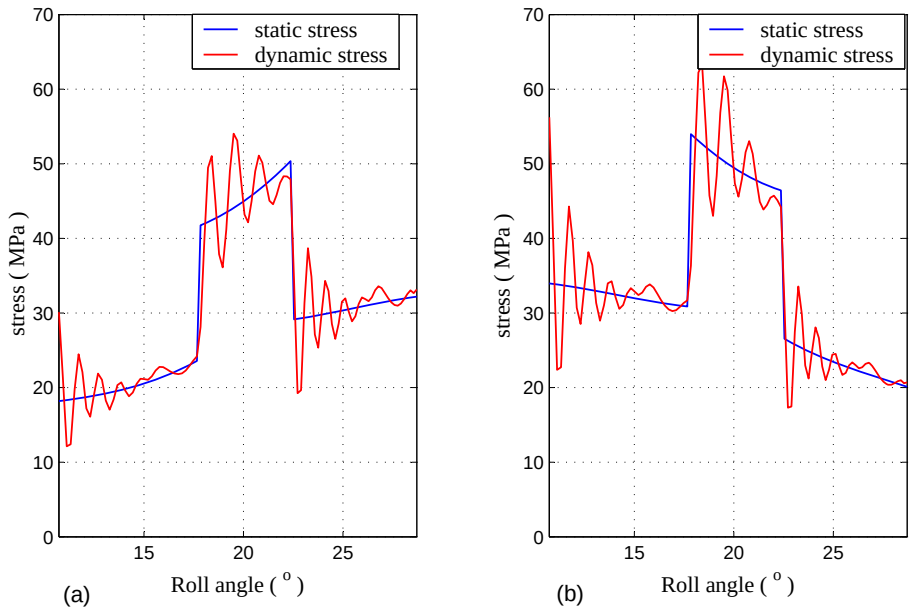

Figure 5.31: Tooth bending stress as a function of the contact position for gears in stage I (gear train 2), (a) pinion, (b) gear

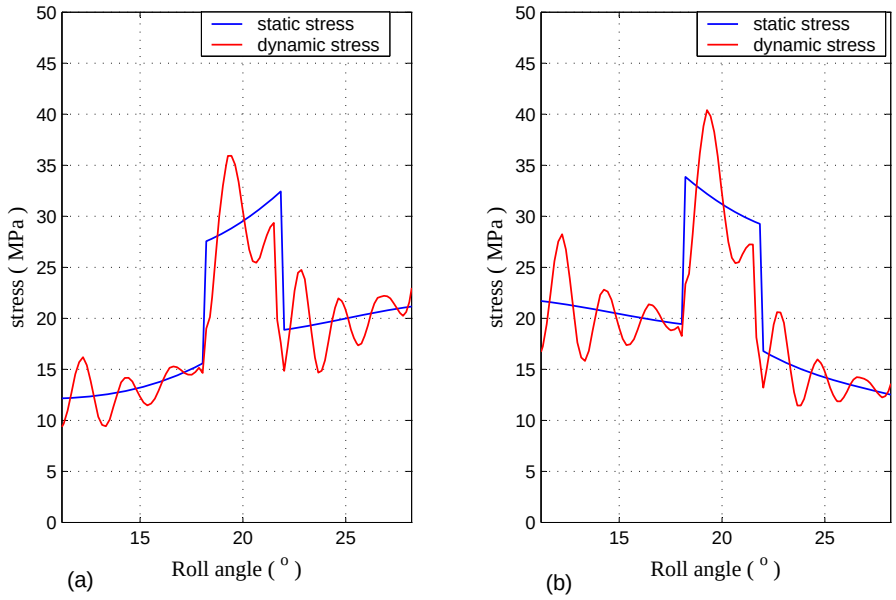

Figure 5.32: Tooth bending stress as a function of the contact position for gears in stage II (gear train 2), (a) pinion, (b) gear

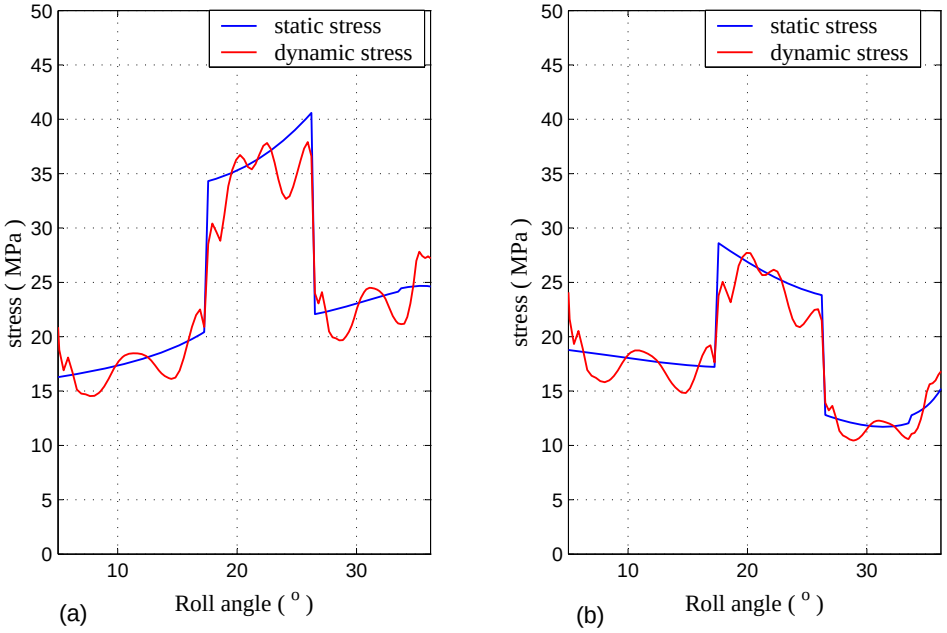

Figure 5.33: Tooth bending stress as a function of the contact position for gears in stage III (gear train 2), (a) pinion, (b) gear

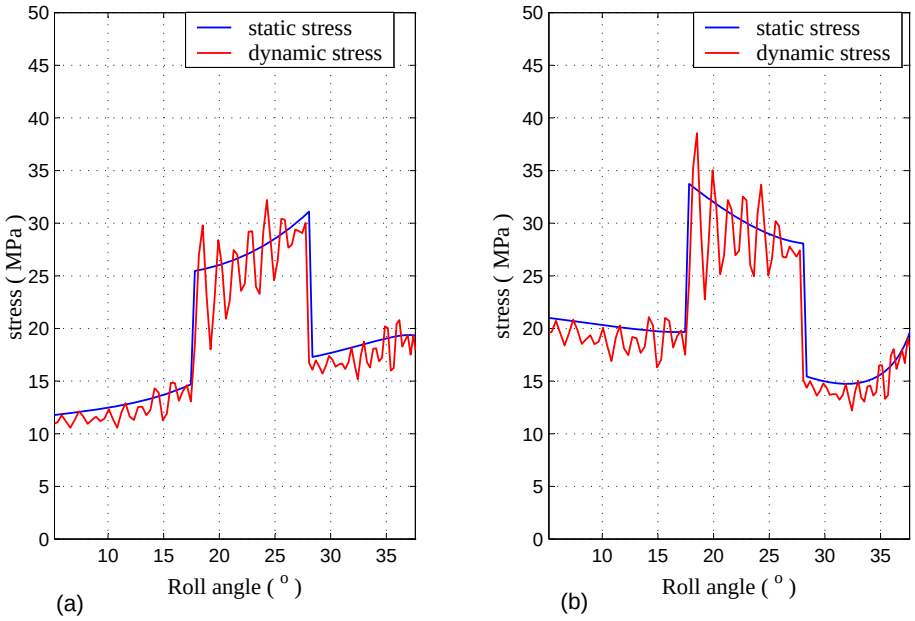

Figure 5.34: Tooth bending stress as a function of the contact position for gears in stage IV (gear train 2), (a) pinion, (b) gear

Table 5.17 shows a comparison of the peak dynamic stress on each gear with the recommended tooth stress by AGMA for 10^7 cycles. It can observed that the peak dynamic stress for all the gears is way below the maximum stress recommended by AGMA implying that the gears on gear train 2 would have a longer fatigue life.

Table 5.17: Recommended and maximum dynamic tooth stresses for gear train 2

Mesh	Gear	No. of Teeth	*V (m/s)*	K_v	σ_j *(MPa)*	*AGMA* σ_{all} *(MPa)*
I	driver	28	6.5973	0.7231	53.56	622.40
	driven	20		0.7231	63.28	
II	driver	30	9.8960	0.6833	36.54	658.60
	driven	24		0.6833	41.11	
III	driver	15	6.1850	0.7291	38.04	617.20
	driven	40		0.7291	30.65	
IV	driver	14	2.0101	0.8217	35.54	547.64
	driven	40		0.8217	36.43	

Table 5.18 shows the natural frequencies corresponding the the system configuration shown in Figure 5.25 while the corresponding mode shapes are shown in Figures 5.22 to 5.24. As explained previously, the first natural frequency is zero for a free-free system. From the mode shapes corresponding to the natural frequencies obtained for this system, Figures 5.22 to 5.24, the mode shape corresponding to the second natural frequency is influenced by the output flywheel assembly whose angular speed is much below the natural frequency. The operating speed range for the system is below any of the natural frequencies implying that resonance is unlikely to occur.

Table 5.18: System Natural Frequencies corresponding to gear train 2

Natural frequency	Predicted value (rad/s)
ω_1	0
ω_2	898 – 920
ω_3	989 – 1003
ω_4	1060 – 1249
ω_5	5540 – 5680
ω_6	11000 – 11625
ω_7	19300 – 22240
ω_8	22533 – 28216
ω_9	26413 – 34650
ω_{10}	42456 – 54318
ω_{11}	75187 - 87227
ω_{12}	79920 – 89450
ω_{13}	135200 - 172250

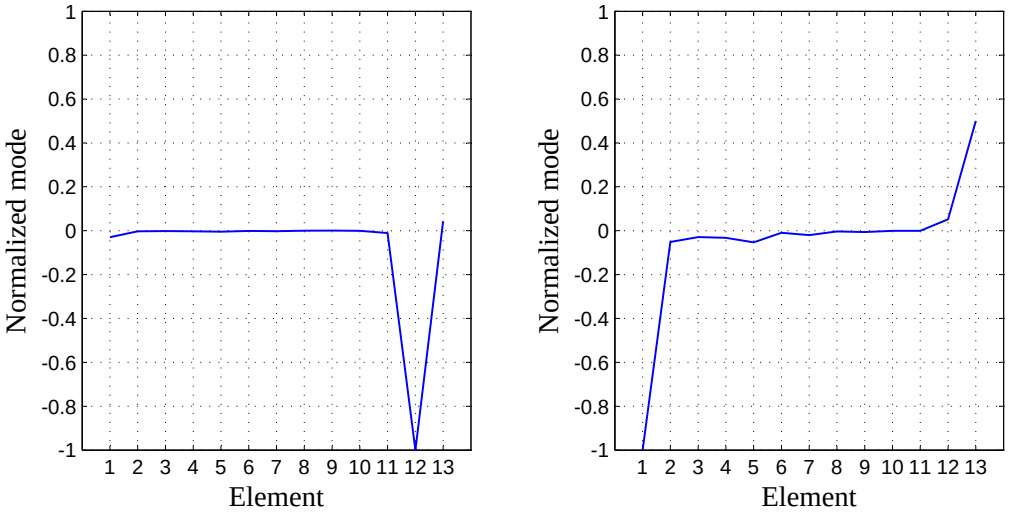

(a) ω_2 (b) ω_3

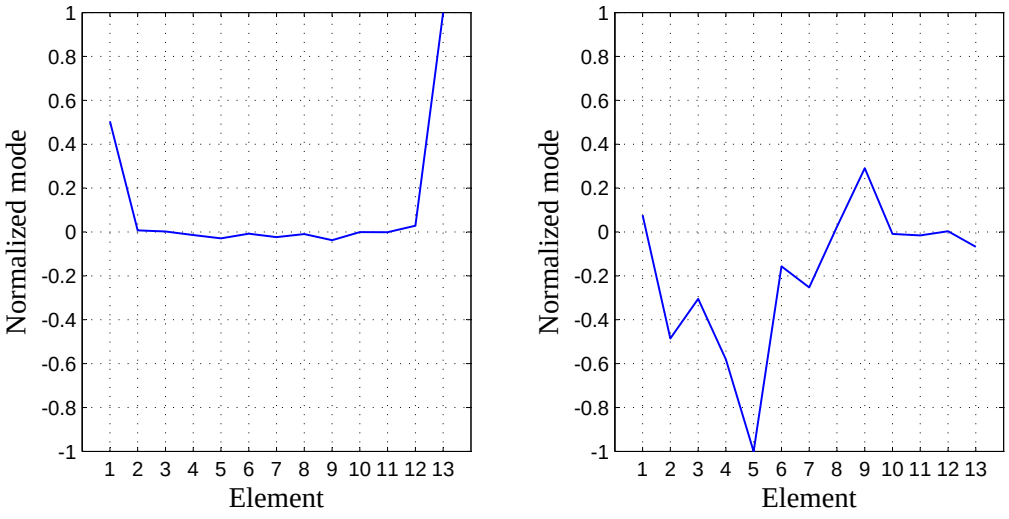

(c) ω_4 (d) ω_5

Figure 5.35: Mode shape corresponding to $\omega_2 - \omega_5$ for gear train 2

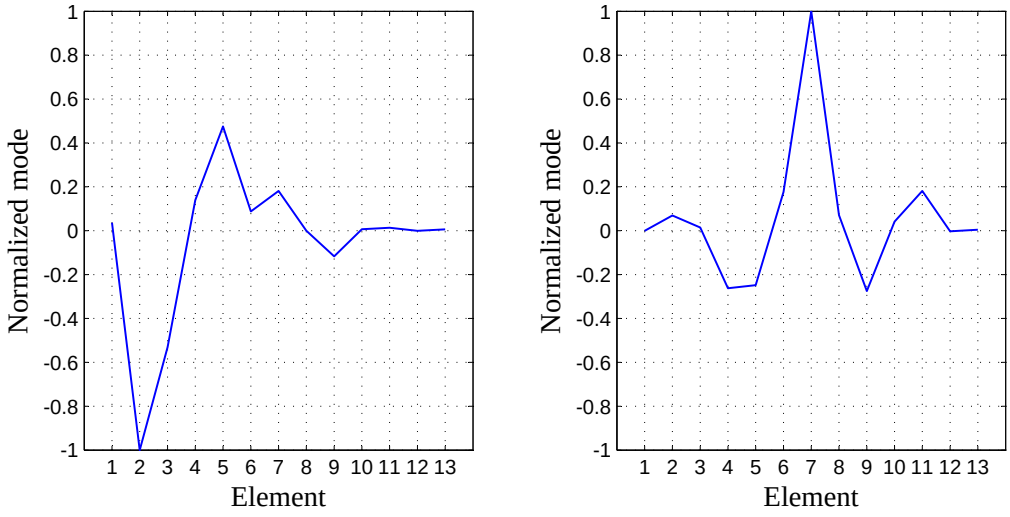

(a) ω_6 (b) ω_7

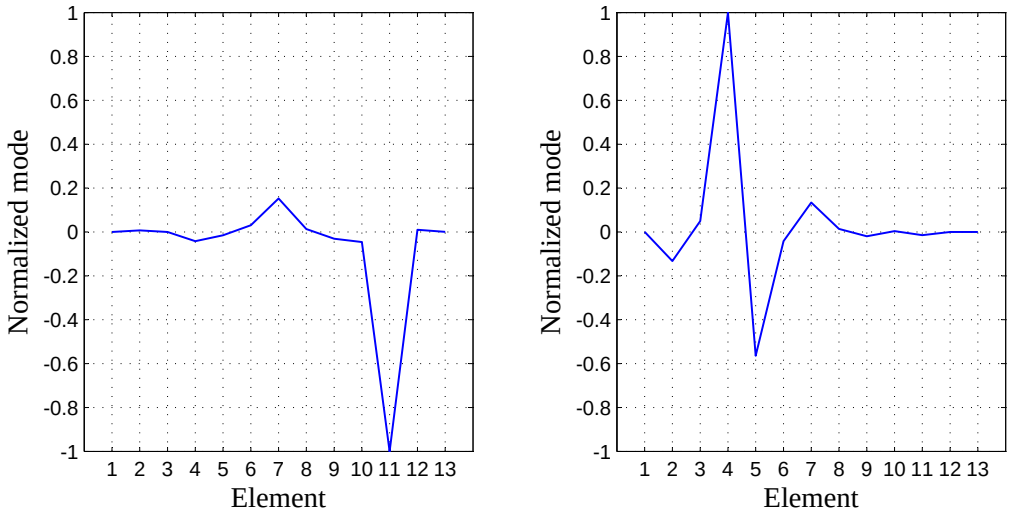

(c) ω_8 (d) ω_9

Figure 5.36: Mode shape corresponding to $\omega_6 - \omega_9$ for gear train 2

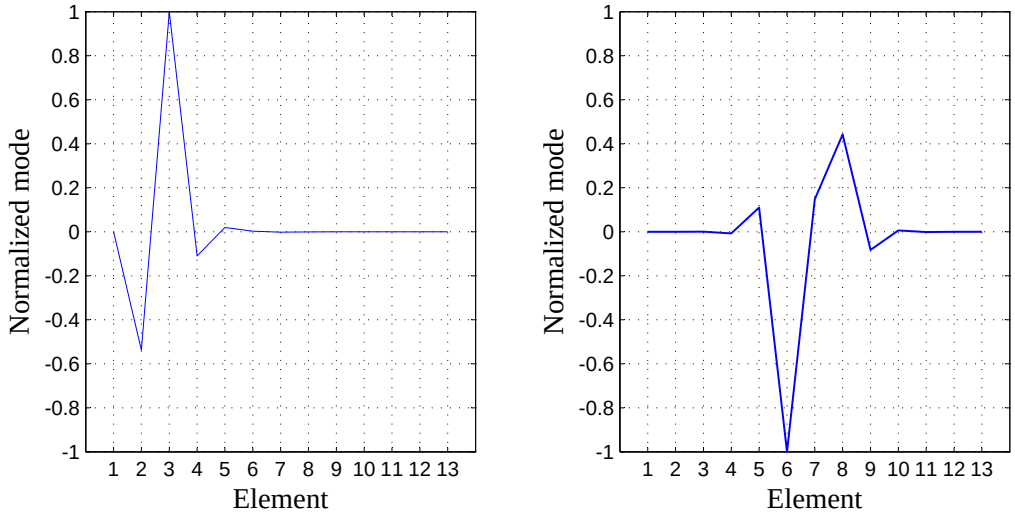

(a) ω_{10} (b) ω_{11}

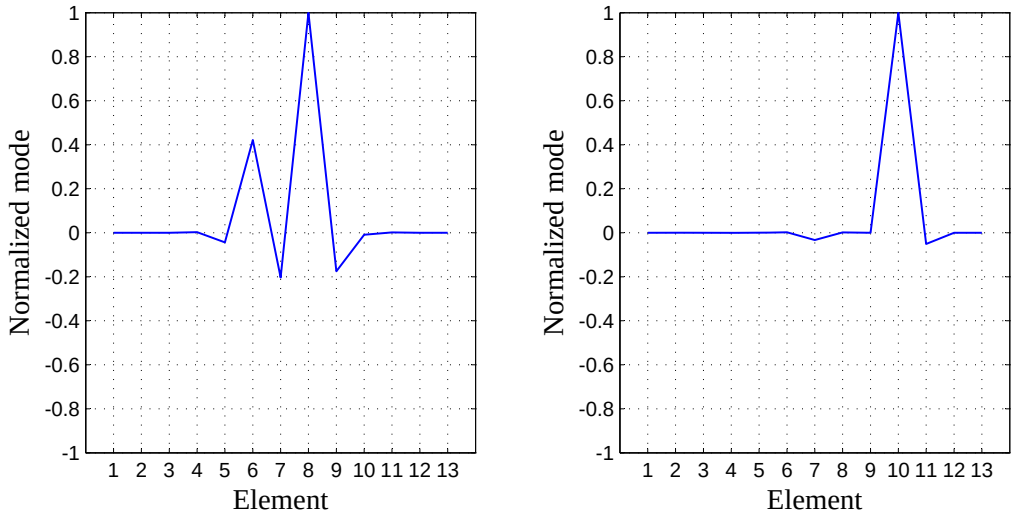

(c) ω_{12} (d) ω_{13}

Figure 5.37: Mode shape corresponding to $\omega_{10} - \omega_{13}$ for gear train 2

5.6 Effect of Gear Design Parameters

In this section, the effect of varying the gear design parameters on the gear vibrations and dynamics is presented. The following gear design parameters are included:

1. Module 2.0, 2.5 and 3.0
2. Contact ratio
3. Pressure angle

5.6.1 Effect of Module on Gear Vibrations

The module of the gears was changed from 3.0 mm to 2.0 mm and 2.5 mm trying to minimize the difference between the original pitch circle diameters and center distances with the new ones by varying the numbers of teeth on the gears as shown on Tables 5.19 and 5.20. The pressure angle, face width and pitch radius were held constant. However, since the number of teeth on a gear is an integer, the pitch radius of some gears varied slightly along with the center distance. Using a module larger than 3.0 would compromise on the space requirements (overall center distance of 325 ± 10 mm) of the gearbox since it would be necessary to increase the number of teeth in order to avoid interference. For instance using a module of 4.0, a gear previously with 14 teeth would be replaced by a gear with 11 teeth which would require an addendum modification factor greater than $0.4m$ resulting to a very small active profile on the mating gear tooth. On the other hand, changing the module alone while holding the number of teeth constant would change the pitch radius and hence the applied load. Figure 5.38 shows sample tooth profiles for selected number of teeth on the gears.

Table 5.19: Corresponding numbers of teeth for different modules on gear train 1 (bottom gear ratio)

Mesh	Module 3.0		Module 2.5		Module 2.0	
	No. of teeth	C (mm)	No. of teeth	C (mm)	No. of teeth	C (mm)
I	14	72.0	17	72.5	21	72.0
	34		41		51	
II	14	81.0	17	81.25	21	81.0
	40		48		60	
III	15	82.5	18	82.5	23	83.0
	40		48		60	
IV	14	81.0	17	81.25	21	81.0
	40		48		60	

Table 5.20: Corresponding numbers of teeth for different modules on gear train 2 (top gear ratio)

Mesh	Module 3.0		Module 2.5		Module 2.0	
	No. of teeth	C (mm)	No. of teeth	C (mm)	No. of teeth	C (mm)
I	28	72.0	34	72.5	42	72.0
	20		24		30	
II	30	81.0	36	81.25	45	81.0
	24		29		36	
III	15	82.5	18	82.5	23	83.0
	40		48		60	
IV	14	81.0	17	81.25	21	81.0
	40		48		60	

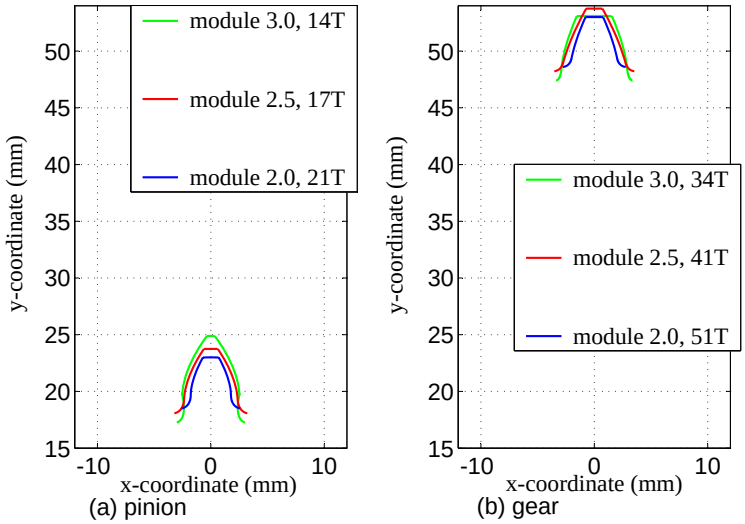

Figure 5.38: Sample tooth profiles for different modules

Figures 5.39 and 5.40 show the vibration levels of the various meshes on gear train 1 in the frequency domain for modules, 2.0, 2.5 and 3.0. It can be seen that the peak amplitude of the vibrations for the different modules are almost the same though gears with module 2.0 show slightly lower amplitudes for mesh I, III and IV. This could be as a result of the high mesh stiffness as shown in Figure 5.41. The stiffness of the gears increases with reduction in the module since the effective length of the tooth as a cantilever beam reduces. However, from Figure 5.42 it can be observed that the root stress on a gear tooth increases by reducing the module. The stresses on the driven gear with a module of 2.0 and 2.5 for the fourth stage (Figure 5.42) are higher than that calculated using the AGMA equation which implies that they would have a lower fatigue life than gears with a module of 3.0. This could be due to the decreased tooth thickness at the fillet area for gears with a smaller module as shown in Figure 5.38.

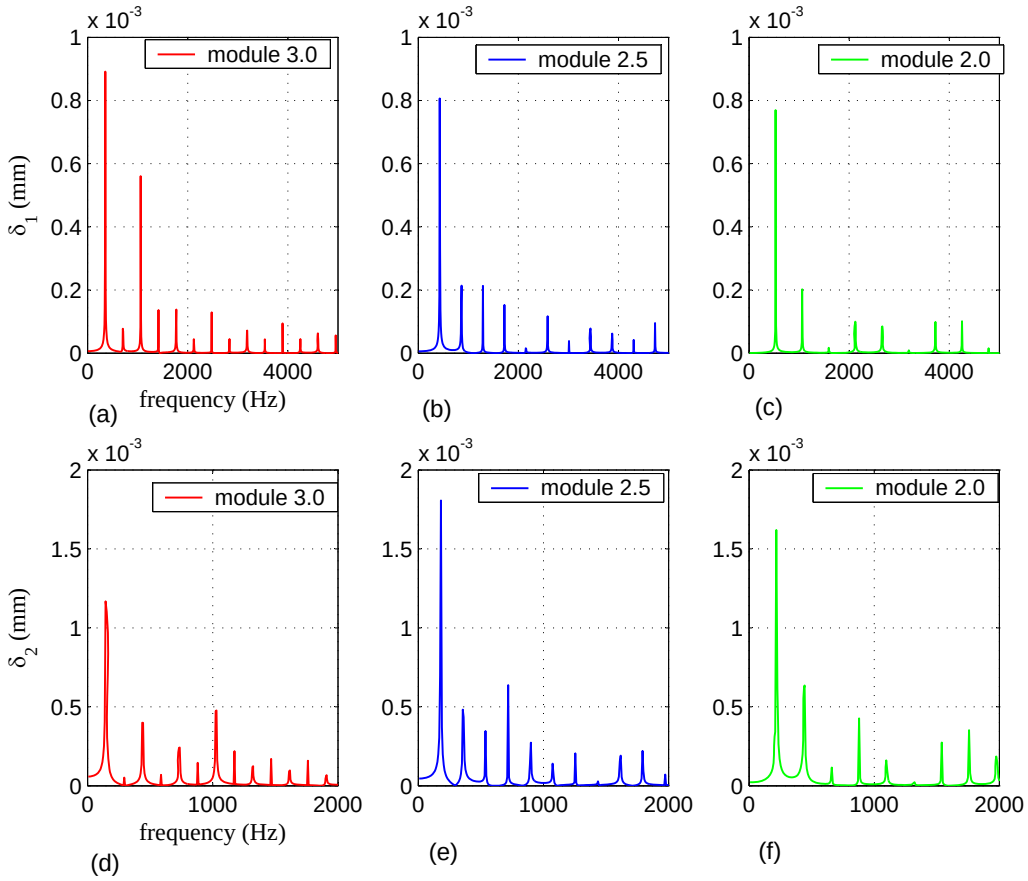

Figure 5.39: Vibration levels for various modules for bottom gear ratio (stage I and II)

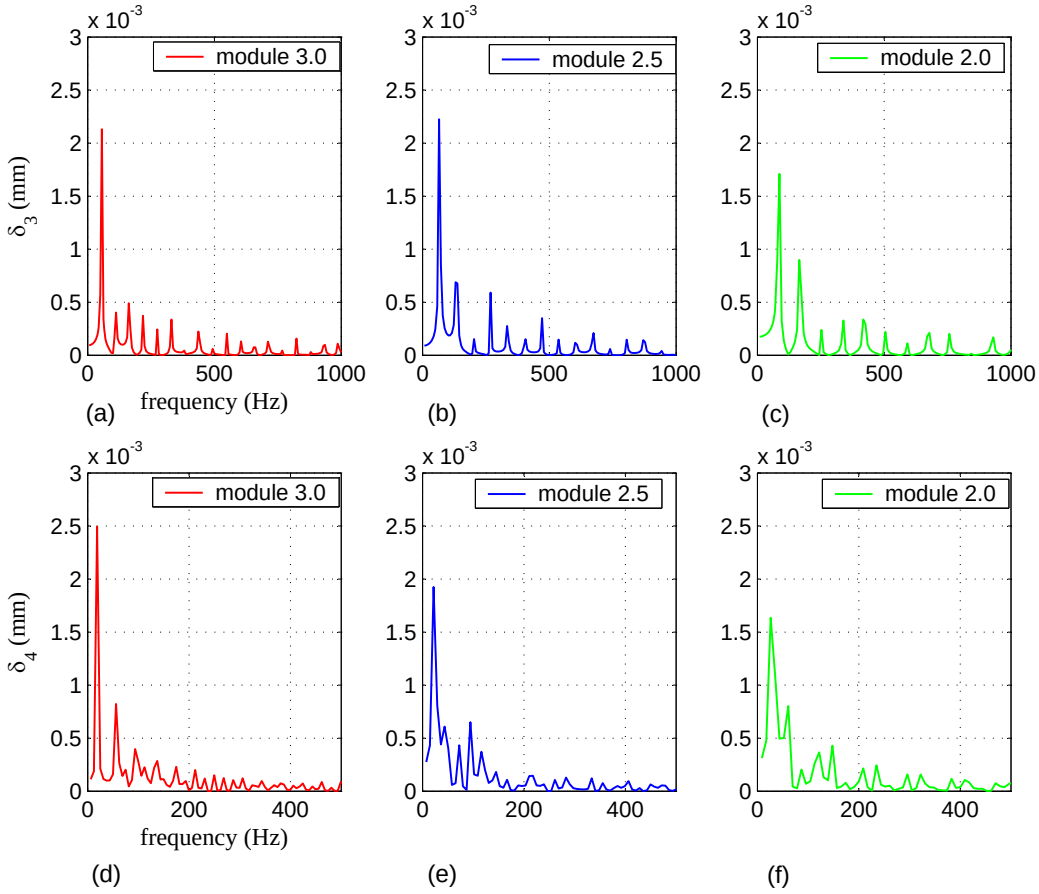

Figure 5.40: Vibration levels for various modules for gear train 1 (stage III and IV)

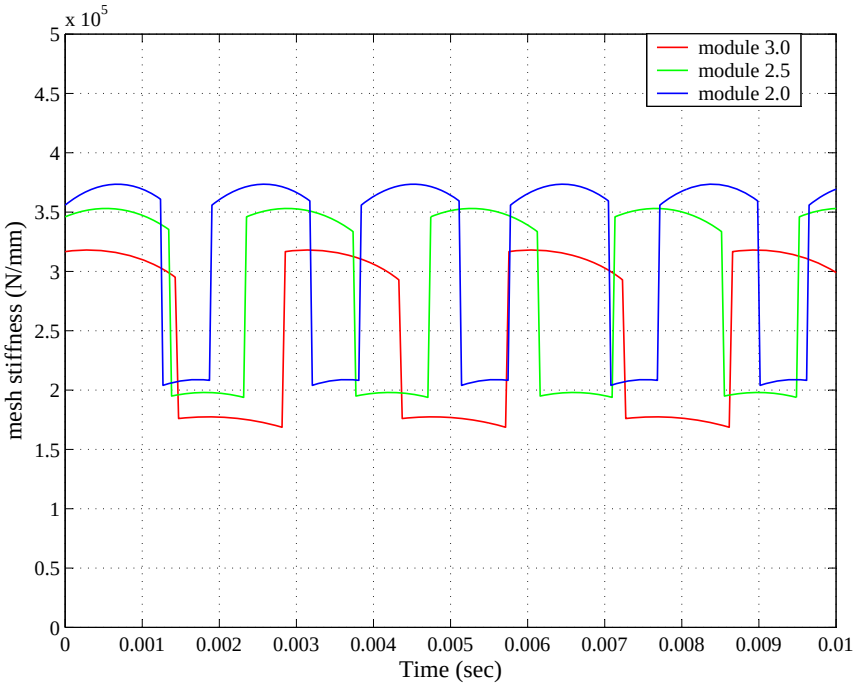

Figure 5.41: Sample mesh stiffness for gears with different modules but the same pitch diameter and face width

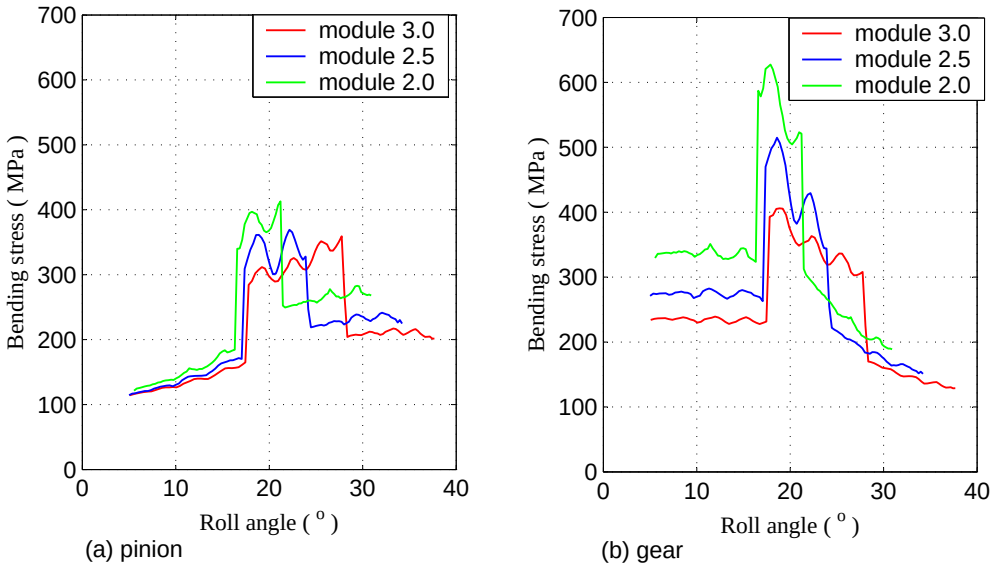

Figure 5.42: Root stress on stage IV of gear train 1 for different modules

5.6.2 Effect of Pressure Angle on Gear Vibrations

The standard pressure angles normally used in the manufacture of gears are 14.5^o, 20^o and 25^o. In this section, the results are presented for pressure angles of 25^o and 20^o only since the minimum number of teeth to avoid interference for pressure angle of 14.5^o is 32 as shown on Table 2.1. This means that we would require very large gears for the gear train and by considering the space requirements (overall center distance of 325 ± 10 mm) of the gearbox, it would be uneconomical to use this pressure angle. The pressure angle was varied while holding the module and number of teeth of the various meshes constant.

Figure 5.43 shows sample profiles for teeth with a pressure angle of 20^o and 25^o respectively.

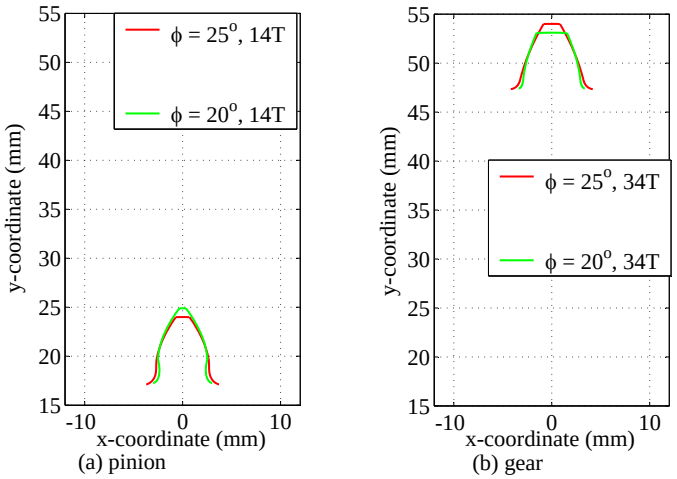

Figure 5.43: Sample tooth profiles for different pressure angles

The tooth with a pressure angle of 25^o has a larger thickness at the fillet area which explains why the gears with pressure angle of 25^o have a higher mesh stiffness than a corresponding pair with a pressure angle of 20^o as shown in Figure 5.44, which is

also attributed to the larger tooth thickness at the fillet area. However increasing the pressure angle reduces the contact ratio and thus increasing the duration of single pair contact zone as shown in Figure 5.44.

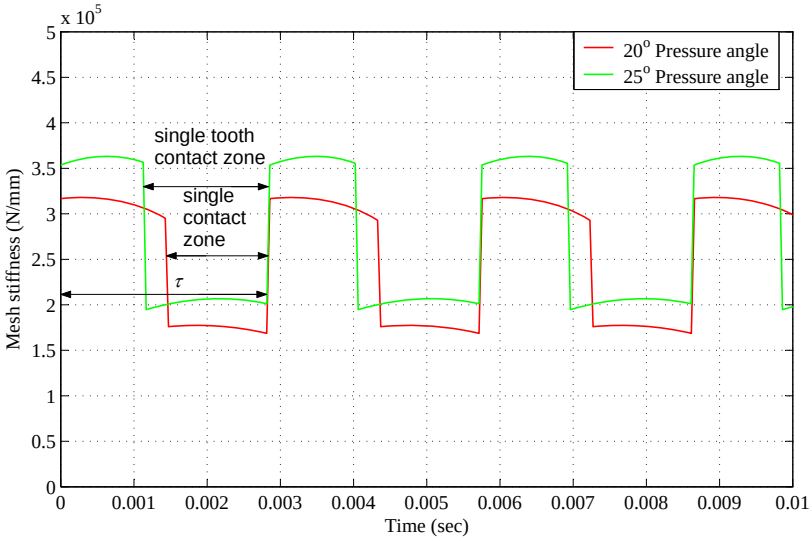

Figure 5.44: Mesh stiffness for different pressure angles

Figures 5.45 and 5.46 show plots of the vibration amplitudes of the various meshes of gear train 1. It can be observed that the vibration amplitudes of gears with a pressure angle of 25^o are slightly lower than those of corresponding gear pairs with a pressure angle of 20^o. This could be due to the higher mesh stiffness for pressure angle of 25^o. The root stress plots (Figure 5.47) show relatively lower root stress for the pinion with a pressure angle of 25^o which is mainly due to the larger tooth thickness at the fillet area and the fact that the addendum of the pinion has not been modified and therefore the effective length of the gear tooth is smaller as shown in Figure 5.43.

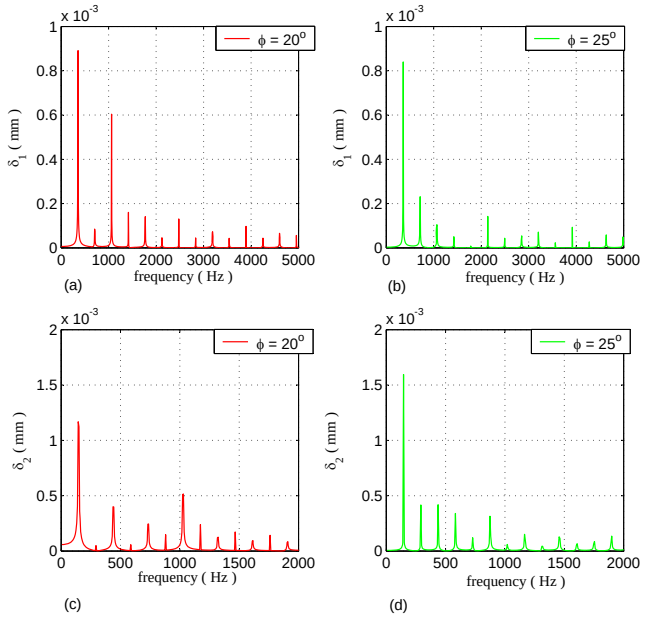

Figure 5.45: Comparison of the vibration amplitudes for different pressure angles (stage I and II)

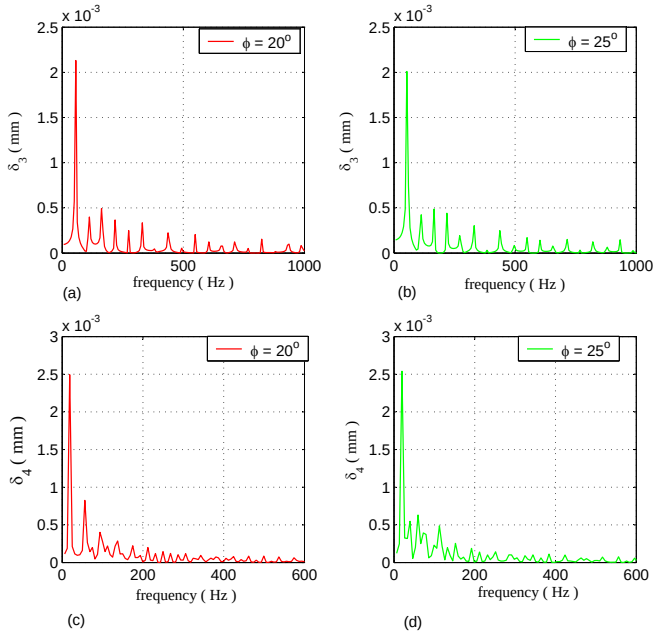

Figure 5.46: Comparison of the vibration amplitudes for different pressure angles (stage III and IV)

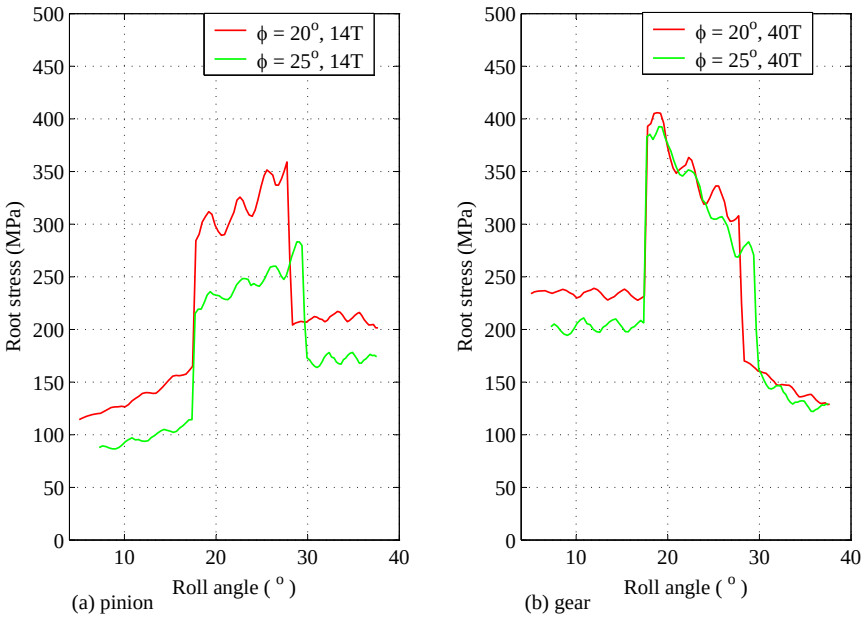

Figure 5.47: Sample root stress for gears with different pressure angle

5.6.3 Effect of Contact Ratio on Gear vibrations

The contact ratio of a pair of gears in mesh is given by equation B.42 and is affected by the following parameters:

- addendum
- center distance
- pressure angle
- module

The contact ratio of a gear pair can be increased by varying one of the above parameters or a combination of two or more of these parameters. Increasing the addendum is normally recommended for increasing the contact ratio since this can be achieved

by simply adjusting the cutter depth [18]. The maximum permissible addendum modification coefficients are obtained by iteratively varying the addendum modification coefficient of the pinion and gear until the top land thickness is equal to the minimum allowable (usually $0.3m$) [74]. In this research work, a code was developed to obtain the maximum possible contact ratio for a gear pair by varying the addendum and adjusting the center distance in order to avoid interference.

Table 5.21: Maximum possible contact ratio for a gear pair with module 3.0

Mesh	Gear	A_x	Contact ratio	Center distance (mm)
I	14	0.348	1.594	72.915
	34	0.156		
II	14	0.348	1.594	81.621
	40	0.009		
III	15	0.364	1.651	83.809
	40	0.341		
IV	14	0.348	1.594	81.621
	40	0.009		

From Table 5.21, it can be observed that for a pair of gears with a high reduction ratio, it is difficult to obtain a contact ratio close to 2.0. However, this can be achieved by using a smaller module as shown on Tables 5.22 and 5.23.

Table 5.22: Maximum possible contact ratio for a gear pair with module 2.5

Mesh	Gear	A_x	Contact ratio	Center distance (mm)
I	17	0.393	1.970	72.969
	41	0.407		
II	17	0.393	1.971	81.503
	48	0.265		
III	18	0.357	1.991	82.903
	48	0.384		
IV	17	0.393	1.971	81.503
	48	0.265		

Table 5.23: Maximum possible contact ratio for a gear pair with module 2.0

Mesh	Gear	A_x	Contact ratio	Center distance (mm)
I	21	0.360	1.992	72.382
	51	0.371		
II	21	0.360	1.992	81.267
	60	0.273		
III	23	0.347	1.998	83.124
	60	0.181		
IV	21	0.360	1.992	81.267
	60	0.273		

Figure 5.48 shows sample tooth profiles for teeth with modified addendum to increase the contact ratio. In this case the minimum allowable top land thickness for the pinions was set to $0.35m$

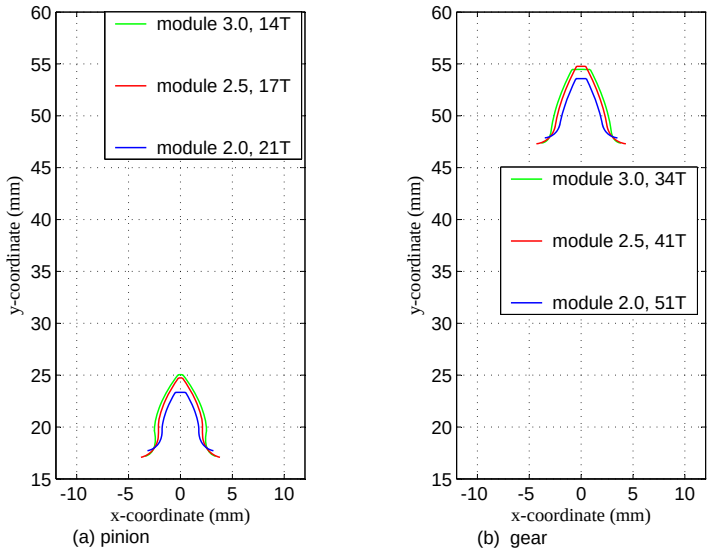

Figure 5.48: Sample tooth profiles for teeth with modified addendum

Figure 5.49 shows the periodic mesh stiffness for various contact ratios. It can be observed that as the contact ratio increases, the band width for single contact zone reduces. As the contact ratio approaches 2.0, the variation in mesh stiffness is mainly due to the change in contact point along the path of contact as shown in Figure 5.49. The discontinuities in the mesh stiffness as the number of teeth in contact changes are eliminated. As one pair of teeth leaves mesh, another pair of teeth enters the mesh ensuring that there are always two pairs of teeth in contact. The applied load is shared between two pairs of teeth at all times. However, the magnitude of the mesh stiffness reduces due to the increase in the tooth height and consequently the effective length of the cantilever beam that represents the tooth.

Figures 5.50 and 5.51 show sample plots for vibration levels of gear pairs with high contact ratio. A pair of gears with a contact ratio close to 2.0 shows relatively low vibration levels especially those with a module of 2.0. A contact ratio of 2.0 reduces the vibration levels by up to 75% in both cases. This effect is due to the very narrow band of single-tooth contact being passed so quickly during gear rotation that the system could not respond until after excitation has passed resulting to a very gentle dynamic response.

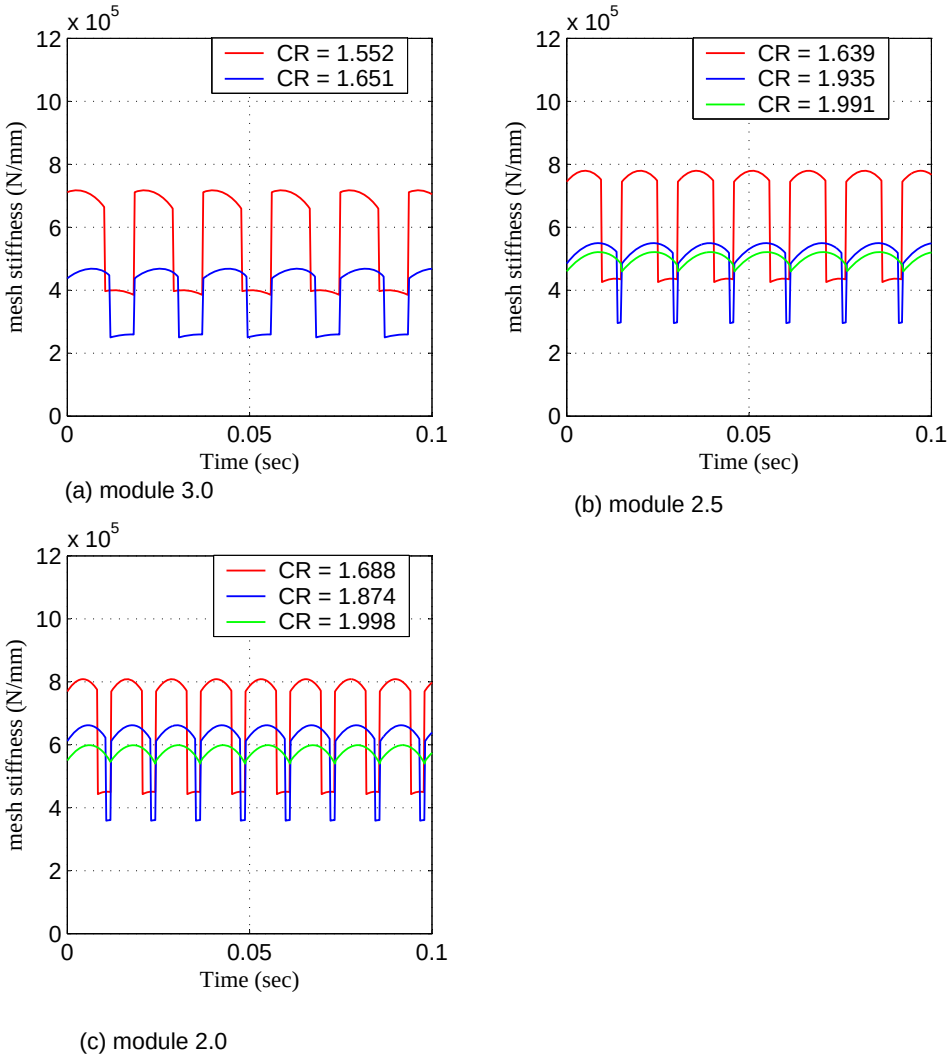

Figure 5.49: Periodic mesh stiffness for different contact ratios

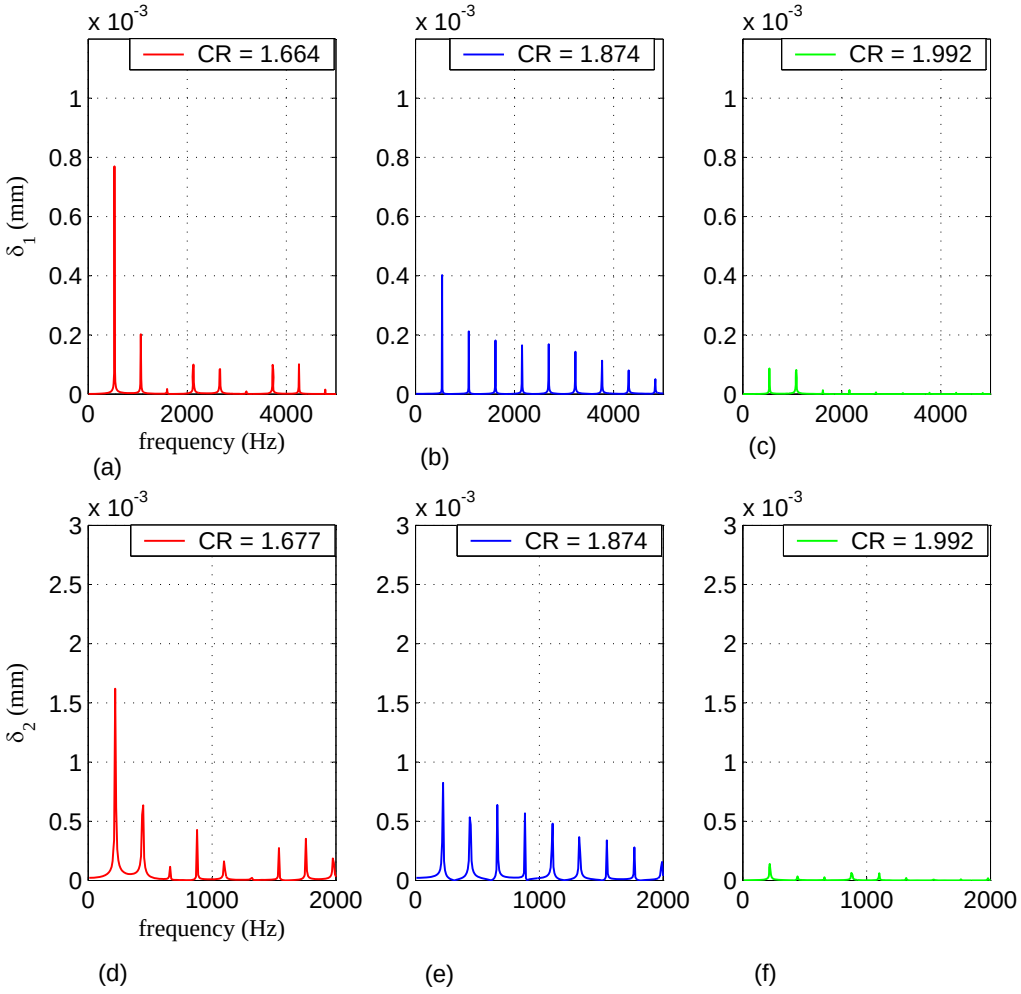

Figure 5.50: Sample vibration levels for gear pairs with increased contact ratio (gears with a module of 2.0 mm)

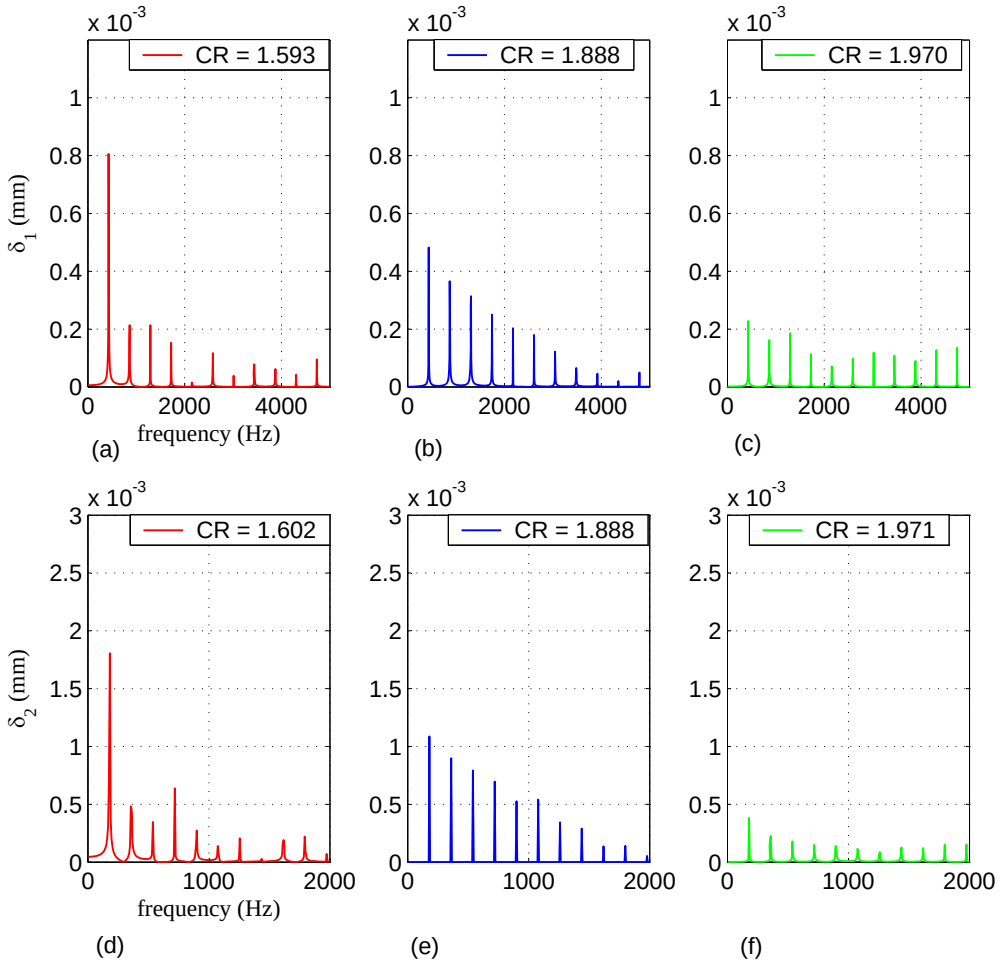

Figure 5.51: Sample vibration levels for gear pairs with increased contact ratio (module 2.5 mm)

A contact ratio close to 2.0 also results to a smooth root stress curve as shown on Figure 5.52 and 5.53. A contact ratio of 2.0 reduces the peak dynamic root stresses on the gear teeth by about 45% in both cases. In addition, the discontinuities in the stress curves that occur during the transition from double tooth contact to single tooth contact and vice versa are eliminated. This implies that the gears with a contact ratio of 2.0 would have a higher fatigue life than those with a contact ratio lower than 2.0. However, the gears with a module of 2.5 show lower root stresses

than those with a module of 2.0 as shown in Figure 5.54. This could be attributed to the larger tooth thickness on the gears with a module of 2.5. As explained in section 3.5, the root stress is dependent on the tooth thickness at the fillet area and the length between the contact point and the critical section of the tooth in addition to the load. The zone of single contact is also eliminated since a contact ratio of 2.0 implies that there are at least 2.0 pairs of teeth in contact at any one point. The only variation in the root bending stress is due to the change in the contact positions.

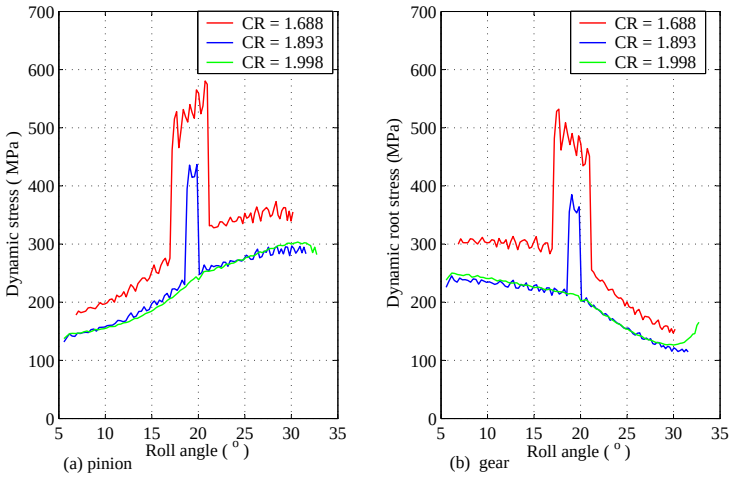

Figure 5.52: Root stress on stage IV gears of gear train 1 for different contact ratios using a module of 2.0

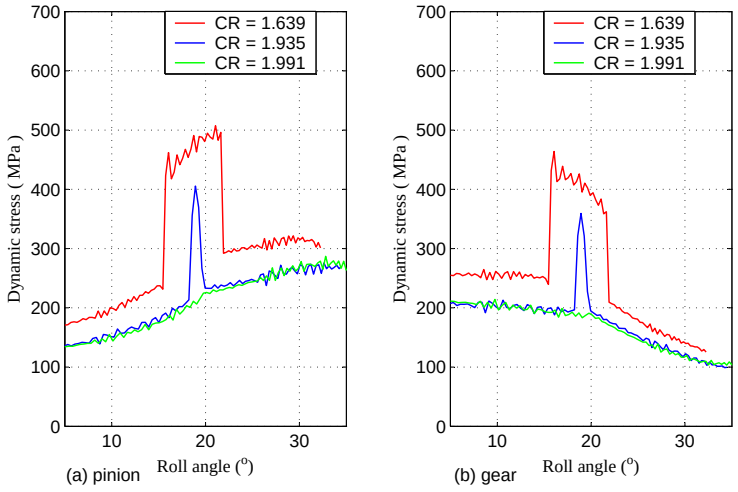

Figure 5.53: Root stress on stage IV gears of gear train 1 for different contact ratios using a module of 2.5

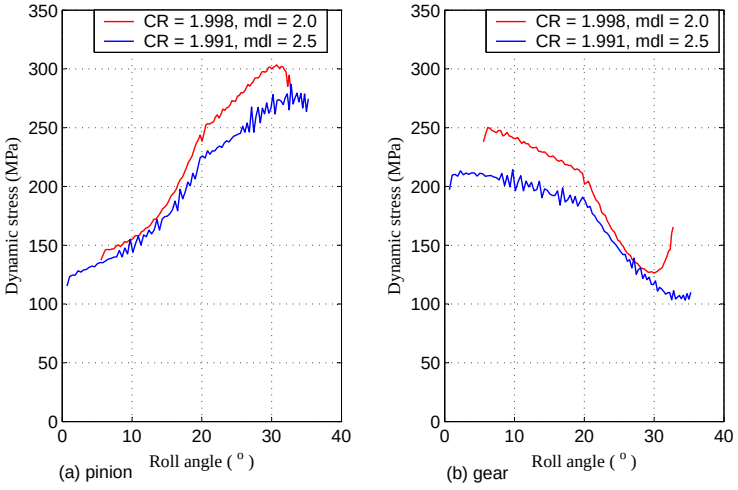

Figure 5.54: Root stress on stage IV gears of gear train 1 for a contact ratio of 2.0

The speed of the gearbox is varied by sliding the speed gears into mesh. This means that the rate of wear for these gears is very high. Thus despite the fact that gears with a module of 2.0 and a contact ratio of 2.0 show lower vibration levels than those with a module of 2.5 and a contact ratio of 2.0, those with a module of 2.5

exhibit lower stresses and have a larger tooth thickness and would therefore be more suitable for this application. It is therefore recommended that the gears with a module of 2.5 and a contact ratio of 2.0 be adopted in the design of the gearbox.

CHAPTER 6

CONCLUSIONS AND RECOMMENDATIONS

6.1 Conclusions

This work investigated parametrically excited torsional vibrations for multistage tractor gearbox through numerical methods. The primary concern of the study was to model the vibrations of a multistage gear train and to analyze the effects of gear design parameters (module, pressure angle and contact ratio) on the vibration levels of the gear pairs in contact and consequently obtain the best configuration of the gear train that would result to minimum vibrations while at the same time maintaining low bending stresses.

Procedures for computing the tooth profile, mesh stiffness, periodic frictional torque and simulation of the model were coded in a FORTRAN program. The validity of the code was verified using experimental results from a single stage gear test rig developed at the NASA Lewis gear research center. The results from the code were found to correlate well with the experimental data which has led to the conclusion that the analysis simulates the physical behaviors of the gears.

The results from this work indicate that parametric variations have a dominant effect on the dynamic response of the system. The dynamic loads were found to be much higher than the corresponding quasi-static load which resulted in much higher dynamic stresses on the gear teeth. This shows that dynamic analysis of geared systems is necessary at the design stage in order to predict the performance and life of the gears. The dynamic stresses obtained from this study were compared with the allowable AGMA bending strength to analyze the possibility of failure.

The results also show that reducing the module of the gears from 3.0 to 2.5 and 2.0, reduces the vibration levels slightly especially for module 2.0. However, this results to relatively high bending stresses which in some cases are above the recommended AGMA bending stress. Increasing the pressure angle to 25^o reduces the vibration levels slightly and also the bending stresses. However, increasing the pressure angle increases the single-tooth contact zone thereby increasing the fraction of time that a single tooth carries all the load. Increasing the contact ratio to a value close to 2.0, reduces the vibration levels significantly and results to a gentle response. For gears with a high reduction ratio, a contact ratio close to 2.0 can only be obtained by using a smaller module. The results showed that increasing the contact ratio to 2.0 reduces the vibration levels by about 75% while the dynamic root stresses on the gears are reduced by about 45%. Though the gears with a high contact ratio and a module of 2.0 exhibit lower vibration levels than corresponding gear pairs with a module of 2.5, they exhibit higher bending stresses. We can therefore conclude that gears with a module of 2.5 and increased addendum to increase the contact ratio produces the best combination of low vibration levels and bending stress.

The computer code developed in this study also predicts the torsional natural frequencies and mode shapes of the system. Knowledge of the natural frequencies can provide an insight on possibilities of resonance occurring within the operating speed range of the gearbox when the rotation speed corresponds to one of the natural frequencies. In this analysis, it was found that the operating speed range of the gearbox is way below the natural frequencies of the system thereby ruling out any possibilities of resonance occurring.

Finally, the computer code developed in this study can be easily adapted to any

multistage gear train with minimal changes. The inputs required by the program are the gear parameters for each reduction stage, inertias of the rotors, lengths and diameters of the shafts and whether they are solid, hollow or splined. For standard gears, the program checks for interference and recommends a value for addendum modification of the gear pair to avoid interference and minimize the bending stress at the lowest point of contact for the pinion. The outputs from the code are the static and dynamic transmission errors, static and dynamic loads, static and dynamic bending stresses and natural frequencies and their mode shapes.

6.2 Recommendations for Future Work

Even though a model to study the parametrically induced vibrations on a multistage tractor gearbox has been developed and verified using available experimental data, there are other fundamental areas that should be addressed in future.

(a) The effect of coupling between lateral and torsional vibrations should be analyzed. This will take into consideration lateral bending of shafts and shaft deflections due to bearing deformations. This will play a vital role in improving the accuracy of the model in determining the dynamic characteristics of a multistage gear train.

(b) The effect of deformation of gear rims to the gear vibrations should be analyzed. This will play a big role in exploring the use of thin-rimmed gears in the system, thereby reducing the weight of the gearbox. The use of finite element analysis should also be considered in this area.

(c) Thorough literature review has shown that experimental work on multistage gear trains is limited. Experimental work will not only play a vital

role in validating the model but also contribute to the data bank on gear dynamics that can be used by other researchers.

(d) The analysis should be extended to include helical gears and synchronizers. This will lead to the design of a smooth running gearbox and a reliable gearshift method.

(e) The development of a user-interface that is user friendly should be explored. This will ensure that even a designer who does not understand the programming language used in this study can use the code to analyze the dynamics of a gearing system.

REFERENCES

[1] J. Wang, "Numerical and Experimental Analysis of Spur Gears in Mesh," PhD Thesis, Curtin University of Technology, 2003.

[2] W. Zeping, "Stresses and Deformations in Involute Spur Gears By Finite Element Method," Master's thesis, College of Graduate Studies and Research, University of Saskatchewan, 2004.

[3] M. Vaishya and R. Singh, "Strategies for Modeling Friction in Gear Dynamics," *Journal of Mechanical Design*, vol. 125, pp. 383–393, 2003.

[4] J. H. Kuang and A. D. Lin, "The Effect of Tooth Wear on the Vibration Spectrum of a Spur Gear Pair," *Journal of Vibrations and Acoustics*, vol. 123, pp. 311–317, 2001.

[5] M. Vaishya and R. Singh, "Analysis of Periodically Varying Gear Mesh Systems with Coulomb Friction Using Floquet Theory," *Journal of Sound and Vibration*, vol. 243(3), pp. 525–545, 2001.

[6] R. G. Parker, S. M. Vijayakar and T. Imajo, "Non-linear Dynamic Response of a Spur Gear Pair: Modelling and Experimental Comparisons," *Journal of Sound and Vibrations*, vol. 237(3), pp. 435–455, 2000.

[7] L. Gelman, V. Giurgiutiu and A. Bayoumi, "Statistical Analysis of the Dynamic Mean Excitation for a Spur Gear," *Journal of Vibrations and Acoustics*, vol. 127, pp. 204–207, 2005.

[8] G. Bonori, A. O. Andrisano and F. Pellicano, "Stiffness Evaluation and Vibration in a Tractor Gear," *ASME International Mechanical Engineering Congress and Exposition*, 2004.

[9] M. A. Faith and O. Milosav, "Gear Vibration in Supercritical Mesh-Frequency Range," *Faculty of Mechanical Engineering (FME), Belgrade*, vol. 32, pp. 87–94, 2004.

[10] R. G. Timothy, "Computer- Aided Design Software for Torsional Analysis," Master's thesis, Virginia Polytechnic Institute and State University, 1998.

[11] J. Lin and R. G. Parker, "Sensitivity of Planetory Gear Natural Frequencies and Vibration Modes to Model Parameters," *Journal of Sound and Vibration*, vol. 228(1), pp. 109–128, 1999.

[12] Hsiang Hsi Lin and Chuen-Huei Liou, "A Parametric Study of Spur Gear Dynamics," Tech. Rep., National Aeronautics and Space Administration (NASA), Lewis Research Center, 1998.

[13] H. H. Lin, C. Lee, F. B. Oswald and D. P Townsend, "Computer-Aided Design of High-Contact-Ratio Gears for Minimum Dynamic Load and Stress," tech. rep., National Aeronautics and Space Administration, 1991.

[14] Tae Hyong Chong, Jae Hyong Myong and Ki Tae Kim, "Tooth Modification of Helical Gears for Minimization of Vibration and Noise," *International Journal of the Korean Society of Precision Engineering*, vol. 2, pp. 5–11, 2001.

[15] Chinwai, L., Hsiang, H. L., Fred, B. O. and Townsend, D. P., "Influence of Linear Profile Modification and Loading Conditions on the Dynamic Tooth

Load and Stresses of High Contact Ratio Gears," Tech Rep., NASA Lewis Research Center, 1990.

[16] Y. Kikaganeshwala, "Vibration Analysis of Geared System as Combined Rotor System based on Complex Rotor Variable," Masters Thesis, University of Cincinnati, 2005.

[17] S. Kim and R. Singh, "Gear Surface Roughness Induced Noise Prediction Based on Linear Time Varying Model with Sliding Friction," *Journal of Vibrations and Control*, vol. 13, pp. 1045–1063, 2007.

[18] Hsiang-Hsi Lin, *Computer - Aided Design and Analysis of Spur Gear Dynamics*. PhD Thesis, University of Cincinnati, 1985.

[19] Shengxiang Jia, Ian Howard and Jiande Wang, "The Dynamic Modeling of Multiple Pairs of Spur Gears in Mesh, Including Friction and Geometric Errors," *International Journal of Rotating Machinery*, vol. 9, pp. 437–442, 2003.

[20] H. Xu and A. Kahraman, "Prediction of Mechanical Efficiency of Parallel - Axis Gear Pairs," *Transactions of ASME*, vol. 129, pp. 58–68, 2007.

[21] R. W. Cornell, "Compliance and Stress Sensitivity of Spur Gear Teeth," *ASME Journal of Mechanical Design*, vol. 103, pp. 447–459, 1981.

[22] A. Crowther, "PowerTrain Vibration: Modelling, Simulation and Testing," Tech. Rep., University of Technology, Sidney, 2004.

[23] P. Heingartner and D. Mba, "Determining Power Losses in the Helical Gear Mesh," *Gear Technology*, pp. 32–37, 2005.

[24] S. M. Mahbub, M. A. Wahed and M. A. Salam, "Parametric Solution of Spur Gear Tooth Under Tip Load," Tech Rep., Mechanical Engineering Department, Bangladesh University of Engineering and Technology, 2004.

[25] N. Sarkar, R. E. Ellis and T. N. Moore, "Backlash Detection in Geared Mechanisms: Modeling, Simulation and Experimentation," *Mechanical Systems and Signal Processing*, vol. 11(3), pp. 391–408, 1996.

[26] Tamminana, V. K., Kahraman, A. and Vijayakar, S., "A study of the Relationship Between the dynamic factor and the dynamic transsmission error of spur gear pairs," in *ASME 2005 International Design Engineering Technical Conferences and Computers and Information in Engineering conference*, September 24-28 2005.

[27] N. V. Khang, M. C. Thai and P. D. Nguyen, "Modelling Parametric Vibration of Gear Pair System as a Tool for Aiding Fault Diagnosis," *Technische Mechanik*, vol. 24, pp. 198–205, 2004.

[28] Shaobin Li, H. Z. Huang, X. Fan, Q. Miao, "Nonlinear Dynamic Simulation of Coupled Lateral-Torsional Vibrations of a Gear Transmission System," *International journal of Computer Science and Network Security*, vol. 6, pp. 27–35, 2006.

[29] K. G. Sejoong Oh and J. R. Barber, "Energy Conserving Equations of Motion for Gear Systems," *Journal of Vibrations and Acoustics, Transactions of ASME*, vol. 127, pp. 208–212, 2005.

[30] R. G. Parker, V. Agashe and S. Vijayakar, "Dynamic Response of a Planetary Gear System Using a finite Element/Contact Mechanics Model," *Transactions of ASME, Journal of Mechanical Design*, vol. 122, pp. 304–310, 2000.

[31] Y. Diab, F. Ville and P. Velex, "Prediction of Power Losses Due to Tooth Friction in Gears," *Tribology Transactions*, vol. 49, pp. 260–270, 2006.

[32] E. Garcia, P. Gonzalez de Santos and C. Canudas de Wit, "Velocity Dependence in the Cyclic Friction Arising with Gears," *International Journal of Robotics Research*, vol. 21, pp. 761–771, 2002.

[33] H. Xu, *Developement of a generalized Mechanical Efficiency Prediction Methodology for Gear Pairs*. Phd Thesis, The Ohio State University, 2005.

[34] F. B. Ostwald, D. P. Townsend, B. Rebbechi and H. H. Lin, "Dynamic Forces in Spur Gears: Measurement, Prediction and Code Validation," Tech. Rep., NASA Lewis Research Center, 1996.

[35] R. Maliha, C. U. Dogruer and H. N. Ozguven, "Nolinear Dynamic Modeling of Gear-Shaft-Disk-Bearing Systems Using Finite Elements and Describing Functions," *Journal of Mechanical Design*, vol. 126, pp. 534–541, 2004.

[36] N. Driot, E. Rigaud and J. Perret-Liaudet, "Variability of Critical Rotational Speeds of Gearbox Induced by Misalignment and Manufacturing Errors," Tech Rep., Laboratoire de Tribologie et Dynamique des Systemes, 2000.

[37] Y. H. Guan, W. S. Shepard Jr., T. C. Lim and Mingfeng Li, "Experimental Analysis of an Active Vibration Control System for Gearboxes," *Journal of Smart Materials and Structures*, vol. 13, pp. 1230–1237, 2004.

[38] J. Leitner, "Transmission Simulation with Adams," tech. rep., Steyr-Daimler-Puch Engineering Center Steyr, 2000.

[39] J. S. Rao, T. N. Shiau and J. R. Chang, "Theoretical Analysis of Lateral Response Due to Torsional Excitation of Geared Rotors," Tech. Rep., National Science Council of Taiwan, 1996.

[40] H. H. Li and R. L. Huston, "Dynamic Loading on Parallel Shaft Gears," Tech Rep., NASA Lewis Research Center, 1986.

[41] S. Vasilios and S. Christos, "Non-linear Dynamic Simulation of Spur Gears with Indexing Errors and Profile Modifications," in *Modelling, Identification and Control*, vol. 500, pp. 354–359, February 2006.

[42] T. L. Krantz and M. Rashidi, "Vibration Analysis of a Split Path Gearbox," Tech. Rep., Army Research Laboratory, NASA, 1995.

[43] Jian Lin and R. G. Parker, "Mesh Stiffness Variation Instabilities in a Two stage Gear System," *Transactions of ASME, Journal of Vibration and Acoustics*, vol. 124, pp. 68–76, 2002.

[44] T. Takuechi and K. Togai, "Gear Whine Analysis with Virtual Power Train," Tech Rep. 16, Mitsubishi Motors, 2004.

[45] D. V. J. Peeters and P. Sas, eds., *Flexible Multibody Model of a Three-stage Planetary Gearbox in a Wind Turbine*, ISMA, 2004.

[46] F. K. Choy, Y. K. Tu and D. P. Townsend, "Vibration Signature Analysis of a Multistage Gear Transmission," Tech Rep., NASA Lewis Research Center, 1989.

[47] P. H. Lin, H. H. Lin, F. B. Oswald and D. P. Townsend, "Using Dynamic Analysis for compact Gear Design," Tech. Rep., National Aeronautics and Space Administration, NASA, 1998.

[48] V. Spitas, T. H. Costopoulos and C. Spitas, "Increasing the Stength of Standard Involute Gear Teeth with Novel Circular Root Fillet Design," *American Journal of Applied sciences*, vol. 6, pp. 1058–1064, 2005.

[49] Hsiang Hsi Lin, Chuen-Huei Liou, F. B. Oswald and D. P. Townsend, "Balancing Dynamic Strenth of Spur Gears Operated at Extended Center Distance," Tech. Rep., National Aeronautics and Space Administration, NASA, 1996.

[50] S. Cananau, "3-D Contact Stress Analysis for Spur Gears," in *National Tribology Conference*, pp. 349–351, September 2003.

[51] S. C. Mohanty, "Tooth Load Sharing and Contact Stress Analysis of High Contact Ratio Spur Gears in Mesh," *IE(I) Journal-MC*, vol. 84, pp. 66–70, 2002.

[52] S. Glodez, D. T. Jelaska and J. Kramberger , "A Computational Model for Calculation of Load Capacity of Gears," Tech. Rep., University of Maribor, Faculty of Mechanical Engineering, 2000.

[53] H. J. Sutherland and D. P. Burwinkle, "The Spectral Content of the Torque Loads on a Turbine Gear Tooth," *Wind Energy, ASME*, vol. 16, pp. 91–97, 1995.

[54] M. Ristivojevic, "Developement of the Theoretical Model for Determining the Stress Athoritative for Checking the Gear Tooth Volume Strength," *Mechanical Engineering*, vol. 1(9), pp. 1135–1145, 2002.

[55] P. Somprakit, R. L. Huston and F. B. Oswald, "Contact Stresses in Gear Teeth-A New Method of Analysis," Tech. Rep., National Aeronautics and Space Administration (NASA), 1991.

[56] G. D. Bibel, S. K. Reddy, M. Savage and R. F. Handschuh, "Effects of Rim Thickness on the Spur Gear Bending Stress," Tech Rep., NASA Lewis Research Center, 1991.

[57] N. E. Anderson and S. H. Loewenthal, "Efficiency of Non-Standard High Contact Ratio Involute SpurGears," Tech Rep., NASA Lewis Research Center, 1984.

[58] A. Kahraman, Donald R. Houser and Hai Xu, "Developement of a Generalized Mechanical Efficiency Prediction Methodology For Gear Pairs," Tech Rep., AGMA Foundation, October 2005.

[59] A. K. H. Xu and D. R. Houser, "A Model to Predict Friction Losses of Hypoid Gears," Tech Rep., AGMA Foundation, October 2005.

[60] E. Podzharov, A. Mozuras and J. A. Sanchez, "Design of High contact Ratio Spur Gears to Reduce Static and Dynamic Transmission Error," *Ngenieria Mecanica Tecnologia y Desarrollo*, vol. 1(003), pp. 85–90, 2003.

[61] E.-S. Aziz and C. Chassapis, "Knowledge-based Geometry Generation for Spur and Helical Gears," *Concurrent Engineering*, pp. 251–261, 2002.

[62] J. D. Smith, *Gears and Their Vibrations*. New York and Basel London and Basingstoke Publishers, 1983.

[63] J. M. Gere and S. P. Timoshenko, *Mechanics of Materials*. PWS Publishers, Boston, second ed., 1987.

[64] P. P. Benham and R. J. Crawford, *Mechanics of Engineering Materials*. Longman Scientific and Technical, 1987.

[65] J. Case and A. H. Chilver, *Strength of Materials and Structures*. Edward Arnold (Publishers) Limited, second ed., 1971.

[66] K. L. Johnson, *Contact Mechanics*. Cambridge University Press, 1985.

[67] B. J. Hamrock, *Fundamentals of Fluid Film Lubrication*. McGraw-Hill, Inc, 1994.

[68] M. L. James, G. M. Smith and P. W. Whaley, *Vibration of Mechanical and Structural systems*. Harper Collins College Publishers, 2nd ed., 1994.

[69] H. Press William, P. Flannery Brian, P. Teukolsky Saul and T. Vetterling William, *Numerical Recipes in Fortran: The Art of Scientific Computing*. Cambridge University Press, 1992.

[70] E. Buckingham, *Analytical Mechanics of Gears*. Buckingham Associates, Inc, Springfield, Vermont in Association with Dover Publications, Inc., Newyork, 1988.

[71] J. S. Rao and K. Gupta, *Introductory Course on Theory and Practice of Mechanical Vibrations*. New Age International (P) Limited, 1995.

[72] J. E. Shigley and C. R. Mischike, *Mechanical Engineering Design*. McGraw-Hill International Editions, 5th ed., 1989.

[73] J. K. Kimotho, "Re-Design of a Tractor Gearbox," Tech. Rep., Jomo Kenyatta University of Agriculture and Technology, 2006.

[74] D. W. Dudley, *GEAR HANDBOOK: The Design, Manufacture and Application of Gears*. McGraw-Hill Publishing Company, Newyork, 1st ed., 1962.

[75] D. P. Townsend, *Dudley's Gear Handbook*. McGraw-Hill, Inc., 2nd ed., 1992.

APPENDIX A

Description of the Gearbox

The gearbox to be studied has been designed by the researcher [**?**] under the supervision of a departmental staff. It is part of the on-going **Tractor Project** at the Department of Mechanical Engineering, JKUAT aimed at developing an affordable tractor for small scale applications such as ploughing, lawn mowing, water pumping and transport.

The gearbox has six forward speeds and two reverse speeds with a maximum road speed of 35 Km/h. The gear train consists of seventeen (17) gears and six (6) shafts and eleven (11) bearings. The gears and shafts are made of low carbon alloy steel (EN9). The gearbox is to be powered by a 6.5 HP diesel engine via V-belts. The speeds are achieved in two stages:

(a) Low range - applied when high torque and low speed is required for instance in off-road duties like ploughing and when moving the loaded tractor up a steep hill.

(b) High range - applied when high speed is required.

Table A.1 shows these speeds and their corresponding gear ratios and maximum road speed. The gearbox is also fitted with a PTO (Power Take Off) shaft to drive auxiliary equipment such as lawn mowers and water pumps. Figure A.1 shows a 3-D section of the gearbox while Figure A.2 shows the front and end views of the gearbox. The speed change is achieved by sliding the speed gears into mesh and this is the reason why the spur gears are recommended for this gearbox.

Table A.1: Speed ratios and corresponding maximum road speed for each speed

Low range		
Speed	Gear ratio	Road speed (Km/h)
Reverse	63.440	2.407
1st	54.087	2.823
2nd	32.182	4.744
3rd	15.144	10.082
High range		
Reverse	18.659	8.183
1st	15.908	9.598
2nd	9.465	16.131
3rd	4.354	35.067

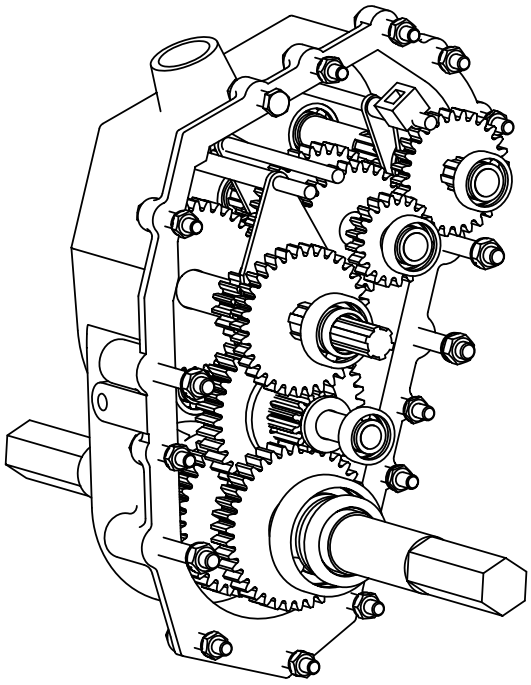

Figure A.1: An isometric section of the gearbox

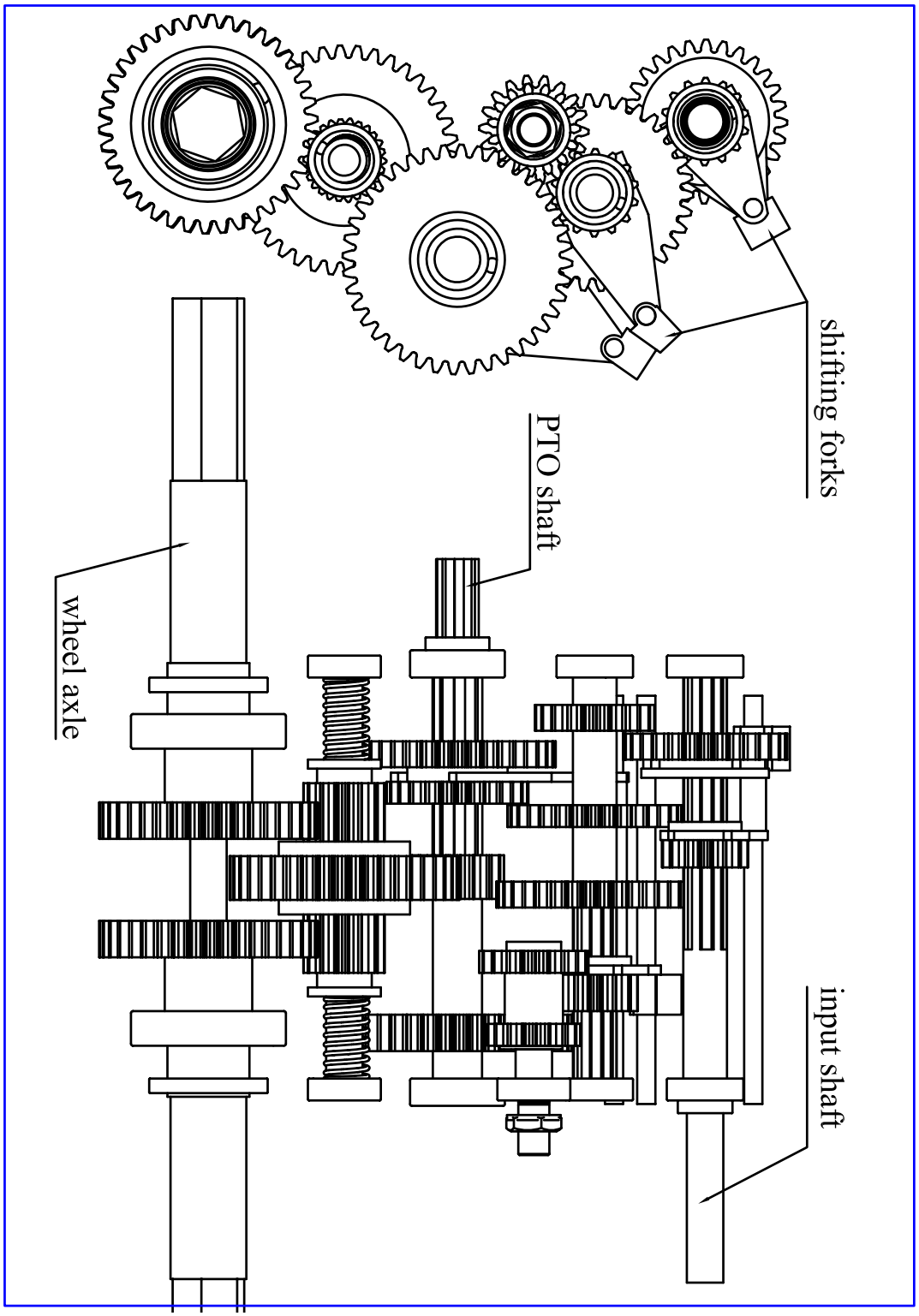

Figure A.2: Orthographic views of the gearbox

APPENDIX B

Analysis of Spur Gear Tooth Geometry

B.1 Introduction

The essential purpose of gear tooth profiles is to transmit rotary motion from one shaft to another. In majority of cases, the additional requirement of uniform rotary motion exists [70]. Gear teeth are a series of cam surfaces that contact similar surfaces on a mating gear in an orderly fashion [75]. In order to drive in a given direction and to transmit power or motion smoothly and with a minimum loss of energy, the contacting cam surfaces on the mating gears must have the following properties [75]:

1. The height and lengthwise shape of the active profiles of the teeth (cam surfaces) must be such that, before one pair of teeth goes out of contact during mesh, a second pair will have picked up its share of load. This is called **continuity of action**.

2. The shape of the contacting surfaces of teeth (active profiles) must be such that the angular velocity of the driving member of the pair is smoothly imparted to the driven member in the proper ratio.

3. The spacing between the successive teeth must be such that a second pair of the tooth contacting surfaces (active profiles) are in the proper positions to receive the load before the first leaves mesh.

Many different shapes of surfaces can be used on teeth to produce uniform transmission of motion. Curves that act on each other with a resulting smooth driving

action and with constant driving ratio are called **conjugate curves**. The fundamental requirements governing the shapes that any pair of tooth form acting on each other must have can be summarized in Buckingham's "Basic law of gearing", which states that, "normals to the profiles of mating teeth must at all points of contact pass through a point located on the line of centers" [75]. In case of spur and helical type gears, the curves used almost exclusively are those of the involute family. In involute curves, the fixed point mentioned in the basic law is the pitch point. The involute curve has the following properties which make it satisfy all the requirements of the basic law of gearing [75]:

i. All contact takes place along the line of action.

ii. The line of action is normal to both the driving and the driven involutes at all possible points of contact.

iii. The line of action passes through the pitch point.

Previously, the cycloidal family of curves was commonly used in power transmission applications, but they have been replaced by involute curves due to the following reasons [75]:

- greater ease of design.
- far less sensitive to manufacturing and mounting errors
- tools used to generate the cycloid are more difficult to make with same degree of accuracy as those of the involute.

However, cycloidal gears still do find application in clockwork.

B.2 Tooth Profiles

The gear tooth profile can be determined analytically from some basic geometrical parameters which are derived based on the simulation of the cutting tool motion on the gear as shown in Figure B.1.

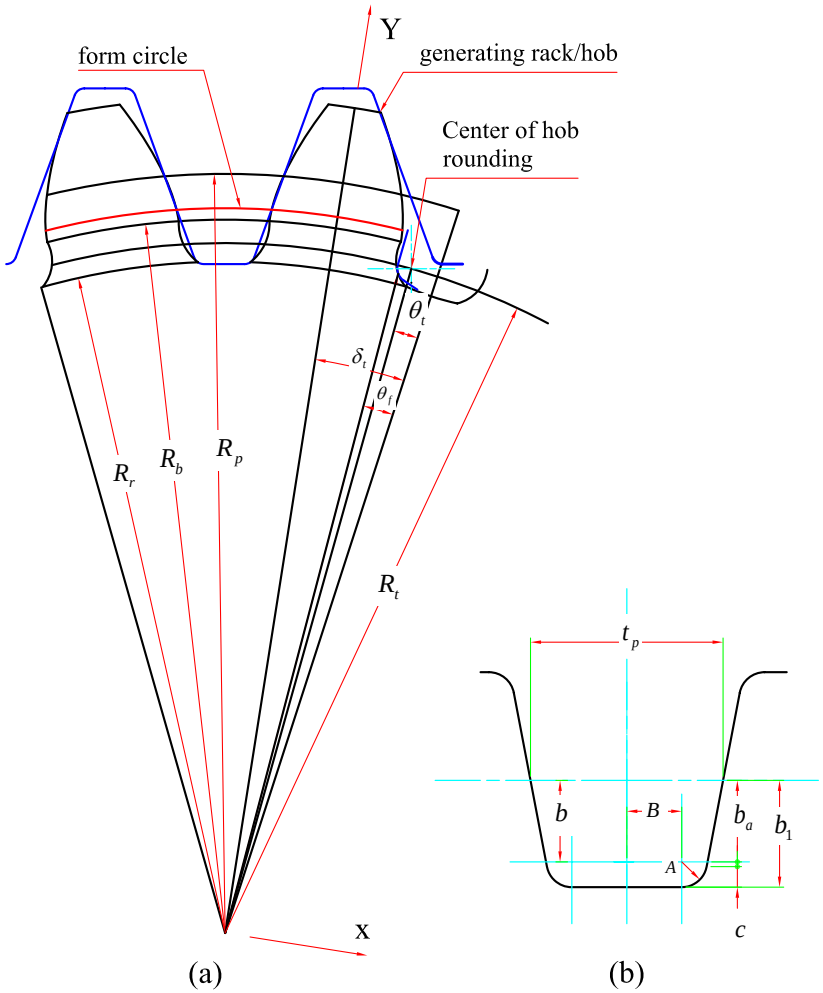

Figure B.1: (a) Kinematics of gear cutting. (b) Hob tooth proportions

The gear tooth profile can be split into three distinct regions. The first part of the gear tooth profile, the working portion (involute) is cut by the linear flank of the

rack cutter. The second part, which is the root circle is generated by the tip of the rack. The third portion, the fillet, connects the working portion to the root circle and is generated by the cutter tip radius.

B.3 The Involute Curve as a Tooth Profile

The involute curve is used almost exclusively for spur gear tooth profiles that are employed to transmit power. The involute meets all the kinematic requirements for a gear tooth profile as explained in section B.1. The involute is the curve that is described by the end of a line that is unwound from the circumference of a circle as shown in Figure B.2. The circle from which the string is unwound is called the **base circle**.

From the geometric conditions shown in Figure B.2, we have:

$$\theta = \beta - \psi = \beta - tan^{-1}\frac{\sqrt{r^2 - R_b^2}}{R_b}, \tag{B.1}$$

The length of the generating line PA is also the length of the circumference of the base circle subtended by the angle β, hence,

$$\sqrt{r^2 - R_b^2} = R_b\beta \Rightarrow \beta = \frac{\sqrt{r^2 - R_b^2}}{R_b}, \tag{B.2}$$

Hence,

$$\theta = \frac{\sqrt{r^2 - R_b^2}}{R_b} - tan^{-1}\frac{\sqrt{r^2 - R_b^2}}{R_b}. \tag{B.3}$$

Equation B.3 is known as the polar equation of the involute curve. The generating line PA is always normal to the involute curve and its length is the radius of curvature of the involute curve at any point described by the end of this line [18]. An involute gear tooth form consists of two similar involute curves with a common base circle. When relative positions are known at any radius, their relative positions at any

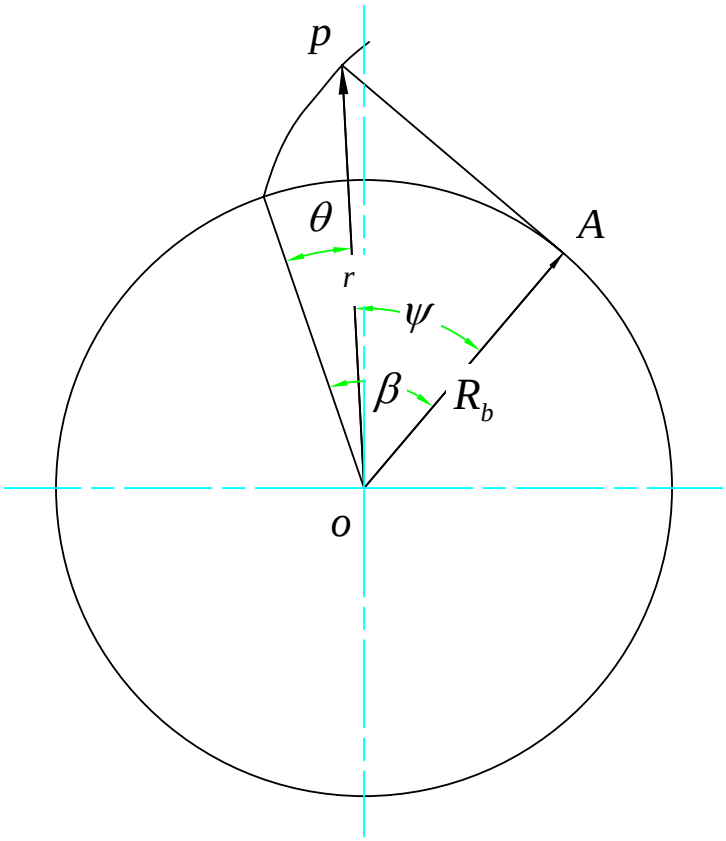

Figure B.2: Involute curve geometry

other radius can be readily determined. In general, this is accomplished by first determining their relative positions at the base circle, and then adding or subtracting the vectorial angle of the involute for any other radius. The process of calculating involute gear tooth relationships is called **involumetry** [70]. These relationships are shown in Figure B.3.

Given the pitch radius R_p, the pressure angle ϕ and the circular pitch p_c, let an X-Y coordinate system be defined as shown in Figure B.3. Along with the determination of all points of the tooth, it is important, for the purpose of analyzing stress and deflection, to be able to compute the thickness of a tooth at any radius. The circular tooth thickness on the pitch circle, t_p is half the circular pitch p_c. The circular tooth

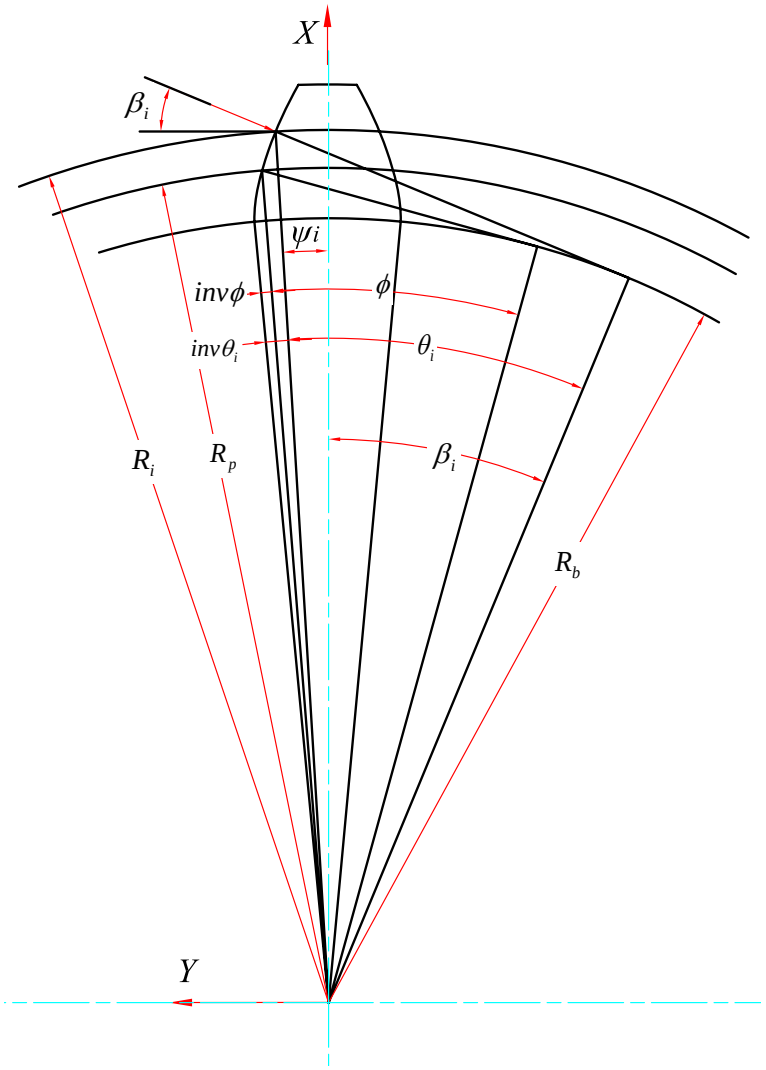

Figure B.3: Involumetry of spur gears

thickness t_i at any point i on the tooth profile, with radius R_i from the gear center can be expressed as:

$$t_i = 2R_i\{\frac{t_p}{2R_p} + inv\phi - inv\theta_i\}, \tag{B.4}$$

where

$$\theta_i = cos^{-1}\frac{R_b}{R_i}, \tag{B.5}$$

and

$$invx = tanx - x. \tag{B.6}$$

The term on the left hand side of equation B.6 is the involute function of an angle x. The angle ψ_i between the Y-axis and radius R can be found as

$$\psi_i = \frac{t_p}{2R_p} + inv\phi - inv\theta_i, \tag{B.7}$$

The direction β_i of the transmitted load at any point i on the tooth profile with respect to X-axis is given by:

$$\beta_i = \theta_i - \psi_i, \tag{B.8}$$

The chordal thickness h at any point i on the tooth profile is given by:

$$h_i = 2_i sin\psi_i, \tag{B.9}$$

The X and Y coordinates of any point i on the tooth profile are:

$$Y_i = R_i sin\psi_i, \tag{B.10}$$

$$X_i = R_i cos\psi_i. \tag{B.11}$$

These coordinates of points on the tooth profile will be used to generate geometry properties for the calculation of deflection of involute gear teeth.

B.4 Root Fillet Profile

The tooth fillet is the curved surface that connects the root circle (dedendum circle) and the tooth flank of the gear and is generated by the trochoidal envelope of the cutter tip. A trochoid is a curve which is traced on a rotating plane by a designated point on a second plane. When the second plane moves in a straight line, we have

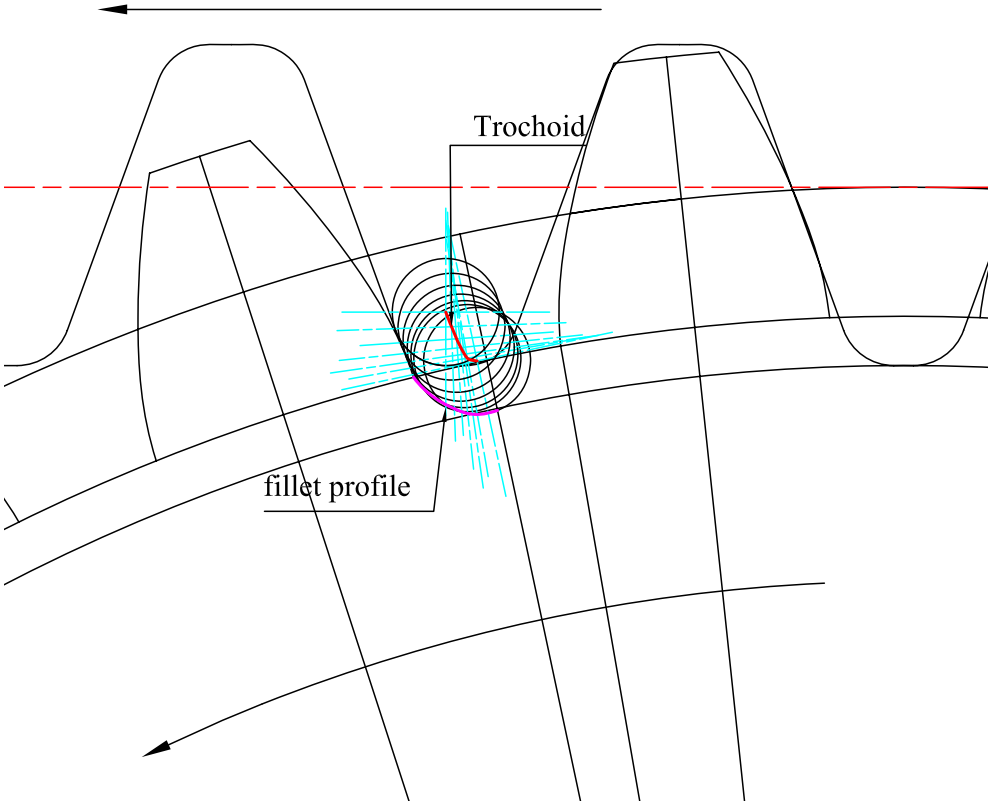

Figure B.4: Simulation of the cutting tool motion on the gear

a rack trochoid, which is the curve on a gear traced by a point on a meshing rack as shown in Figure B.4 [74].

When the rack tooth represents the form of the generating tool, then this trochoid gives the form of the fillet of the gear tooth. When no undercut is present, this trochoid will be tangent to the generated gear-tooth profile. When the rack is represented by the cutting tooth of a rack-shaped cutter or of a hob, the corners of these cutting teeth are generally rounded. In such cases the center of the rounding will follow the trochoidal path but the actual form of the fillet will be the envelope of the path of a series of circles equal in size to the rounding of the corners, and

with their centers on the trochoidal path as shown if Figure B.4.

Coordinates of a point on the fillet portion can be calculated from the geometric conditions shown in Figure B.5

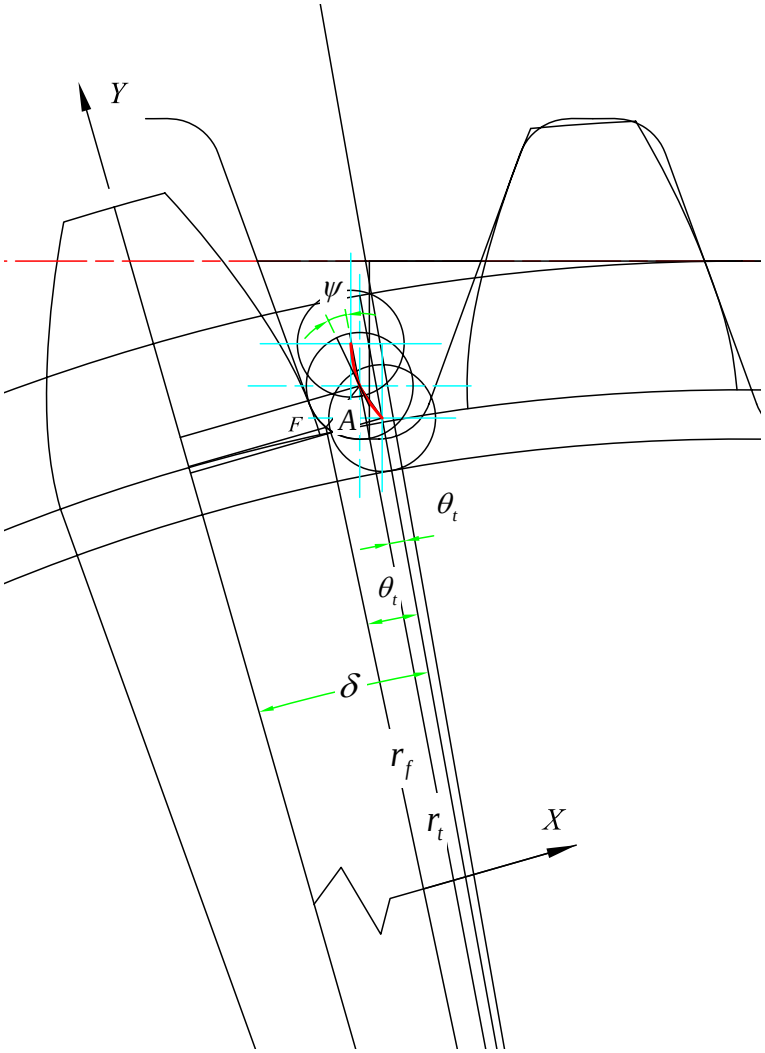

Figure B.5: Geometry for calculation of fillet coordinates

From the geometric conditions shown in Figure B.5,

$$\theta_t = tan^{-1}\{\frac{\sqrt{r_t^2-(R_p-b)^2}}{R_p-b} - \frac{\sqrt{r_t^2-(R_p-b)^2}}{R_p}, \tag{B.12}$$

$$tan\psi_t = \frac{R_p(R_p-b)-r_t^2}{R_p\sqrt{r_t^2-(R_p-b)^2}}, \tag{B.13}$$

$$r_f = \sqrt{r_t^2 + A^2 - 2Ar_t sin\psi_t}, \tag{B.14}$$

$$\theta_f = \theta_t + cos^{-1}\{\frac{r_t - Asin\psi_t}{r_f}\}. \tag{B.15}$$

where:

b distance from pitch line of hob to center of rounding

A radius of rounding of the hob edges.

r_t any radius of trochoid curve.

θ_t vectorial angle of trochoid radius.

ψ_t angle between tangent to trochoid curve and radius vector.

r_f any radius of the fillet profile.

θ_f Vectorial angle of fillet radius

c clearance

Other symbols remain as defined in the text.

$$A = \frac{c}{(1 - sin\phi)}, \tag{B.16}$$

$$b = b_1 - A, \tag{B.17}$$

and

$$B = \frac{t_p}{2} - (btan\phi + \frac{A}{cos\phi}). \tag{B.18}$$

To determine the coordinates of the actual fillet when the corner of the hob is rounded, we must first calculate the coordinates of the trochoid of the center of the rounded corner and then calculate the actual fillet.

Let,

δ_t angle between centerline of gear tooth and origin of trochoid

θ_s vectorial angle of fillet radius in reference to the centerline of the tooth.

X_f abscissae of the fillet profile.

Y_f ordinate of the fillet profile.

then,

$$\delta_t = \frac{t_p - B}{R_p}, \tag{B.19}$$

$$\theta_s = \delta_t - \theta_f, \tag{B.20}$$

$$X_f = r_f cos\theta_s, \tag{B.21}$$

$$Y_f = r_f sin\theta_s. \tag{B.22}$$

When no undercut is present, the trochoidal fillet will be tangent to the involute profile. This point of tangency for a hob will be the point where the end of the straight-line profile of the hob or basic rack form crosses the path of contact. The intersection of the involute and root fillet profiles lies on the form circle, whose radius can be obtained from equation B.23.

$$R_t = \sqrt{\left(Rsin\phi - \frac{b_a}{sin\phi}\right)^2 + R_b^2}, \tag{B.23}$$

The root radius R_r is given by

$$R_r = R_p - b_1. \tag{B.24}$$

When $r_t = (R_p - b)$, then $\psi_t = 90^o$ and $r_f = R_r$. The above procedure for profile generation were coded into a FORTRAN program. The process starts with the input of gear parameters such as module, number of teeth, pressure angle, clearance and cutter tip radius. The involute and trochoid curves of the gear tooth can then be plotted on a cartesian coordinate system emanating from the center of the gear

as shown in Figure B.6. For the pair of gears in Figure B.6(a), the pinion has a number of teeth less than that recommended to avoid interference and therefore the addendum of both gears are modified by increasing that of the pinion and reducing that of the gear by the same amount.

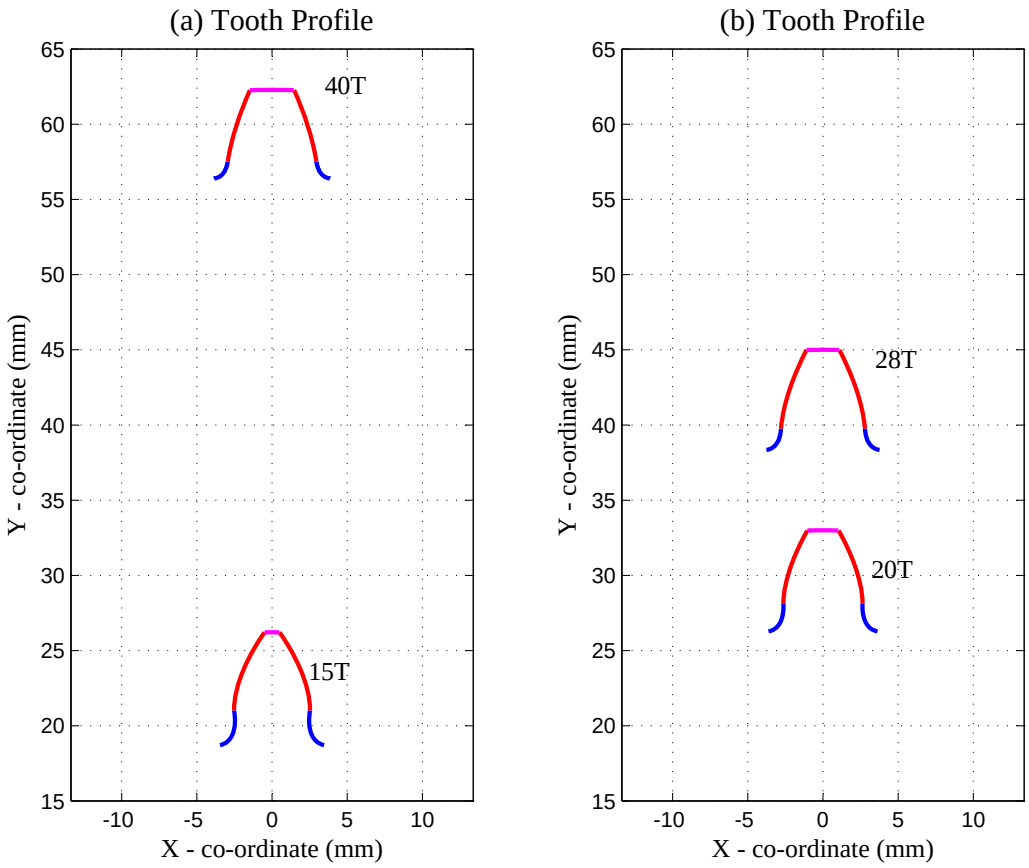

Figure B.6: Generated gear tooth profile (a) with addendum modification (b) standard teeth

Tables B.1 and B.2 shows the parameters used in the generation of the above tooth profiles.

Table B.1: Gear data for a pair of teeth with modified addendum

Parameter	**Pinion**	**Gear**
No. of teeth	15	40
module m	3.0 mm	3.0 mm
pressure angle	20^o	20^o
addendum	1.2385m	0.7615m
clearance	0.157m	0.157m
tip radius	0.7mm	0.7mm

Table B.2: Gear data for a pair of standard teeth

Parameter	**Pinion**	**Gear**
No. of teeth	28	20
module m	3.0 mm	3.0 mm
pressure angle	20^o	20^o
addendum	1.0m	1.0m
clearance	0.157m	0.157m
tip radius	0.7mm	0.7mm

B.5 Kinematics of Gears

Contact between a pair of meshing gears is arranged to occur purely along a specified line of action as shown in Figure B.7. When two involutes are acting on each other, a combined rolling and sliding action takes place between them because of the varying lengths of equal angular increments on the profiles [70].

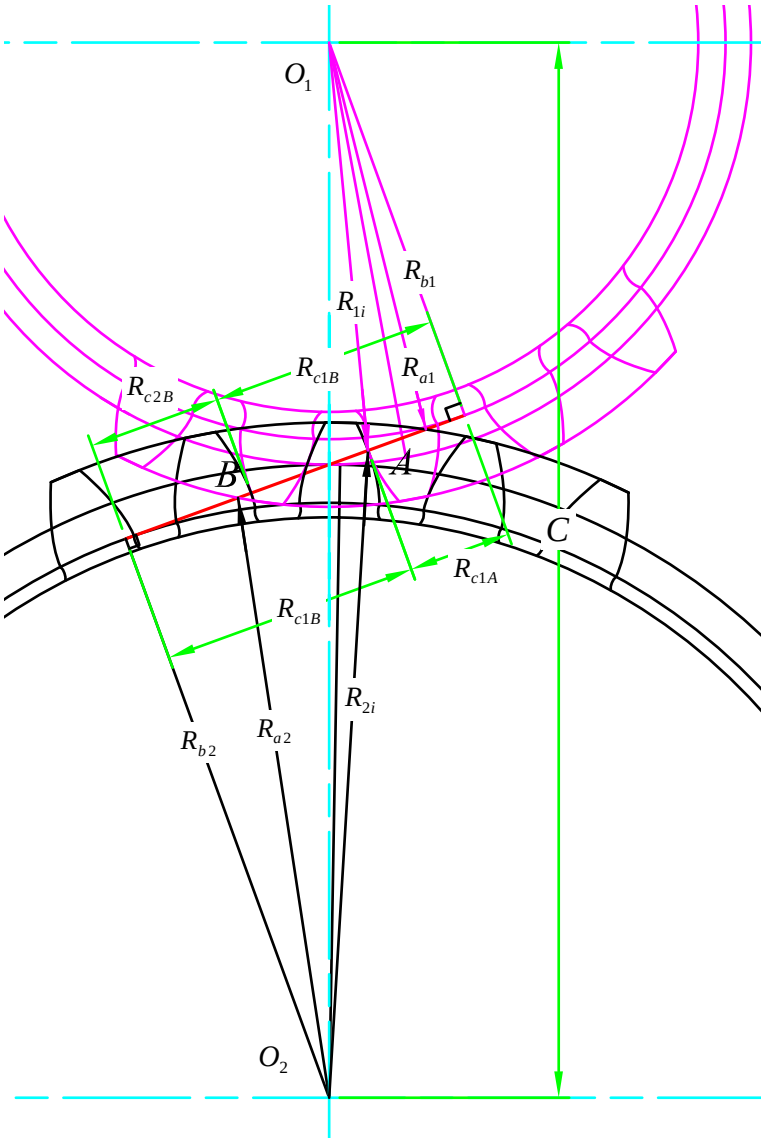

Figure B.7: Meshing action of a pair of spur gears

If we define the sliding velocity as the difference in speed at the ends of the generating lines of the involutes as they pass through the line of action, we can obtain equations for the sliding velocity from the kinematic relations in Figure B.7. The angular velocities of these generating lines will be the same as the angular velocities of the gears themselves. The actual sliding velocities will be the products of these relative

angular velocities and the length of the generating lines or radii of curvature.

Let,

V_p pitch line velocity of the gears.

V_s sliding velocity of the gears.

r_1 any radius of driving gear tooth profile.

r_2 mating radius of driven gear tooth profile.

R_{c1} radius of curvature of driving gear at radius r_1

R_{c2} radius of curvature of mating gear at radius r_2

Then,

$$V_p = R_{p1}\omega_1 \Rightarrow \omega_1 = \frac{V_p}{R_{p1}}, \tag{B.25}$$

$$V_s = (R_{c1}\omega_1 - R_{c2}\omega_2), \tag{B.26}$$

$$\omega_2 = \frac{R_{p1}}{R_{p2}}\omega_1, \tag{B.27}$$

and,

$$R_{c1} + R_{c2} = Csin\phi, \tag{B.28}$$

$$R_{c1} = \sqrt{r_1^2 - R_{b1}^2}, \tag{B.29}$$

Therefore,

$$R_{c2} = \sqrt{r_2^2 - R_{b2}^2} = Csin\phi - \sqrt{r_1^2 - R_{b1}2}. \tag{B.30}$$

Substituting these equations into equation B.26, combining and simplifying, we obtain:

$$V_s = V_p\frac{R_{p1} + R_{p2}}{R_{p1}R_{p2}}(\sqrt{r_1^2 - R_{b1}^2} - R_{p1}sin\phi), \tag{B.31}$$

Equation B.31 may also be written as:

$$V_s = V_p\{\frac{1}{R_{p1}} + \frac{1}{R_{p2}}\}(\sqrt{r_1^2 - R_{b1}^2} - R_{p1}sin\phi), \tag{B.32}$$

From equation B.32, if,

$$\sqrt{r_1^2 - R_{b1}^2} - R_{p1} sin\phi = 0, \tag{B.33}$$

then

$$r_1 = R_{p1} \Rightarrow V_s = 0. \tag{B.34}$$

This implies that the rate of sliding is zero at the pitch point. Actually, the rate of sliding starts quite high, reduces to zero at the pitch point, changes direction and increases again [70]

The active profile of a gear-tooth is that portion of the tooth profile which actually comes into contact with its mating tooth along the line of action. Considering Figure B.7,

let,

R_{a1} radius to bottom of active profile on driving gear.

R_{a2} radius to bottom of active profile on driven gear.

$$R_{a1} = \sqrt{[Csin\phi - \sqrt{(R_{o2}^2 - R_{b2}^2)}]^2 + R_{b1}^2}, \tag{B.35}$$

$$R_{a2} = \sqrt{[Csin\phi - \sqrt{(R_{o1}^2 - R_{b1}^2)}]^2 + R_{b2}^2}. \tag{B.36}$$

Given the radius of the driving gear at any point of contact, the corresponding radius on the mating gear can be obtained from equation B.37

$$R_{2i} = \sqrt{[Csin\phi - \sqrt{(R_{1i}^2 - R_{b1}^2)}]^2 + R_{b2}^2}. \tag{B.37}$$

B.6 Analysis of Gear Teeth Meshing Cycle

The numbers of teeth in contact for a meshing pair of gears vary along the path of contact depending on the contact position and contact ratio. For low contact

ratio gears, the number of teeth in contact alternates between 1 and 2. For the case shown in Figure B.8, we have two pairs of teeth in contact, at point A and point C. Figure B.8, illustrates the motion of a pair of meshing teeth when a gear rotating about center O_1 drives another gear rotating about center O_2.

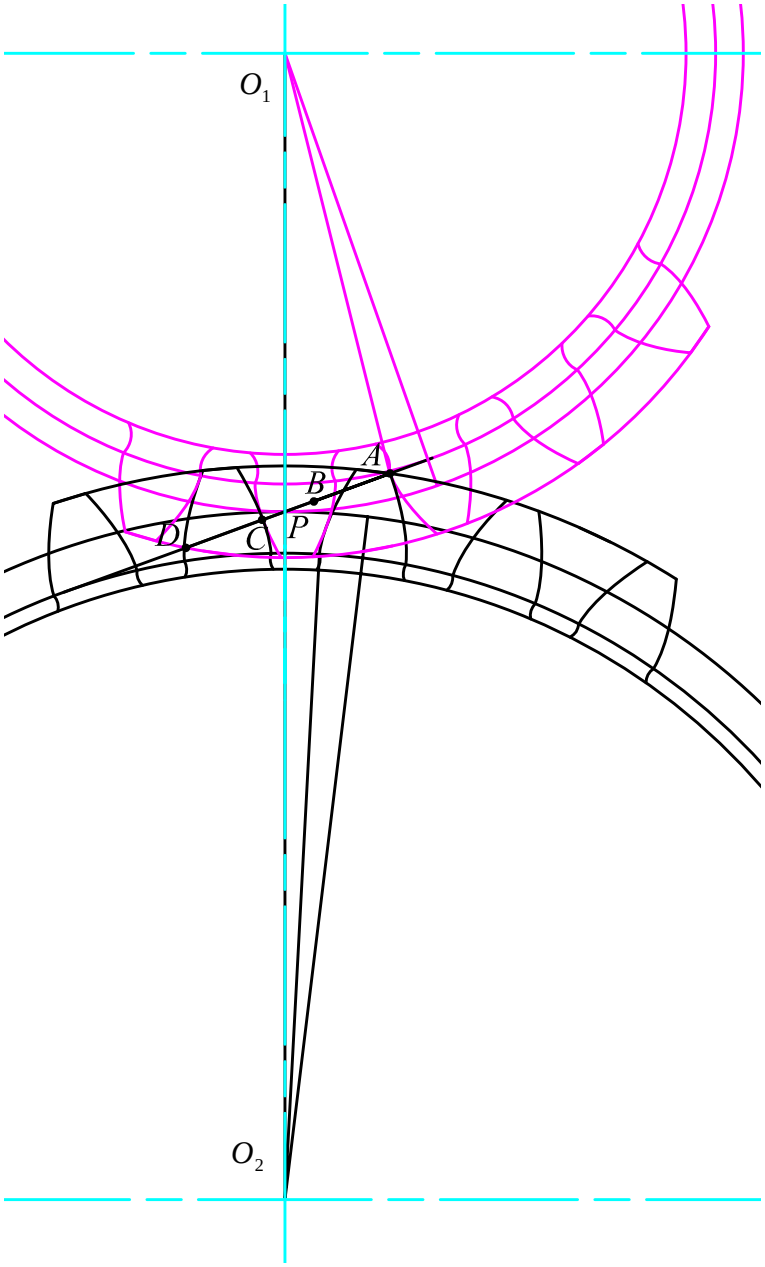

Figure B.8: Gear teeth meshing action

The initial contact occurs at A, where the addendum circle of the driven gear intersects the line of action. As the gears rotate, the point of contact will move along the line of contact, $\overline{APD}$.

When the approaching tooth pair contacts at B, the recessing tooth pair disengages at D leaving only one tooth pair in contact. From B through P to to C is a single contact zone. When the tooth pair reaches point C, the next tooth pair begins engagement at A and starts another meshing cycle. to perform a systematic analysis, the position of contact of the gear teeth along the line of action is expressed in terms of roll angles of the driving gear. The roll angle ε is given by:

$$\varepsilon_i = cos^{-1}\frac{r_i}{R_b}. \tag{B.38}$$

B.7 Contact Ratio

The contact ratio is defined as the average number of tooth pair(s) in contact [12]. It may also be defined as the ratio of the length of contact for one tooth to the base pitch. The path of contact is the length of the line of action where actual contact between the mating gears takes place. For most practical designs of spur gears, the contact ratio CR has a value between 1.0 and 2.0, implying that two teeth are in contact $2(1-\frac{1}{CR})$ fraction of total mesh time and a single tooth pair is transmitting torque during the rest of the mesh cycle. The path of contact may be divided into two portions:

i. Path of approach, line (AP) in Figure B.8

ii. Path of recess, line (PD)

From the geometric properties shown in Figure B.8, the path of approach and recess can be obtained using the following relations:

$$AP = \sqrt{R_{o2}^2 - R_{b2}^2} - R_{p2} sin\phi, \tag{B.39}$$

$$PD_2 = \sqrt{R_{o1}^2 - R_{b1}^2} - R_{p1} sin\phi, \tag{B.40}$$

Therefore, the path of contact is given by:

$$\overline{AD} = \overline{AP} + \overline{PD} = \sqrt{R_{o1}^2 - R_{b1}^2} + \sqrt{R_{o2}^2 - R_{b2}^2} - (R_{p1} + R_{p2}) sin\phi, \tag{B.41}$$

and the contact ratio is given by:

$$C.R = \frac{\sqrt{R_{o1}^2 - R_{b1}^2} + \sqrt{R_{o2}^2 - R_{b2}^2} - (R_{p1} + R_{p2}) sin\phi}{p_c cos\phi}. \tag{B.42}$$

APPENDIX C

Parameters for Redesigned Gear Train

Table C.1 shows the gear parameters adopted for the new design. In the design of subsequent gear trains, the center distance was held constant while the addendum of the corresponding gear trains were varied to obtain a contact ratio close to 2.0 while avoiding interference. The gear properties of subsequent speeds' gear trains are given in Tables C.2 to C.6.

Table C.1: Adopted gear parameters for speed 1 gear train

Mesh	Gear	A_x	C (mm)	CR	J_i (Kg mm^2)
I	17	0.39338	72.969	1.970	52.075
	41	0.40766			1273.234
II	17	0.35522	81.503	1.971	64.478
	48	0.27664			3178.655
III	18	0.35690	82.903	1.991	77.725
	48	0.38380			4192.515
IV	17	0.39338	81.503	1.971	141.703
	48	0.26455			4767.982

Table C.2: Adopted gear parameters for speed 2 gear train

Mesh	Gear	A_x	C (mm)	CR	J_i (Kg mm^2)
I	17	0.39338	72.969	1.970	52.075
	41	0.40766			1273.234
II	24	0.35522	81.503	2.000	149.711
	41	0.27664			1627.157
III	18	0.35690	82.903	1.991	77.725
	48	0.38380			4192.515
IV	17	0.39338	81.503	1.971	141.703
	48	0.26455			4767.982

Table C.3: Adopted gear parameters for speed 3 gear train

Mesh	Gear	A_x	C (mm)	CR	J_i (Kg mm^2)
I	17	0.39338	72.969	1.970	52.075
	41	0.40766			1273.234
II	36	0.35522	81.503	2.000	757.653
	29	0.27664			1627.157
III	18	0.35690	82.903	1.991	77.725
	48	0.38380			4192.515
IV	17	0.39338	81.503	1.971	141.703
	48	0.26455			4767.982

Table C.4: Adopted gear parameters for speed 4 gear train

Mesh	Gear	A_x	C (mm)	CR	J_i (Kg mm^2)
I	34	0.42084	72.969	1.990	743.553
	24	0.35522			149.711
II	17	0.39338	81.503	1.972	64.478
	48	0.27664			3178.655
III	18	0.35690	82.903	1.991	77.725
	48	0.38380			4192.515
IV	17	0.39338	81.503	1.971	141.703
	48	0.26455			4767.982

Table C.5: Adopted gear parameters for speed 5 gear train

Mesh	Gear	A_x	C (mm)	CR	J_i (Kg mm^2)
I	34	0.42084	72.969	1.990	743.553
	24	0.35522			149.711
II	24	0.35522	81.503	1.972	149.711
	41	0.27664			1627.157
III	18	0.35690	82.903	1.991	77.725
	48	0.38380			4192.515
IV	17	0.39338	81.503	1.971	141.703
	48	0.26455			4767.982

Table C.6: Adopted gear parameters for speed 6 gear train

Mesh	Gear	A_x	C (mm)	CR	J_i (Kg mm^2)
I	34	0.42084	72.969	1.990	743.553
	24	0.35522			149.711
II	36	0.35522	81.503	2.000	757.653
	29	0.27664			1627.157
III	18	0.35690	82.903	1.991	77.725
	48	0.38380			4192.515
IV	17	0.39338	81.503	1.971	141.703
	48	0.26455			4767.982